Late Neogene biogenic sedimentation and carbon isotope shifts in the southwest Pacific Ocean

Thesis submitted by

Katharine Mary Grant ***(BSc[Hons] University of Southampton)***

in September 2005

for the degree of Master of Science
in the School of Earth Sciences
James Cook University, North Queensland, Australia

STATEMENT OF ACCESS

I, the undersigned author of this work, understand that James Cook University will make this thesis available for use within the University Library and, via the Australian Digital Theses network, for use elsewhere.

I understand that, as an unpublished work, a thesis has significant protection under the Copyright Act and;

I do not wish to place any further restriction on access to this work

Katharine Grant 04/02/10

Signed ~~on behalf of~~ Katharine Grant

Paul Dirks

Head of School

Earth and Environmental Sciences

5/02/10

STATEMENT ON SOURCES

Declaration

I declare that this thesis is my own work and has not been submitted in any form for another degree or diploma at any university or other institution of tertiary education. Information derived from the published or unpublished work of others has been acknowledged in the text and a list of references is given.

Katharine Grant 04/02/10

Signed on behalf of Katharine Grant

Paul Dirks

Head of School

Earth and Environmental Sciences

5/02/10

ELECTRONIC COPY

I, the undersigned, the author of this work, declare that the electronic copy of this thesis provided to the James Cook University Library, is an accurate copy of the print thesis submitted, within the limits of the technology available.

Katharine Grant 04/02/10

Signed on behalf of Katharine Grant

Paul Dirks

Head of School

Earth and Environmental Sciences

5/02/10

STATEMENT OF THE CONTRIBUTION OF OTHERS

I sincerely thank James Cook University for provision of an International Postgraduate Research Scholarship (IPRS) in conjunction with a scholarship from the School of Earth Sciences. Extension of candidature was made possible thanks to additional funds from an IPRS and Bob Carter. Research activities were also funded through Australian Research Council (ARC) grants to R. M. Carter and G. R. Dickens, and through the Ocean Drilling Program, which invited me to sail as a student technician on Leg 181 and supplied the core samples for my project.

This project was chiefly supervised by Bob Carter, and his contribution is hugely appreciated. In addition the project was aided to a large degree by Jerry Dickens, a brilliant geochemist and inspiring teacher. Further assistance was provided by Keith Turnbull and Paul Gammon at Adelaide University - for stable isotope analyses - and by Elvi Grigolato at the JCU-AAC for XRF analyses.

ACKNOWLEDGMENTS

Above all I am indebted to Jerry Dickens and Bob Carter, without whom this thesis would not have been possible. Their continual assistance, encouragement and empathy throughout my struggles have been deeply appreciated and I thank them wholeheartedly. I am also enormously grateful to Helene Marsh for being so understanding with respect to my situation and very generously extending my candidature; similarly, I extend my thanks to Bob Henderson for his enduring approval and moral support.

During my time at James Cook University I was extremely fortunate to meet many wonderful people and I want to thank them all. I can only mention a few here; the others know who they are. Inspiring colleagues at the School of Earth Sciences include Rhonda Welch (né Adkins), a truly great friend who has helped steer me through everything; members of the 'Marine Group', especially Gavin Dunbar, Peter Crosdale, and Andrew Heap for their help and advice, particularly when they were so busy themselves; Nicole Patison, Jo Muller, Belinda Kinna, and Haidi Hancock, for their long-lasting friendship; and lastly (but very loudly) the jolly madness of Nick "The Youth" Timms and Aaron Stallard with whom I celebrated life's quirkier moments.

In the UK, Canada, and elsewhere in Australia, I want to expressly thank Astrid, Gnomes, Jools, Angelique, Rose, and Sr. Lucy Kert for their constant positivity, love, and thoughtfulness. And finally, a very special mention to Mum and Dad, who have done so much that I can't convey my thanks on a page. I am eternally grateful and owe everything to them.

Abstract

Biogenic components of sediment accumulated at high rates beneath frontal zones of the Indian and Pacific oceans during the late Miocene and early Pliocene. The $\delta^{13}C$ of bulk and foraminiferan carbonate also decreased during this time interval. Although the two observations may be causally linked, and signify a major perturbation in global biogeochemical cycling, no site beneath a frontal zone has independent records of export production and $\delta^{13}C$ on multiple carbonate phases across the critical interval of interest. Furthermore, most of the $\delta^{13}C$ data for the late Miocene-early Pliocene are not calibrated on the same timescale. In the Southwest Pacific Ocean, Deep Sea Drilling Project (DSDP) site 590 and Ocean Drilling Program (ODP) site 1125 lie beneath major frontal zones: the Tasman Front and Subtropical Convergence (STC), respectively; DSDP site 594 lies just outside the STC. Late Neogene records of $CaCO_3$ mass accumulation rate (MAR), bulk carbonate $\delta^{13}C$, and Ca/Ti, Si/Ti and Al/Ti ratios have been constructed at all three sites, and are complemented at sites 590 and 1125 by $\delta^{13}C$ records of planktic and benthic foraminifera; a record of Ba/Ti has also been produced for site 590.

At site 590, $CaCO_3$ MARs, Ca/Ti, Al/Ti and Ba/Ti ratios are 2 to 3 times higher in upper Miocene and lower Pliocene sediment relative to overlying and underlying units. A significant decrease (between 1 and 2 ‰) also occurs in all $\delta^{13}C$ records. All evidence indicates that enhanced export production - the “biogenic bloom” - extended to the Tasman Front between ca. 9 and 3.8 Ma, and this phenomenon is coupled with changes in $\delta^{13}C$ - the “Chron C3AR carbon shift”. However, $CaCO_3$ MARs peak ca. 5 Ma whereas elemental ratios are highest ca. 6.5 Ma; foraminiferan $\delta^{13}C$ starts to decrease ca. 8 Ma whereas bulk carbonate $\delta^{13}C$ begins to drop ca. 5.6 Ma. Temporal discrepancies between the records can be explained by changes in the upwelling regime at the Tasman Front and by depth differences between coccolithophorid and foraminiferan carbonate precipitation.

The sediment records from site 1125 show very similar trends to those from site 590. $CaCO_3$ MARs are eight-fold higher between 5.66 and 5.38 Ma, relative to average Neogene values, and this maximum coincides with elevated Ca/Ti ratios and faunal abundance patterns indicative of elevated upwelling and primary productivity. These observations, and their absence from the site 594 records, are interpreted as evidence of

the biogenic bloom in the STC. The suite of $\delta^{13}C$ records from site 1125 all show significantly lower values for the early Pliocene compared to the latest Miocene, and the depletion occurs mainly in two distinct shifts. The "Chron C3Ar carbon shift" (between –0.6 and –1.5 ‰ magnitude) is recorded by planktic and benthic foraminifera between 7.0 and 6.4 Ma, and an "early Gilbert carbon shift" is recorded by both the bulk sediment (–1.8 ‰; 5.1-3.6 Ma) and all species of foraminifera (~ –1.0 ‰; 5.3-4.9 Ma). Bulk sediment from site 594 also decreases markedly (–1.7 ‰) between 5.0 and 3.6 Ma. These isotopic excursions are explained by coupled variations in hydrography, productivity, and depth of calcite precipitation, as well as an increase in terrigenous fluxes to Chatham Rise ca. 5.4 Ma. The overall driving force of the biogenic bloom and late Neogene carbon isotope shifts in the southwest Pacific Ocean can be related to climate-driven changes in ocean circulation, probably arising from Antarctic glaciation.

Table of Contents

List of Tables

List of Figures

PART I

BACKGROUND

1 Introduction

For most of the earth's 4.6 billion year history, marine sediments have been accumulating beneath an ocean free from polar ice cover and freely circulating in a largely 'global' oceanic basin. These conditions changed dramatically, however, during the late Neogene (11.2-1.8 Ma; Berggren et al., 1995b); this interval encompasses the late Miocene and Pliocene, and marks the initiation of significant ice sheet growth in the Antarctic and Northern Hemisphere, and of modern-day global circulation patterns in the atmosphere and ocean. Changes within the biosphere are also an integral part of the earth's evolution, so the research of global biogeochemical cycles during the late Neogene is fundamental to an understanding of past, and possibly future, large-scale changes in ocean productivity, chemistry, and circulation. Deep-sea sediment cores are valuable archives of such changes, hence this study investigates a variety of geochemical proxies in late Neogene sediments.

1.1 Background to this thesis

For more than 20 years, studies of late Miocene and early Pliocene marine sediments have encountered two observations that require major perturbations in global biogeochemical cycling. First, sediment components linked to primary productivity in surface waters (e.g., $CaCO_3$, SiO_2, P) accumulated at very high rates beneath upwelling zones throughout the Indian and Pacific oceans (e.g., Van Andel et al., 1975; Peterson et al., 1992; Delaney and Filippelli, 1994; Farrell et al., 1995a; Dickens and Owen, 1999) and the Atlantic ocean (Diester-Haass et al., 2002, 2004). This widespread and significant increase in export production, coined the "biogenic bloom", relates to an elevated supply of nutrients to the ocean, a major redistribution of nutrients within the ocean, or both (Delaney and Filippelli, 1994; Farrell et al., 1995a; Dickens and Owen, 1996, 1999; Hermoyian and Owen, 2001). Second, carbon isotope ($\delta^{13}C$) records of bulk carbonate and benthic and planktic foraminifera at many locations decrease by 0.5 to 1.0 ‰ (e.g., Keigwin, 1979; Vincent et al., 1980; Savin et al., 1981; Loutit et al., 1983; Keigwin et al., 1987; Müller et al., 1991). This change in the isotopic composition of water masses, often referred to as the "Epoch 6" or "Chron C3Ar" carbon shift (Vincent et al., 1980; Müller et al., 1991), signifies a change in the marine carbon cycle,

possibly because of variations in deep water circulation, carbon supply to the ocean, or both (above references).

In addition to increased export production and a depletion in the $\delta^{13}C$ content of marine carbonates, there is further evidence for profound changes in global oceanography between 8 and 4 Ma, as previously mentioned, that would have affected nutrient and carbon cycling. For example, the maximum depth of the carbonate compensation depth (CCD) switched from the Atlantic to the Pacific (e.g., Van Andel, 1975; Rea and Leinen, 1985); the West Antarctic ice sheet developed (e.g., Drewry, 1978; Ciesielski et al., 1982); the Isthmus of Panama emerged, separating Pacific and Atlantic circulation (e.g., Keigwin, 1982a; Farrell et al., 1995a; Haug and Tiedemann, 1998); and, the Mediterranean basin became dessicated (the "Messinian Salinity Crisis"; e.g., Hsü et al., 1973, 1977; Hodell et al., 1986; Clauzon et al., 1996).

The biogenic bloom and Chron C3Ar carbon shift were probably associated with some or all of the aforementioned oceanographic phenomena. Of particular interest in this regard is how the biogenic bloom and Chron C3Ar carbon shift are related to one another, because widespread changes in nutrient distribution and productivity should cause global variations in carbon isotopes.

1.2 Unanswered questions

Although the biogenic bloom and Chron C3Ar carbon shift may be causally related and hint at fundamental oceanographic differences from the Miocene to the Pliocene, there are four immediate problems with placing these phenomena into scenarios of late Neogene global change.

First, absolute ages for isochronous datums have changed significantly over the last 15 years, especially in the late Miocene (cf. Berggren et al., 1985, 1995b). Many key records across the time interval of interest are therefore not calibrated to a similar or current time scale (Dickens and Owen, 1999). Second, the timing and magnitude of the Chron C3Ar carbon shift is problematic. Whereas $\delta^{13}C$ records from benthic and planktic foraminifera exhibit an abrupt – 0.5 to – 1.5 ‰ shift before Chron 3An (e.g., Bender and Graham, 1981; Keigwin et al., 1987), the excursion appears gradually after Chron 3An in bulk carbonate records (Mead et al., 1991; Shackleton and Hall, 1995, 1997).

Third, no previous studies have analysed the $\delta^{13}C$ content of planktic and benthic foraminifera, coccoliths, and bulk sediment in a single core. Because $\delta^{13}C$ varies down through the water column, coccolithophores, benthic foraminifera, and different species of planktic foraminifera, will record different values of $\delta^{13}C$. Despite this vertical variability, no previous study of the stable carbon isotopic ratios in sedimentary carbonate has analysed each of the different carbonate phases at the one site. Finally, despite potential links between enhanced productivity and the Chron C3AR carbon shift (Vincent et al., 1980, 1985; Berger and Vincent, 1986), no study has examined independent proxies of palaeoproductivity and $\delta^{13}C$ in multiple carbonate phases at the same location. Thus, timing relationships between the two phenomena have remained uncertain.

1.3 Thesis aims

In order to address some of the aforementioned problems, the aims of my thesis are fourfold: (1) provide up-to-date reviews of the "Epoch 6" carbon shift and "biogenic bloom" phenomena, particularly with respect to current timescales, (2) establish $\delta^{13}C$ records of different carbonate phases (benthic and planktic foraminifera, and bulk sediment fractions) at the same site, (3) compare these records with independent proxies of palaeoproductivity at the same site, and (4) establish similar datasets at more than one site in the same region, for comparison and interpretation within the framework of current palaeoceanographic hypotheses for the late Miocene – early Pliocene.

1.4 Structure of thesis

This thesis is divided into two parts. Part I provides a background to my research by reviewing evidence of the late Miocene ("Epoch 6") carbon shift (chapter 2) and the "biogenic bloom" (chapter 3), finishing with a review of the present-day oceanography of the New Zealand region of the Southwest Pacific (chapter 4). Part II contains my own analyses, divided into chapters 5-7. First I describe a multi-proxy study at a single site (DSDP 590; chapter 5), and then I compare sediment records from site 590 with those from two other sites in same region (DSDP 594 and ODP 1125; chapter 6). I conclude Part II with a synopsis of my completed research project (chapter 7), in which

I summarise the main findings, highlight some of the problems with the project, and suggest possible directions for future research in this field. All references cited in the body of the thesis are listed in one bibliography following chapter 7, and all figures and tables are in appendices after the bibliography.

2 The "Chron C3Ar Carbon Isotope Shift"

2.1 Introduction

Stable carbon isotope records constructed using marine carbonates reveal a series of characteristic trends from the Paleogene through the Quaternary (**Fig. 2F1**; see also Zachos et al., 2001). These $\delta^{13}C$ variations represent changes in the operation of the global carbon cycle. One of the most widely recognised excursions is the negative shift of ~0.5-1.0 ‰ occurring in magnetic polarity subchronozone C3Ar (formerly magnetic Epoch 6; see Keigwin, 1979; Haq et al., 1980; Bender and Graham, 1981; Vincent et al., 1980, 1985; Berger and Vincent, 1986; **Fig. 2F2**). These pioneering investigations showed that the $\delta^{13}C$ depletion was recorded by both benthic and planktic foraminifera, occurred in Pacific, Indian, and Atlantic sediment cores, and was globally isochronous (based on the resolution of core sampling and age models employed at that time).

The combination of an increasingly large carbon isotope database, as isotope stratigraphy has become a standard tool in palaeoceanography, and revised Cenozoic geomagnetic timescales (e.g., Berggren et al., 1985, 1995b; Cande and Kent, 1992; Shackleton et al., 1995) permits an updated review of the "Chron C3Ar carbon shift". Evidence of the isotopic excursion will therefore be presented, incorporating stable carbon isotope records from different carbonate phases and recent high-resolution records. Explanations for a decrease in marine carbonate $\delta^{13}C$ during the late Miocene will then be outlined, concluding with a summary of the literature discussed.

2.2 Neogene records of marine carbonate $\delta^{13}C$

Pioneering work by Douglas and Savin (1973, 1975) established that the $\delta^{13}C$ of planktic and benthic foraminifera from sediment cores of the Pacific tended to be increasingly depleted in $\delta^{13}C$ from the Miocene/Pliocene boundary to the Holocene. A comparison of subsequent higher resolution analyses revealed that a depletion of ~0.6-1.0 ‰ occurred just above the First Appearance Datum (FAD) of *Amaurolithus primus* (7.2 Ma [Berggren et al., 1995b]) in benthic foraminiferan $\delta^{13}C$ records from Deep Sea Drilling Program (DSDP) sites 77, 158, 289, and 310 in the equatorial and North Pacific Ocean, sites 207 and 208 in the southwest Pacific Ocean, sites 214, 237, and 238 in the

Indian Ocean, and site 357 in the South Atlantic Ocean (Haq et al., 1980, and references therein). Initial studies had therefore concluded that the late Miocene $\delta^{13}C$ shift was a benthic signal, mainly confined to the Indo-Pacific region (e.g., Bender and Keigwin, 1979; Shackleton and Cita, 1979; Vincent et al., 1980), but subsequent work documented the isotopic excursion in planktic foraminifera (e.g., Loutit et al., 1983; Vincent et al., 1985; Müller et al., 1991; **Fig. 2F2**) and in the North and South Atlantic at DSDP sites 502, 525, 526, and 552, and at Ocean Drilling Program (ODP) sites 704, 982, and 1088 (Keigwin, 1982c; Shackleton et al., 1984; Keigwin et al., 1987; Müller et al., 1991; Hodell et al., 2001; Billups, 2002; **Fig. 2F2**).

Curiously, not all marine carbonates record a 0.5-1.5 ‰ depletion in $\delta^{13}C$ within Chron C3Ar; in bulk carbonate records the excursion is either younger (DSDP site 525 [Shackleton and Hall, 1984]) or gradual (ODP site 704 [Mead et al., 1991], ODP sites 844-854 [Shackleton and Hall, 1995], and ODP site 926 [Shackleton and Hall, 1997]; **Fig. 2F2**). This disparity has been noted but not adequately explained (Broecker and Woodruff, 1992; Shackleton and Hall, 1995, 1997).

2.3 Stratigraphic framework

Absolute ages on the geomagnetic polarity timescale have been repositioned over the last 15 years, especially in the late Miocene, hence many of the aforementioned $\delta^{13}C$ records are not calibrated to a similar or current timescale. The isochroneity of the Chron C3Ar carbon shift in sediment cores from different regions was therefore initially confirmed by key biostratigraphic datums.

The late Miocene carbon shift has been observed near the top of the radiolarian *Ommatartus penultimus* Zone, often coinciding with the FAD of *Stichocorys peregrina* - 6.96 Ma [cf. Berggren et al., 1995b] - (Keigwin, 1979; Haq et al., 1980; Keigwin and Shackleton, 1980; Vincent et al., 1980, 1985; Savin et al., 1981). With respect to nannofossil datums, the shift has been recorded just above the FAD of *Amourolithus primus* - 7.2 Ma [Berggren et al., 1995b] - (Loutit and Kennett, 1979; Haq et al., 1980; Shackleton et al., 1984; Elmstrom and Kennett, 1986; Keigwin et al., 1987) and below the Last Appearance Datum (LAD) of *Amourolithus amplificus* - 6.2 Ma [Berggren et al., 1995b] - (Savin et al., 1981; Shackleton et al., 1984; Vincent et al., 1985). It has also

been observed close to the N16/N17 boundary - 8.26 Ma [Berggren et al., 1995b] - (Bender and Keigwin, 1979; Keigwin, 1979).

In addition, the diatom biostratigraphic FADs of *Thalassiosira praeconvexa* and *Nitzschia miocenica* var. *elongata* have been documented near the carbon shift (Haq et al., 1980), as well as the planktic foraminiferan FADs of *Globorotalia plesiotumida, Globigerinoides obliquus extremus* and *Gs. conglobatus* (Keller, 1981). The FADs of the planktic foraminifera *Globorotalia ciboaensis* and *Ga. conomiozea* (7.8 and 7.12 Ma, respectively [Berggren et al., 1995b]) have also been identified near the isotope shift (Bender and Keigwin, 1979; Loutit and Kennett, 1979; Keigwin 1979, 1982b; Shackleton et al., 1984). These datums appear to be diachronous, however, and may be unreliable (see Hodell and Kennett [1986] and Berggren et al. [1995b]).

The development of well-constrained age models has continually resolved the timing of the carbon shift. The observation of the shift within magnetic Epoch 6 (7.43-6.57 Ma [Berggren et al., 1995b]), in the east Equatorial Pacific piston core RC12-66 (Keigwin and Shackleton, 1980), led to the event being coined the "Epoch 6 Carbon Shift". Subsequent revision of the geomagnetic polarity timescale (Berggren et al., 1985) gave rise to an update in terminology -- the "Chron C3Ar carbon shift" (Müller et al, 1991). A few years later, the astronomically-tuned chronology of ODP site 926 in the west Equatorial Atlantic (Shackleton and Crowhurst, 1997) dated a negative shift in bulk carbonate $\delta^{13}C$ at 7.31-5.90 Ma (Shackleton and Hall, 1997). Most recently, Billups (2002) constrained the timing of the shift to between 7.62 ($\delta^{13}C$ maximum) and 6.65 Ma ($\delta^{13}C$ minimum) based on a high resolution $\delta^{13}C$ record from ODP site 982 in the North Atlantic which had been astronomically-tuned (Hodell et al., 2001).

2.4 What caused the "Chron C3Ar Carbon Shift"?

Widespread recognition of the Chron C3Ar carbon shift as a significant late Neogene event has generated much debate about the cause of such a distinct drop in marine carbonate $\delta^{13}C$, leading to a variety of explanatory hypotheses. Depletion of marine carbonate $\delta^{13}C$ requires either a) redistribution of the relative proportions of ^{13}C and ^{12}C between the ocean basins ("internal fractionation"), b) a fundamental change in the average $\delta^{13}C$ composition of seawater ("external fractionation"), or (c) a

combination of both. Alternatively, the $\delta^{13}C$ of carbonate shells may not be a true approximation of seawater $\delta^{13}C$ at the time of precipitation. Suggested mechanisms for the Chron C3Ar carbon shift differ according to the relative importance assigned to each causal factor, although there is general agreement that no single process is responsible.

2.4.1 Internal fractionation

The Upwelling / Phosphate (PO_4^{3-}) signal

The carbon shift was initially believed to reflect either a rapid change in oceanic cycling of TCO_2 (total carbon dioxide) incurred by dampened rates of global upwelling, or an increase in the fraction of particulate inorganic phosphate (PO_4^{3-}) reaching the deep ocean (Bender and Keigwin, 1979; **Fig. 2F3(a)**). These authors based their argument on the intimately linked cycles of marine organic matter and phosphate (Broecker, 1971; Froelich et al., 1977; Kroopnick et al., 1977). As a corollary to this hypothesis, they deduced that an alternative origin of the $\delta^{13}C$ depletion would be a change in abyssal circulation, because nutrient cycling is dependent on deep water dynamics. Vincent et al. (1980) dismissed the "decreased upwelling" hypothesis, citing an increase in sedimentation of siliceous fossils at the time of the carbon shift to be indicative of elevated fertility and hence upwelling. However, it has long been accepted by palaeoceanographers that deep water circulation plays a key role in the carbon isotope record (see following discussion).

The Deep-water 'conveyor belt'

Modern-day abyssal circulation was characterised by Broecker (1974) as the deep arm of a global conveyor belt, flowing from the North Atlantic to the Pacific basin. It has been suggested that the carbon shift marks the on-set of this hydrographic regime (Bender and Graham, 1981; Keigwin, 1982c; Keigwin et al., 1987; Savin et al., 1981; Vincent et al., 1980, 1985). This hypothesis is based on the fact that modern-day Atlantic-Pacific gradients in $\delta^{13}C$, amongst other basin-basin gradients, are mirrored at the time of the carbon shift and thereafter (e.g., Billups, 2002), and these gradients are closely tied to deep water circulation patterns (**Fig. 2F3(a))**.

The aging of water masses towards the Pacific is reflected in higher values of $\delta^{12}C$, "apparent oxygen utilisation" (AOU), and carbonate dissolution in Pacific waters,

resulting from the continual decomposition of organic matter along the Atlantic-Pacific deep water conveyor belt. Consequently, there is an accumulation of corrosive, isotopically light bottom waters in the Pacific, with a concomitant depletion of oxygen. Such oceanic contrasts have been documented for $\delta^{13}C$ (Miller and Fairbanks, 1983, 1985; Shackleton and Hall, 1984), AOU (Bender and Graham, 1981; Bender and Keigwin, 1979; Keigwin, 1979), and Carbonate Compensation Depth (CCD) (Van Andel et al., 1975), and these oceanic gradients are more pronounced since the time of the Chron C3Ar carbon shift. A coincident trend is an amplification of climate-forcing mechanisms (Vincent et al., 1980, 1985). The production of North Atlantic Deep Water (NADW) is one such mechanism, and its coupling to climate change has been widely demonstrated in palaeoceanographic studies of the Quaternary glaciations (e.g., Broecker et al., 1985; Boyle and Keigwin, 1987; Ruddiman et al., 1989; Maslin et al., 1995). Further evidence of a link between the Chron C3Ar carbon shift and initiation of NADW production is a distinctly variable oxygen isotope record from the late Neogene onwards (Vincent et al., 1980, 1985).

Clearly, these explanations presume that NADW production pre-dates, or coincides with, the isotopic excursion. Yet the origin and timing of changes in global deepwater flow during the late Miocene are still debated (see also **chapter 3**). Some investigators of the Chron C3Ar carbon shift have speculated on the fundamental trigger of these changes. Bender and Keigwin (1979) invoked tectonic movements, whereby the Isthmus of Panama shoaled above some critical depth and thus altered North Atlantic circulation (e.g., Keller et al., 1989; Duque-Carol, 1990; Farrell et al., 1995a). Alternatively, Loutit and Kennett (1979) and Loutit and Keigwin (1982) considered Antarctic ice sheet growth as the instigator of deepwater circulation change. A major expansion of southern ice caps, and corresponding global regression, characterises the late Miocene (Kennett and von der Borch, 1986; Shackleton and Kennett, 1975; Van Andel et al., 1975; Adams et al., 1977; Berggren and Haq, 1976; Vail and Hardenbol, 1979). Regression also controls the flux of terrestrial organic carbon from continental margins, and it is therefore a key process in the "external fractionation" hypothesis (see below).

2.4.2 External fractionation

Several investigators have surmised that the covariance of benthic and planktic signals during the Chron C3Ar carbon shift indicates a compositional change in seawater ΣCO_2 towards lighter isotopic fractions (e.g., Loutit et al., 1983; Berger and Vincent, 1986; Keigwin et al., 1987). Such a fundamental change in isotopic composition will arise from a change in either the fraction or rate of flux of carbon from or to a major reservoir in communication with the ocean (Kump and Arthur, 1999). These principal reservoirs and fluxes are illustrated in **Fig. 2F3(b)**, and their potential role in the depletion of marine carbonate $\delta^{13}C$ during the late Miocene is discussed below in terms of the physical processes involved.

Deep sea burial, continental weathering

Enhanced decomposition of organic matter in the deep sea enriches ΣCO_2 in ^{12}C (**Fig. 2F3(b)**), and a decline in the proportion of organic:inorganic carbon burial through the late Miocene is well documented (Tappan, 1968; Berger, 1977; Fischer and Arthur, 1977; Shackleton, 1987). The breakdown of organic carbon consumes oxygen, so an increase in the oxygen content of bottom waters favours a decrease in organic:inorganic carbon burial (Berger and Vincent, 1986), and this is conducive with the initiation of NADW production (the "internal fractionation" hypothesis). Alternatively, a greater flux of inorganic carbon to the oceans over long (My) periods would effectively reduce the ratio of organic:inorganic carbon burial. By this reasoning, Miller and Fairbanks (1985) proposed that an increased input of HCO_3^- to the global ocean modified net carbon and strontium riverine fluxes in the late Miocene (**Fig. 2F3(b)**). An increase in continental weathering during the late Neogene has been inferred from strontium isotope analyses (Hodell et al., 1989). However, a decrease in the average $\delta^{13}C$ of river-borne HCO_3^- is considered insufficient in its capacity to lower marine $\delta^{13}C$ values by the magnitude observed across the Chron C3Ar carbon shift (Vincent et al., 1980). Many studies have therefore concluded that such a depletion requires a substantial input of isotopically light carbon to the oceans, and hence involved the organic carbon reservoirs (Vincent et al., 1980, 1985; Bender and Graham, 1981; Loutit et al., 1983; Berger and Vincent, 1986; Keigwin et al., 1987).

Late Neogene regression

The growth of Antarctic ice sheets in the late Neogene was accompanied by a substantial fall in global sea-level, which in turn augmented the weathering of organic-rich marginal sediments and thence caused a drop in marine carbonate $\delta^{13}C$ (Vincent et al., 1980; Bender and Graham, 1981; Berger and Vincent, 1986). This scenario was mathematically proven using simple models of the carbon cycle (Bender and Graham, 1981; Berger and Vincent, 1986; Vincent et al., 1980), and subsequently linked to orbital forcing (Keigwin et al., 1987; Bickert et al., 2004). Keigwin et al. (1987) first detected a cyclic variability in $\delta^{13}C$ values post-carbon shift, and speculated that fluctuations in the earth's orbit during the late Miocene affected the size of the continental biomass reservoir. Now Bickert et al. (2004) have observed 100-kyr cyclicity in benthic foraminiferan $\delta^{13}C$ between 8.5 and 5.3 Ma (ages based on oxygen isotope stratigraphy, see authors' age model) at ODP site 999 in the Caribbean. This cyclic variability was positively correlated with that of magnetic susceptibility - a proxy of terrigenous inputs - in the same sediments, leading these authors to conclude that the Chron C3Ar carbon shift apparent in their record was caused by erosion of organic carbon from terrigenous soils and shelf sediments.

2.4.3 "Vital effects"

Foraminifera precipitate their carbonate shells in disequilibrium with ambient seawater, hence isotope analyses of their shells will not provide absolute values of seawater $\delta^{13}C$ at the time of precipitation (Vergnaud-Grazzini, 1976; Berger et al., 1978b). It is therefore possible that the Chron C3Ar carbon shift reflects, to a certain extent, an increase in disequilibrium between seawater and foraminiferan carbonate (Vincent et al., 1980). This disparity may occur at times of elevated growth rates, and by inference, increased fertility. An association between fertility and foraminiferan $\delta^{13}C$ has been established (Berger et al., 1978a) and subsequent studies have demonstrated that species in highly fertile areas exhibit larger $\delta^{13}C$ fractionation than those from less fertile regions (Vincent et al., 1981). However, the relative contribution of vital effects to the Chron C3Ar carbon shift may be minimal, given that 1) no vital effects are apparent in corresponding $\delta^{18}O$ curves, 2) both planktic and benthic foraminifera record

a near-identical shift, and 3) bulk sediment $\delta^{13}C$ also decreases in the latest Miocene-earliest Pliocene.

The above review of possible causes of the Chron C3Ar carbon shift reveals that there are many plausible explanations for it, and more than one mechanism may have been responsible. Vincent et al. (1980, 1985) offered a breakdown of the relative influence of each hypothesised cause, suggesting that the $\delta^{13}C$ depletion owed 50% to external fractionation, 30% to internal fractionation, and 20% to "vital effects".

2.5 Summary

A decline of approximately 0.5-1.0 ‰ in the $\delta^{13}C$ values of foraminiferan shells and some bulk carbonate sediments occurred in the late Miocene ca. 7.6-6.6 Ma. The frequent covariance of benthic and planktic records, combined with inter-oceanic contrasts in the magnitude of the depletion, imply that both the composition and distribution of seawater $\delta^{13}C$ changed at that time. This implication is consistent with independent records of late Neogene palaeoceanography. However, not all marine carbonates record a depletion in $\delta^{13}C$ in the late Miocene, and this has not been adequately explained. So although there is overwhelming evidence of a major change in global carbon cycling at this time (and in the early Pliocene), deciphering the cause of this change is not straightforward and more than one mechanism was probably involved.

The carbon cycle is one part of a bigger global system - biogeochemical cycling. A better understanding of changes in the global carbon cycle during the late Neogene can therefore be gained from examining variations in biogeochemical cycling at that time. A commonly used tool in such studies is the analysis of biogenic sediment deposits, and it is intriguing to note that down-core records from these deposits show dramatic changes during the late Miocene and early Pliocene, i.e., broadly time-coincident with the aforementioned shifts in marine $\delta^{13}C$ records. The observations form the basis of the "biogenic bloom" hypothesis (Farrell et al., 1995a) and are examined in the following chapter.

3 The "biogenic bloom" hypothesis

3.1 Introduction

The observation of a dramatic increase in the accumulation of biogenic components in Upper Neogene sediments from the east equatorial Pacific Ocean led Farrell et al. (1995a) to propose their "biogenic bloom" hypothesis. This states that primary productivity increased substantially at Indo-Pacific divergence zones during the latest Miocene and earliest Pliocene. The observations, therefore, have been interpreted as an increase in the supply, as opposed to preservation, of the biogenic component in question.

Evidence of higher rates of export production during the latest Miocene and earliest Pliocene will be presented geographically (**Fig. 3F1, Table 3T1**), and then compared chronologically in order to investigate the timing of this acme in palaeoproductivity. Finally, potential causes of elevated productivity in the late Neogene will be reviewed with respect to nutrient availability in the ocean.

3.2 Global evidence for increased primary productivity during the latest Miocene-earliest Pliocene

Pacific Ocean

An acme in export production during the late Neogene was first reported by Van Andel et al. (1975), who showed that $CaCO_3$ Mass Accumulation Rates (MARs) in Cenozoic sediments from the central equatorial Pacific Ocean (CEP) peaked during the latest Miocene-earliest Pliocene (**Fig. 3F1, Table 3T1**). Subsequently, Theyer et al. (1985, 1989), Berger et al. (1993), and Farrell et al. (1995a) demonstrated that $CaCO_3$ MARs were elevated across the entire equatorial Pacific Ocean (in the CEP, west (WEP), and east (EEP), respectively) during the time interval in question (**Fig. 3F2**). A similar, co-eval peak has also been observed in the southwest Pacific Ocean (Kennett, von der Borch, et al., 1986). All these observations were interpreted as an increase in rates of export production rather than decreased carbonate dissolution.

Accumulation rates of biogenic Si in the CEP over the past 50 My were first calculated by Leinen (1979), who showed that they were highest during the late

Miocene and Pliocene. Over this time interval, diatom and radiolarian abundances increase in sediments from the WEP (Kroenke et al., 1991), and opal MARs and Ba/Sc ratios all increase significantly in the EEP and north Pacific (Farrell et al., 1995a; Rea et al., 1995; Dickens and Owen, 1996; Schroeder et al., 1997); these rises have been linked to elevated productivity. Furthermore, the deposition of pennate diatom mats and/or oozes in the EEP and north Pacific during the latest Miocene-early Pliocene (Kemp and Baldauf, 1993; Kemp et al., 1995; Dickens and Barron, 1997; **Fig. 3F2**) may be a signature of the biogenic bloom (Dickens and Owen, 1999).

Maximum accumulation rates of organic matter in the latest Miocene-earliest Pliocene have been recorded in the WEP (Stax and Stein, 1993). This trend is mirrored by the accumulation rate of benthic foraminifera (BFAR) - considered to be a reliable proxy for export production (Herguera and Berger, 1991; Diester-Haass et al., 2004, and references therein) - in the same area (Berger et al., 1993).

Down-core microfaunal changes in sediments from the Pacific also support the biogenic bloom hypothesis. An increase in the abundance of planktic and benthic foraminiferan tests indicative of intensified upwelling and palaeoproductivity has been observed in latest Miocene-earliest Pliocene sediment from the WEP (Berger et al., 1993) and southwest Pacific (Woodruff and Douglas, 1981; Woodruff, 1985; Kennett and von der Borch, 1986). Elevated primary and export production tends to increase the surface-to-deep water $\delta^{13}C$ gradient ($\Delta\delta^{13}C$), and in the WEP, peak values of $\Delta\delta^{13}C$ occur in latest Miocene sediments (Berger et al., 1993).

Enhanced primary productivity leads to greater rates of sinking, and thence decomposition, of organic matter. The latter process utilises oxygen, resulting in the development of "Oxygen Minimum Zones" (OMZs) at intermediate water depths beneath high-productivity regions of the oceans (Kroopnick, 1985). In shallower regions of the oceans, such as continental margins and ocean ridges, the OMZ can reach the seafloor and so there is a positive correlation between surface productivity, OMZ expansion, and seafloor hypoxia. As a consequence, some evidence for the biogenic bloom is based on sediment proxies for an oxygen-depleted benthic environment. This evidence includes a decrease in Fe/Sc ratios and bulk sediment Fe concentrations, and an increase in the burial of Fe-Mn nodules, in the central North Pacific during the late Miocene and/or early Pliocene (Arnold et al., 1995; Dickens and Owen, 1996), and an increase in the abundance of the benthic foraminifera *Uvigerina* spp. (tolerant of low oxygen concentrations [e.g., Streeter and Shackleton, 1979]) in the North, West

Equatorial, and Southwest Pacific (Keigwin, 1979; Kennett and von der Borch, 1986; Berger et al., 1993).

Most of the aforementioned sedimentary changes are also seen in drill cores from the Indian Ocean (see below), thus implying that the biogenic bloom encompassed the Indo-Pacific region at least.

Indian Ocean

Significantly increased MARs of carbonate during the latest Miocene-earliest Pliocene have been documented for the Mascarene Plateau (western Indian ocean), the northwest Arabian Sea, and the eastern Indian Ocean (Prell et al., 1989; Pierce et al., 1989; Peterson and Backman, 1990; Peterson et al., 1992; Dickens and Owen, 1999), and have been interpreted together as evidence of the biogenic bloom in the Indian ocean (**Figs. 3F1, 3F2; Table 3T1**). Further indications of heightened primary productivity in different regions of the Indian Ocean during this key interval are summarised below.

In the northwest Arabian Sea, deposition of silica and organic carbon was elevated during the latest Miocene-earliest Pliocene (Prell et al., 1989), and coincides with changes in diatom and benthic foraminiferan assemblages suggestive of enhanced palaeoproductivity (Nigrini, 1991; Hermelin, 1992). Sediment cores from the southeast Arabian Sea also record changes in benthic foraminiferan assemblages in the earliest Pliocene, and these are thought to reflect a high food supply to a poorly-oxygenated benthos (Gupta and Thomas, 1999). Further south in the western Indian ocean, down-core abundance patterns of diatoms from the Mascarene Plateau imply strengthened upwelling and high productivity during the late Miocene and early Pliocene (Mikkelsen, 1990).

Evidence from the eastern Indian Ocean for the biogenic bloom mainly comprises proxies of oxygen depletion in the benthos (indicative of elevated productivity at the surface) during the time interval of interest, including sediment colour changes characteristic of Fe reduction (**Fig. 3F2**; Backman et al., 1988; Robinson, 1990), decreased Mn/Sc ratios (Dickens and Owen, 1994), and benthic foraminiferan assemblage changes (Nomura, 1991). A questionable peak in PMARs ca. 5.5-4 Ma at ODP Sites 756 and 757 may be further evidence of the biogenic bloom in this region (Hermoyian and Owen, 2001).

Atlantic Ocean

There is much less evidence for a late Miocene-early Pliocene productivity maximum in sediment records from the Atlantic Ocean, compared with those from the Indo-Pacific region (**Fig. 3F1, Table 3T1**). Nonetheless, accumulation rates of $CaCO_3$, organic carbon, benthic foraminifera, and *Uvigerina* spp. in particular, all dramatically increase ca. 6.7 Ma in parallel with a rise in organic carbon $\delta^{13}C$, number of benthic foraminifera (NBF), and number of *Uvigerina* spp. at ODP site 1085 off southwest Africa (Diester-Haass et al., 2002, 2004; Twitchell et al., 2002). These observations were explained by heightened productivity, and were recognised as part of a global signal. Previous studies from the southeast Atlantic (DSDP leg 74 – the Walvis Ridge) also interpreted elevated $CaCO_3$ MARs in the earliest Pliocene as a peak in surface productivity (Shackleton et al., 1984).

Drilling in the western equatorial Atlantic (Ceara Rise – ODP leg 154) revealed a significant rise in the flux of sand fraction (Shackleton and Crowhurst, 1997) and $CaCO_3$ (Murray and Peterson, 1997) in the latest Miocene, and this was attributed to an increase in "blue ocean productivity". However, there remains no evidence for the biogenic bloom in the Atlantic Ocean at locations away from the Equator or distal from upwelling regions (Dickens and Owen, 1999).

Southern Ocean

The geographic extent of the biogenic bloom phenomenon may have included the Southern Ocean (**Fig. 3F1, Table 3T1**). The first, and most comprehensive, integrated study of biogenic sedimentation in this region showed that - within the past 50 My interval - siliceous productivity dramatically increased in the early Pliocene (Brewster, 1980). Barron and Baldauf (1989) subsequently reported a major increase in opal MARs in the latest Miocene in sediments from the Kerguelen Plateau (ODP leg 119); all these authors related their observations to upwelling-induced surface productivity. More recently, Hillenbrand and Fuetterer (2002) estimated opal depositional rates (derived from records of biogenic opal contents and opal accumulation rates) in Neogene to Quaternary sediments on the continental rise west of the Antarctic Peninsula (ODP leg 178). Their results suggest that palaeoproductivity was slightly enhanced during the late Miocene and high during the early Pliocene.

In the subantarctic South Atlantic, ODP site 704 records maxima in opal and $CaCO_3$ MARs, and a change in diatom assemblages, during the latest Miocene; these

trends were thought to reflect elevated production in the overlying surface waters at that time (Froelich et al., 1991). However, the authors associated the increase with movement of the Polar Front across site 704, as opposed to either a change in the rate of primary production in a specific water mass or an expansion of a high-productivity zone.

3.3 Timing of increased primary productivity

The continual refinement of geomagnetic polarity timescales over the past three decades means that the aforementioned studies (**section 3.1**) are not calibrated to the same timescale. Furthermore, some of these studies have relatively low-resolution records, hence a global, high-resolution chronology (<10 ky) of the biogenic bloom is not straightforward. However, recent key studies of the biogenic bloom employ high-precision astronomical polarity timescales (Cande and Kent, 1992; Berggren et al., 1995b; Shackleton et al., 1995; **Table 3T2**), and a comparison of the revised Cande and Kent (1995) geomagnetic polarity timescale with that of Shackleton et al. (1995) revealed excellent agreement for the 0-5.23 Ma interval and a mean difference of 118 ka between 5.23 and ca. 10 Ma (Kent, 1999). This error margin is significantly less than the duration of the biogenic bloom (up to 5 My; see Dickens and Owen, 1999), so a crude comparison of a few key studies yields a reliable estimate of the timing of this event over a wide geographic area (**Table 3T2**).

From this tabulated summary (**Table 3T2**)**,** three general observations are significant. First, the biogenic bloom is likely to have begun after 9 Ma and terminated by 3.5 Ma. Second, all key studies of the phenomenon suggest that heightened or maximum productivity occurred between 5.5 and 5.0 Ma. And finally, there appears to be no spatial trend in the timing of the biogenic bloom between ocean basins. Similarly, the most comprehensive analysis to date of the global timing of the biogenic bloom concluded that surface production was most intense ca. 6 - 5 Ma (calibrated to the timescale of Shackleton et al. [1995]) and was demonstrably elevated between 9.0 - 3.5 Ma and 8.5 - 3.5 Ma in the Indian and Pacific Oceans, respectively (Dickens and Owen,1999). These dates are based on revised ages for polarity chron boundaries and nannofossil events at 16 ODP sites in the Indian and Pacific Oceans (Dickens and Owen,1999; their table 1). To conclude, maximum productivity probably lasted for about 0.5 – 1 My within the latest Miocene–earliest Pliocene, and overall there was a

prolonged period of higher-than-average productivity that lasted ~5 My. All ocean basins experienced the biogenic bloom contemporaneously, although further relevant studies in the Atlantic Ocean would provide a more thorough global context for comparisons.

3.4 Possible causes of increased primary productivity

Primary production in the oceans is controlled by a complex combination of physical (e.g., light, temperature), biological (e.g., growth rate), and chemical (e.g., availability of nutrients) variables. In most marine environments, the limiting factor is the availability of nutrients (Neinhuis, 1981), and these are usually considered to be nitrate, phosphate and silicate (Parsons, 1975). Phytoplankton growth may also be limited by iron availability (Martin et al., 1994; Coale et al., 1996). Oceanic residence times for these elements are ~10^2-10^5 years (see Chester, 1990); on timescales longer than this, nutrient inputs to and outputs from the global ocean should therefore be balanced. Palaeoceanographic records imply that the "biogenic bloom" phenomenon lasted up to 5 My or more (see previous section), so it follows that maintaining enhanced primary production over a period of such length requires an elevated nutrient supply over a similar duration (Farrell et al., 1995a; Dickens and Owen, 1999). Fundamentally, there are two processes which can achieve this: (1) an increase in the net flux of nutrients to the global ocean from an external source, or (2) a redistribution of nutrients in the global ocean, such that surface waters of some areas become nutrient-enriched at the expense of other areas. A similar distinction between "external" and "internal" causal mechanisms was recognised in studies of the Chron C3Ar carbon shift, and these two categories will now be used to group the possible causes of the biogenic bloom.

3.4.1 External nutrient inputs

Enhanced continental weathering

On a global scale, the main pathways by which material is brought to the ocean are river run-off, atmospheric deposition, and hydrothermal activity (Chester, 1990). The most significant of these sources in the supply of major nutrients (N, P, Si) to the ocean is the riverine flux derived from continental weathering. Some authors have

therefore proposed that the biogenic bloom was caused by increased nutrient inputs to the ocean as a result of enhanced continental weathering (Delaney and Filippelli, 1994; Filippelli, 1997; Hermoyian and Owen, 2001). Changes in continental weathering over geologic time are commonly approximated from records of $^{87}Sr/^{86}Sr$ in marine carbonates (Elderfield, 1986; Hess et al., 1986; Hodell et al., 1989, amongst others). Such records reflect changes in the strontium isotopic composition of seawater over time, and this in turn provides information about the geochemical cycling of Sr in the ocean. The major processes involved in the mass balance of Sr in the ocean are continental weathering, hydrothermal circulation at mid-ocean ridges, and dissolution of marine carbonates (Brass, 1976; Palmer and Elderfield, 1985). Records of marine $^{87}Sr/^{86}Sr$ for the late Neogene reveal a sharp increase from ~6 to 5 Ma, and this has been interpreted as an increase in the dissolved riverine flux of Sr to the ocean following enhanced continental weathering (Hodell et al., 1989; Farrell et al., 1995b).

Three more lines of evidence suggest that continental weathering (and hence riverine fluxes) increased during the late Miocene and early Pliocene (Hodell et al., 1989; Delaney and Filippelli, 1994). First, uplift of the Himalayas, Andes, and Tibetan Plateau intensified during the late Neogene and can be linked to the onset of monsoonal circulation and enhanced terrigenous sediment fluxes to the oceans (Raymo et al., 1988; Kroon et al, 1991; Edmond, 1992; Raymo and Ruddiman, 1992; Rea 1992; Richter et al., 1992; Curry et al., 1995). Second, a major cooling episode in the latest Miocene, and consequent ice sheet expansion (e.g., Shackleton and Kennett, 1975; Hodell and Kennett, 1986; Larsen et al., 1994; Kennett, 1995), may have increased the weathering rates of continental basement underlying the ice sheets (Hodell et al., 1989; Miller et al., 1991). Third, a well-documented lowering of sea level during the late Miocene (e.g., Haq et al., 1987; Adams et al., 1977) would have exposed more continental area, leading to increased terrigenous (and therefore nutrient) fluxes to the ocean (Hodell et al., 1989); this scenario is substantiated by records of enhanced terrigenous deposition during the late Miocene (Rea, 1992; Dobson et al., 2001; Vidal et al., 2002).

Quantitative measurements of nutrient inputs

Few studies have attempted to directly quantify nutrient fluxes to the ocean throughout the Cenozoic. However, Delaney and Filippelli (1994) have determined P accumulation rates in the WEP and EEP for the past 18 My, and have interpreted the results in concert with P mass balance models and proxy records of weathering fluxes.

They observed a substantial peak in P accumulation rates in all records between 9 and 3 Ma, with the maximum centred at 6-5 Ma (ages corrected to Shackleton et al. [1995]). A similar peak was previously observed in Pacific sediments by Moody et al. (1988). This pulse could represent a net increase in the supply of P to the global ocean (Delaney and Filippelli, 1994); if so, sediments underlying more oligotrophic regions would also record a peak in P accumulation rates over the same period. Hermoyian and Owen (2001) calculated PMARs for the late Neogene at sites beneath the central Indian Ocean gyre. Their reported increase in P accumulation at ~5 Ma (using the timescale of Berggren et al., 1995b) was interpreted as evidence of globally enhanced nutrient fluxes to the world oceans at that time. This finding corroborates Wright and Miller's (1996) conclusion that mean nutrient concentrations in the ocean were higher during the latest Miocene-earliest Pliocene, based on oceanic contrasts in benthic foraminiferan $\delta^{13}C$ values.

The iron hypothesis

A final consideration in the argument for a net increase in nutrient inputs is that an inadequate supply of iron can limit primary production in some regions of the ocean, and therefore past fluctuations in the deposition of iron-bearing dust may have driven large changes in productivity (Martin et al., 1994; Coale et al., 1996). None of the investigations into the biogenic bloom have suggested this causal mechanism, yet it is pertinent to note that sediment records from the EEP show an increase in aeolian deposition coincident with peak opal MARs in the latest Miocene and earliest Pliocene (Hovan, 1995). Furthermore, Wells et al. (1999) suggested that increased iron concentrations in the source waters of the upwelling Equatorial Undercurrent (EUC), combined with climate forcing, influenced primary productivity in the EEP during the latest Miocene and earliest Pliocene. These authors based their "increased iron" argument on evidence of intensified tectonic activity in Papua New Guinea between ~8 and 3 Ma (Hill and Gleadow, 1989; Abbott, 1995; Musgrave, 1990), which in turn led to Fe-enrichment of the EUC by erosional and diffusive processes. The localised nature of this productivity-driving mechanism does not account for the wide geographic extent of the biogenic bloom, yet the feasibility of similar scenarios in other locations remains to be investigated.

Evidence against the 'nutrient inputs' theory

Although there is substantial evidence for an increase in the net supply of nutrients to the ocean during the late Neogene, some authors have disputed this mechanism as the sole cause of the biogenic bloom because key sediment records are off-set in time (Rea et al., 1995; Dickens and Owen, 1997, 1999). For example, records of $^{87}Sr/^{86}Sr$ and terrigenous deposition are highest ~3.5 Ma, implying that continental weathering peaked after the biogenic bloom interval (Dickens and Owen, 1999). These authors also questioned the resolution of Filippelli's (1997) chronological correlation between records of monsoon-related processes and export production at the time of the biogenic bloom. And Rea et al. (1995) noted that a significant increase in the terrigenous and aeolian flux to the North Pacific at 2.6 Ma corresponds with a decline in palaeoproductivity, concluding that increased primary production during the latest Miocene and early Pliocene was not fertilized by an enhanced external flux of nutrients to this region.

These criticisms of the 'nutrient inputs' theory led to an alternative explanation for the biogenic bloom: late Neogene ocean circulation changes caused nutrients to be redistributed within the ocean basins, resulting in concommitent increases and decreases in biological productivity in nutrient-enriched and depleted regions, respectively (e.g., Peterson et al., 1992; Rea et al., 1995; Dickens and Owen, 1996, 1997, 1999; see below).

3.4.2 Nutrient redistribution

In general, present-day nutrient distributions in the oceans reflect two processes: (1) deepwater circulation patterns – an aging of deep water masses from the Atlantic to the Pacific, with corresponding increases in dissolved N, P, and Si concentrations (Broecker and Peng, 1982), and (2) vertical mixing within the water column, which determines the depth and gradient of the subsurface nutricline (Parsons et al., 1984). The main pathway by which these nutrients reach the euphotic zone, where they drive primary production, is by the upwelling of deeper water masses (Parsons et al., 1984), and as a result present-day biological productivity and opal accumulation are highest where upwelling is most intense (see Summerhayes et al., 1992). It follows that past changes in deepwater circulation or vertical mixing should cause variations in

palaeoproductivity via changes in the nutrient content or dynamics of upwelling water (e.g., Lyle and Pisias, 1990).

Deepwater circulation

A dramatic rise in carbonate accumulation in the Indian ocean during the latest Miocene was interpreted as an increase in palaeoproductivity in reponse to the development of modern deepwater circulation patterns (Peterson and Backman, 1990; Peterson et al., 1992). Similarly, Berger et al. (1993) and Rea et al. (1995) linked the late Miocene-early Pliocene interval of enhanced productivity in the West Equatorial and North Pacific, respectively, to North Atlantic Deepwater (NADW) formation, which drove the upwelling of nutrient-enriched deepwaters at the end of the global conveyor. Palaeocirculation reconstructions indicate that NADW formation and the modern deepwater 'conveyor' were established in the latest Miocene-earliest Pliocene, and both were probably more intense during this time interval relative to today (Raymo et al., 1996; Wright and Miller, 1996; Billups et al., 1997; Kwiek and Ravelo, 1999). The early Pliocene climate was anomalously warm (e.g., Ciesielski and Weaver, 1974; Hodell and Warnke, 1991; Billups, 2002), and high latitude warmth has been positively correlated with an acceleration of the deepwater conveyor and increased rates of upwelling at Indo-Pacific divergence zones (Rind and Chandler, 1991; Haug et al., 1995; Maslin et al., 1996). These observations support Dickens and Owen's (1996) conclusion that elevated productivity in the North Pacific during the early Pliocene was a result of accelerated deepwater flow, which brought a greater flux of nutrients to divergence zones at the expense of other oceanic areas.

Surface and atmospheric circulation

The geographic distribution of divergence (upwelling) zones in the world's oceans is determined by coupled surface water and atmospheric circulation, and upwelling rates intensify with increasing windstress on the sea surface (Pinet, 1992). It has therefore been suggested that the deposition of pennate diatom oozes in the Pacific during the latest Miocene and early Pliocene represents increased upwelling at the Polar Front and in the EEP in response to stronger zonal winds (Kemp et al., 1995; Dickens and Owen, 1996, 1999; Dickens and Barron, 1997). Pacific sediment records of past aeolian inputs and grain size variations imply that windstress at both low and high latitudes was significantly stronger over this key time interval (Stein and Robert, 1986;

Hovan; 1995), and several previous studies linked opal accumulation on the seafloor to the position and strength of divergence zones in the overlying surface waters (e.g., Brewster, 1980; Pisias and Leinen, 1984; Leinen et al., 1986; Lyle et al., 1988; Froelich et al., 1991; Rea et al, 1995). In particular, Leinen (1979) specified that upwelling associated with equatorial surface circulation was probably the main control on siliceous productivity in the equatorial Pacific throughout the Cenozoic.

Beyond the Pacific, an increase in the abundance of *Globigerina bulloides* in the Arabian Sea in the late Miocene has been attributed to an intensification of monsoon-driven upwelling (Kroon et al., 1991), in agreement with models of the onset of monsoonal circulation ca. 7 Ma (Prell and Kutzbach, 1992; Molnar et al., 1993). This inferred change in atmospheric circulation is also supported by records of climate change from the Indian subcontinent. For example, palaeosol $\delta^{13}C$ increases substantially ca. 7 Ma, reflecting a climate-driven turnover from C_3 to C_4 grasses (Quade et al., 1989; 1995).

The above sections show that elevated productivity during the late Miocene and early Pliocene could have been caused by increased nutrient fluxes to divergence zones resulting from changes in surface or deepwater circulation. A likely trigger for global circulation change during this period is an alteration of the physical dimensions of major inter-oceanic gateways, and many studies have attributed variations in palaeoproductivity directly to these events (see below).

Late Neogene seaways, circulation change, and palaeoproductivity

A significant influence on global circulation patterns (and hence nutrient distributions) is the opening and closure of major 'gateways' between ocean basins (see Hay, 1996), and such movements occured throughout the late Neogene. One of the most significant gateways with respect to Cenozoic history is the Central American Passage. Many studies have attempted to reconstruct the closure of the Panamanian seaway (e.g., Keigwin, 1982a; Keller et al, 1989), and there is a general consensus that circulation between the Atlantic and Pacific Oceans became progressivly restricted between about 13 and 2 Ma (see Farrell et al., 1995a). Comparisons of stable carbon and oxygen isotopes in late Neogene foraminifera shells from the Caribbean and EEP regions indicate that modern-day thermohaline circulation patterns were established at about 4 Ma (Keigwin, 1982; Haug et al., 2001), and this coincides with a distinct and permanent

shift in opal MARs in the EEP (Farrell et al., 1995a). These authors concluded that spatial patterns in productivity may be causally linked to circulation changes resulting from the Panamanian seaway closure.

In the western Pacific Ocean, the Indonesian seaway has become gradually restricted since ~20 Ma (Hamilton, 1979; Dercourt et al., 1992). Kennett et al. (1985) suggested that the closing of this passage resulted in a strengthening of the equatorial undercurrent and of the Kuroshio current, and a general intensification of the gyral circulation in both the North and South Pacific. There is also evidence that the closure of this gateway ca. 3-4 My dramatically altered flow between the Indian and Pacific oceans, which in turn affected the African - and possibly global - climate (Cane and Molnar, 2001). It follows that the strength and location of divergence zones (and hence nutrient availability) in the Indo-Pacific region would be affected by such circulation changes.

Finally, two smaller but significant seaways which also underwent tectonic change in the late Neogene are the Bering and Atlas-Iberian straits (see Hay, 1996). The Bering Strait probably formed ca. 5-3.2 Ma (Pollitz, 1986; Mudie et al., 1990), resulting in a restriction of circulation between the Pacific and Arctic oceans, and closure of the Atlas-Iberian seaway in the Messinian epoch (ca. 7-5.2 Ma, based on the timescale of Berggren et al. [1995b]) effectively isolated the Mediterranean Sea from the Atlantic Ocean (Hsü et al., 1973; 1978). The latter event has been associated with dessication of the Mediterranean basins (the "Messinian Salinity Crisis") and a significant reduction in the contribution of Mediterranean outflow to NADW circulation (Blanc and Duplessy, 1982), possibly affecting primary productivity in the Indian Ocean as a consequence (Gupta and Thomas, 1999; see also **section 3.3.3** 'Dual delivery mechanism').

Evidence against 'nutrient redistribution' theory

Although there are convincing arguments for circulation change as a trigger of the biogenic bloom, some palaeoceanographic records are inconsistent with this hypothesis (Dickens and Owen, 1999; Diester-Hass et al., 2004). For example, deepwater nutrient concentrations in the WEP (as proxied by the difference in $\delta^{13}C$ between planktonic and benthic foraminifera) do not decrease in concert with sedimentation rate in post-Miocene time (Berger et al., 1993). Likewise, a suite of palaeoproductivity proxies from the EEP do not show a close temporal link with reconstructions of NADW flow (Farrell et al., 1995a), based on a reduction of NADW

formation between 7.8 and 6.3 Ma (Wright et al., 1991) and a strengthened flow between 6.4 and 5.9 Ma (Bohrmann et al., 1990). Finally, the observation of peak PMARs ca. 4-5.5 Ma (based on the Berggren et al. [1995b] timescale) in sediment cores from low-productivity regions of the Atlantic and Indian oceans implies that the biogenic bloom was not caused by nutrients being funneled out of the Atlantic (Hermoyian and Owen, 2001).

In summary, there is evidence for a net increase in global nutrient concentrations and a reorganisation of nutrient distributions within the ocean basins during the late Miocene and early Pliocene. There is also evidence which counters both of these interpretations. Some studies have therefore surmised that more than one mode of nutrient delivery may have driven the biogenic bloom (Berger et al., 1993; Farrell et al., 1995a; Dickens and Barron, 1997; Dickens and Owen, 1999; Gupta and Thomas, 1999; Diester-Haass et al., 2002, 2004).

3.4.3 Dual delivery mechanism

Two studies have explicitly invoked a dual causal mechansim for the biogenic bloom. Gupta and Thomas (1999) attributed its manifestation in the Indian ocean primarily to an increase in external nutrient inputs following the development of the Indian monsoon, but also to a redistribution of nutrients within the water column caused by reduced deepwater ventilation. These authors concluded that the flow of NADW – a major contributor to North Indian Deep Water (NIDW; e.g., Schmitz, 1995) – probably diminished in the late Miocene owing to isolation of the Mediterranean basin from the North Atlantic, and this resulted in poorly-ventilated NIDW. Deeper waters consequently accumulated more nutrients via suppressed oxidative decomposition of organic matter, thus fuelling greater primary production when they upwelled. Diester-Haass et al. (2002, 2004) also invoked the onset of the Indian monsoon as a potential cause of the biogenic bloom in the southeast Atlantic: as an amplifier of external nutrient fluxes to the ocean via continental weathering, and as a means of nutrient redistribution via the effects of zonal wind patterns on the dynamics of upwelling systems. These authors additionally proposed that expansion of Antarctic ice (Shackleton and Kennett, 1975; Hodell et al., 1994, 2002) and initiation of northern hemisphere ice caps at 7 Ma (Larsen et al., 1994) would have increased the pole-equator

temperature gradient, thus intensifying atmospheric and oceanic zonal circulation, increasing vertical mixing of dissolved nutrients, and therefore increasing new production in surface waters.

These dual-mechanism hypotheses imply that the biogenic bloom was caused by a combination of local and global processes. Not all investigators of the biogenic bloom have proposed a specific forcing mechanism, but there is general agreement that the phenomenon is associated with global-scale processes (Berger et al., 1993; Farrell et al., 1995a; Dickens and Owen, 1999; Diester-Haass et al., 2002, 2004).

3.5 Summary

The biogenic bloom was defined by Farrell et al. (1995a) as a substantial increase in primary productivity at Indo-Pacific divergence zones during the latest Miocene and earliest Pliocene. A comparison of studies pertinent to this hypothesis indicates that the phenomenon probably occurred at divergence zones in the Atlantic and Southern oceans too, broadly encompasing the period from 9 to 3.5 Ma and centred at 5.5-5 Ma. The heightened productivity could have been caused by an increased external flux of nutrients to the global ocean, a redistribution of nutrients within it, or a combination of both mechanisms; there is evidence to support all three scenarios. Despite some regional differences in key palaeoceanographic records, all have been linked to global-scale processes. It is likely, therefore, that global nutrient and biogeochemical cycling changed dramatically ca. 5.5-5 Ma.

4 The New Zealand region of the Southwest Pacific

4.1 Present-day oceanography

The waters around New Zealand are situated in one of the most diverse and interconnected regions of the world's oceans, owing to the confluence of major, basin-wide subtropical and subantarctic currents (e.g., Warren, 1970; Stanton, 1979, 1981; Heath, 1985; Tilburg et al., 2001). The major surface features of this region are the East Australian Current (EAC), the Tasman Front (TF), the East Auckland Current (EAUC), the East Cape Current (ECC), the Southland Current (SC), and the Subtropical Convergence (STC) (**Fig. 4F1**). Issuing from the South Equatorial Current (SEC), the EAC is the western boundary current of the South Pacific subtropical gyre (Tilburg et al., 2001). This current connects with the EAUC and the ECC northeast of New Zealand by the TF, an eastward "zonal jet" between 152º and 173º E (Warren, 1970). The separation of the ECC off the eastern coast of New Zealand and its confluence with the eastward-flowing SC marks the STC zone, and the merger of these two currents forms the South Pacific Current (Stramma et al., 1995).

The physical and biological characteristics of the two frontal zones pertinent to this study, the TF and the STC, will now be described in more detail. First, however, it is appropriate to mention some properties of the EAC given that it dominates the present surface circulation in the Tasman Sea (see below).

4.1.1 The East Australian Current

The EAC is a western boundary current flowing southward off the east coast of Australia (Marchesiello and Middleton, 2000) **(Fig. 4F1).** It is fed by the SEC, which bifurcates at the Australian coast near 18°S; the resulting southward flow varies between 22 and 42 Sv (see Tilberg et al., 2001, and references therein) although it measures ~29 Sv for most of the year (Sokolov and Rintoul, 2000). This narrow, swift, and highly variable current is centered at 40 km from the coast, has strong shear in the upper 1000 m, and mean velocities are 0.6 m/s in the core (Mata et al., 2000). Chiswell et al. (1997) observed considerable eddy energy in the EAC system, supporting Boland

and Hamon's (1970) description of a permanent, extended eddy field off the east coast of Australia.

At ~30°S the EAC separates from the coast: about 40 % of the total geostrophic transport continues east as a meandering jet across the Tasman Sea (the Tasman Front) whilst the remainder recirculates north and then west (Chiswell et al., 1997; Sokolov and Rintoul, 2000). Most observations of flow in the TF are within the range of 7.6-16.5 Sv (see Tilberg et al., 2001), and the front's oscillation and propagation have been associated with eddy formation - in particular a large warm core eddy in the western Tasman Sea (Marchesiello and Middleton, 2000).

Clearly, the strength and position of the EAC will affect the dynamics of the Tasman Front. Interannual variability of the EAC, however, is insignificant relative to the seasonal cycle (Chiswell et al., 1997). Furthermore, Godfrey et al. (1980) found that although the exact separation point of the EAC from the Australian coast varies seasonally, it is generally centred at 32.5°S.

4.1.2 The Tasman Front

Several investigators have described the physical oceanography of the TF (e.g., Warren, 1970; Stanton, 1979, 1981; Andrews et al., 1980; Heath, 1985; Mulhearn, 1987; Sokolov and Rintoul, 2000; Tilburg et al., 2001). These studies support the notion that the TF is a meandering, eastward flowing arm of a South Pacific gyre, characterised by an abrupt change in sea surface temperature (SST) and salinity (Heath, 1985). Levitus (1982) summarised a comprehensive global dataset of oceanographic measurements that were averaged on 5° latitude-longitude grids. In the vicinity of the TF, winter and summer SSTs are 18-20°C and 22-24°C, respectively. Referring to this dataset, Martínez (1994) observed that maximum seasonal fluctuations in the upper water column were concentrated along the TF, and that the thermocline structure during summer was relatively shallow (~100 m) between 15°S and 45°S. In winter, the base of the thermocline extends to approximately 200m between 20°S and ~40°S owing to mixing in the upper water column along the TF (Levitus, 1982).

A two and a half year analysis of the TF position using satellite imagery (Mulhearn, 1987) has shown that it migrates between 30 and 38ºS, but lies between 31 and 32.5ºS for over half of the year. These observations support earlier studies (Stanton,

1979, 1981) which described the front meandering east-west over the Lord Howe Rise (LHR) between 30 and 35°S. Mulhearn linked latitudinal variability of the TF to the EAC system and the activities of the associated eddy field. These eddies are permanent features of the flow field and have a deep structure that extends from the sea surface to abyssal depths (Mulhearn, 1983; Mulhearn et al., 1986; Lilley et al., 1986).

The hydrodynamics of the TF have been linked to biological production. Scott (1981) analysed phytoplankton fluorescence in the vicinity of a large-scale eddy in the Tasman Sea and found it to be higher in some surface eddies along the front compared with the average measure for the study area. Comiso et al. (1993) reported that there was some seasonal coherence between elevated chlorophyll concentrations (>1 mg/m^3) and the strength of Ekman upwelling in the Tasman Sea. These observations have been substantiated by Behrenfeld and Falkowski (1997), who estimated annual phytoplankton primary production in the Tasman Sea using satellite chlorophyll data. They concluded that production rates in the vicinity of the TF (and STC) were higher than those in non-frontal areas. Quantitative measurements of primary production within the TF are lacking; it is likely, however, that rates are greater than 50 gCarbon/ m^2/year, which is the average rate of primary production for the majority of oceanic waters (Pinet, 1992).

4.1.3 The Subtropical Convergence

East of New Zealand, the physical and biological properties of the Subtropical Convergence (STC), and of offshore waters in general, have been widely studied (e.g., Heath, 1985; Currie and Hunter, 1998; Chiswell, 2001; Murphy et al., 2001; and references therein). A description of the physical oceanography of the front will therefore be followed by a summary of its main biological characteristics.

Physical oceanography

The STC is one of the world's major circumglobal oceanic fronts, formed by the confluence of subantarctic and subtropical surface waters between ~40 and 50°S, and underlain by Subantarctic Mode Water (SAMW) and Antarctic Intermediate Water (AAIW) at water depths of ~600 to 1500 m (McCartney, 1977; Emery and Meincke, 1986; Tomczak and Godfrey, 1994; **Fig. 4F2**). In the vicinity of New Zealand,

relatively warm (summer >15°C, winter >10°C), saline (35.7-35.8 ‰), nutrient-poor subtropical waters from the north mix with colder (summer <15°C, winter <10°C), less saline (~34.5 ‰), nutrient-rich subantarctic waters from the south (e.g., Heath, 1985; Chiswell, 1994).

The position of the STC is dependent on the strength of the surface currents from which it is sourced, and on seafloor topography (see below). This hydrodynamic-bathymetric coupling is illustrated in **Fig. 4F1**. The TF gives rise to the East Auckland Current (EAUC) as it flows around the tip of the North Island; part of this current continues southwards along the east coast as the East Cape Current (ECC) (Heath, 1985; Stanton et al., 1997). At ~42°S the ECC leaves the coast and follows the northern edge of Chatham Rise, while the southern slopes of the CR deflect the northward flowing Southland Current/Front system (SC, SF) eastwards off the coast of the South Island. The confluence of the ECC and the SC, and the topography of CR, therefore determine the position of the STC east of New Zealand.

It was initially suggested that the STC follows the southern flank of the rise in spring and the northern edge in late summer (Heath, 1985; Chiswell, 1994), but a more recent study concluded that latitudinal movement of the front appears to be more or less constrained by Chatham Rise (Chiswell, 2001). This submarine ridge extends ~800 km eastward from the South Island to ~170°W (Heath, 1985). The ridge crest is generally flat and at water depths of 200-400 m, and its slopes descend to the Hikurangi Plateau to the north and the Bounty Trough to the south (Thompson, 1991).

Biological oceanography

Satellite images and *in situ* measurements (**Table 4T1**) indicate that biological production east of New Zealand is elevated within the STC zone relative to subtropical (STW) and subantarctic (SAW) surface waters (Comiso et al., 1993; Banse and English, 1997; Chang and Gall, 1998; Murphy et al., 2001, and references therein). This trend is consistent with a decrease in dissolved CO_2 in surface waters of the STC compared with SAW (Currie and Hunter, 1998), as a result of greater CO_2 utilisation by a stronger 'biological pump' in the upwelling waters of the STC.

Seasonal measurements of organic cell carbon, chlorophyll *a*, and fluxes of particulate biogenic material in the STC east of New Zealand all show peak values during spring (Howard-Williams et al., 1995; Bradford-Grieve et al., 1997, 1998; Chang

and Gall, 1998; Nodder and Northcote, 2001), but regardless of season the phytoplankton assemblages are dominated by diatoms, whose high abundance is supported by nitrate-rich (NO_3^-, 5-12 μmol/l) waters over the Chatham Rise (Chang and Gall, 1998). Low concentrations of dissolved reactive silicate (DRSi) in these waters and the build-up of diatoms in spring implies DRSi limitation (Chang and Gall, 1998). These observations agree with Zentara and Kamykowski's (1981) findings of "excess" NO_3^- and "impoverished" DRSi in SAW of the southwest Pacific, although Broekhuizen et al. (1998) concluded that the spring diatom bloom in STW to the east of New Zealand is terminated by N rather than Si limitation, according to ecological models of photoadaptation.

4.2 Drill site locations

Three sites in the southwest Pacific were chosen for my study: Deep Sea Drilling Project (DSDP) sites 590 and 594, and ODP site 1125 (**Fig. 4F1, Table 4T2**). Site 590, the most northerly location, was drilled on the Lord Howe Rise and underlies the TF. Sites 594 and 1125, however, are located on Chatham Rise. Site 1125 lies on the northern flank, well within the STC zone, whereas Site 594 lies on the southern slope, just outside the STC. In this frontal zone, subantarctic and subtropical surface waters mix when the east-flowing East Cape Current (ECC) from the north meets the east-flowing Southland Current (SC) from the south (Heath, 1985).

Sites 590 and 1125 were chosen because of their location beneath obvious frontal boundaries, and because there is preliminary evidence at both sites for the biogenic bloom (Kennett et al., 1986; Carter et al., 1999). Site 594 was chosen to contrast with the former sites, being located on the southern, cold-water side of the STC, as manifest by its distinctly different Linear Sedimentation Rates (LSRs) during the late Miocene-early Pliocene (Kennett et al., 1986). In addition, sites 594 and 1125 create a latitudinal transect across the STC; analyses of palaeoproductivity at these locations may indicate whether there was any movement of the frontal zone coinciding with the biogenic bloom. Importantly, all three sites lie at a similar water depth (~1.3 km; **Table 4T2**). This is well above the present-day CCD in the Southwest Pacific (~3.5-4.5 km, see Berger and Winterer, 1974), so downcore records should be minimally affected by dissolution. Furthermore, any depth-dependent changes to bulk sediment chemistry should be consistent across the three sites.

4.3 Palaeoceanography: The Tasman Front and Subtropical Convergence in the late Neogene

Changes in atmospheric circulation and in the dynamics of surface currents over geologic time may affect the manifestation or position of oceanic fronts over similar periods. It follows that drill sites located beneath present-day frontal/upwelling regions may have been overlaid by less dynamic, more oligotrophic surface waters at certain times in the past. Similarly, tectonic movements may alter the position of the seafloor relative to surface water features (cf. Pisias et al., 1995). It is therefore crucial to establish the potential effect of either scenario on sediment cores, particularly when these records are explicitly being investigated in the context of palaeoceanographic change at ocean fronts.

The Tasman Front may have migrated several degrees north during Pleistocene glacial intervals (Martínez, 1994; Kawagata, 2001). These authors ascribed changes in planktic foraminiferan assemblages to latitudinal shifts of subtropical and subantarctic water masses. Using a similar approach, combined with $\delta^{18}O$ analyses, Wei (1997) concluded that the TF shifted south at 4.4 Ma (based on the timescale of Berggren et al., 1985), possibly in response to an expanded West Pacific Warm Pool (WPWP). In addition, studies of benthic foraminifera and nannofossil assemblages from Quaternary sediments beneath the present-day STC in the Tasman Sea associate northward shifts of the front with glacial periods (Wells and Connell, 1997; Nees, 1997).

However, the extent of latitudinal variation in the location of these fronts remains debatable. A recent study concluded that northward movement of the TF during glacial times occurred over no more than 3° latitude (Kawahata, 2002), and several studies agree that the STC east of New Zealand shifted little during the last glaciation and remained above Chatham Rise near 43°S (Fenner et al., 1992; Nelson et al., 1993, 1994, 2000; Neil, 1997; Weaver et al., 1998). Nelson and Cooke (2001) reviewed these studies, amongst other data, and concluded that "it is highly likely that the location of the STC east of New Zealand has been relatively constant from the Neogene to the Present". Finally, the average latitudinal position of the STC is strongly influenced by bathymetry, and the latter has been relatively stable in the vicinity of Chatham Rise for at least the past 15 My (Lewis et al., 1985; Wood et al., 1989). The bathymetry of the

Central Tasman Basin has also been relatively stable over the same interval (Hayes and Ringis, 1973; Gaina et al., 1998).

In summary, the position of the TF and the STC during the late Neogene probably compares well with their present location, although the TF probably shifted slightly north-/southwards during cooler/warmer periods, respectively.

PART II

DATA ANALYSES AND SYNTHESES

5 Results from the Tasman Front (DSDP site 590)

5.1 Introduction

A widespread increase in export production – the "biogenic bloom" – and a change in the isotopic composition of water masses – the "Chron C3Ar Carbon Shift" – characterise the latest Miocene-earliest Pliocene time interval. There appears to be some overlap in the timing of these events (see **Chapters 2** and **3**), and both signify a major perturbation in global carbon and nutrient cycling. The two phenomena may therefore be intrinsically related to each other and/or share a common trigger mechanism. Discerning such relationships, however, is not straightforward owing to inconsistencies and offsets within current databases of the biogenic bloom and carbon shift. Furthermore, as previously stated, no study has independently examined past changes in productivity and $\delta^{13}C$ in multiple carbonate phases at the same location.

Deep Sea Drilling Project (DSDP) site 590 (31°10.02′S; 163°21.51′E) lies on the eastern flank of the Lord Howe Rise (**Fig. 4F1**), a topographic high of thinned continental crust in the central Tasman Sea between Australia and New Zealand (Willcox et al., 1980; Auzende et al., 2000). Located at a water depth of 1299 m, this site is bathed by Antarctic Intermediate Water (AAIW) whilst the overlying surface waters form the Tasman Front (TF), a region of eddy-induced mixing. Upper Miocene to lower Pliocene sediments beneath the TF show elevated linear sedimentation rates (LSRs) and a significant drop in the $\delta^{13}C$ of foraminifera (Elmstrom and Kennett, 1986; Kennett, 1986; Nelson, 1986). Thus, sediment at this site may be ideal for investigating the biogenic bloom and Chron C3AR carbon shift together. In this chapter, I supplement previous work beneath the TF with records of export production and $\delta^{13}C$ on multiple carbonate phases. By placing all information on a current and common timescale (Berggren et al., 1995a,b), I document timing relationships between the biogenic bloom and the Chron C3AR carbon shift in the Tasman Sea and then discuss possible explanations for both.

5.2 Previous observations at site 590

Upper Miocene to Holocene sediments at site 590 are dominantly white, foraminifera-bearing nannofossil ooze (Kennett et al., 1986) with carbonate concentrations generally exceeding 90 % (Stein and Robert, 1986). Despite this uniform lithology, sedimentation rates (SRs) appear to have doubled in the late Miocene to early Pliocene (Nelson, 1986). This apparent increase in SRs coincided with a mixing of warm and cool-water planktonic foraminifera assemblages and a drop in the $\delta^{13}C$ gradient between surface and deep-dwelling planktonic foraminifera (Elmstrom and Kennett, 1986). The collective observations may reflect an increase in surface productivity caused by enhanced upwelling (Elmstrom and Kennett, 1986; Kennett and von der Borch, 1986). About 1 to 2 My before these oceanographic changes, planktonic and benthic foraminiferan $\delta^{13}C$ records also decrease by 1.5 and 0.9 ‰, respectively (Kennett, 1986). Thus, initial work at site 590 provides evidence for both the biogenic bloom and the Chron C3AR carbon shift, with a temporal offset between the phenomena.

5.3 Revised age model and sedimentation rates

Numerous nannofossil, foraminifera, and polarity chron events have been identified at site 590 (Jenkins and Srinivasan, 1986; Lohman, 1986; Barton and Bloemendal, 1986). Previous workers (Kennett et al., 1986; Lazarus et al., 1992) have calibrated these datums to the time scale by Berggren et al. (1985), providing a detailed but now inaccurate age model. I assume that all datums have been correctly identified and positioned; I therefore have reassigned their ages (**Table 5T1**; **Fig. 5F1**) to the current and widely used time scale by Berggren et al. (1995a,b).

Typically SRs at a location are determined by fitting lines through age datums to obtain a stepped series of linear sedimentation rates (LSRs) over time (**Fig. 5F1**). Although this approach is convenient, it often leads to artificial LSRs over certain depth intervals, especially where they change significantly. Polynomial fits through age datums provide an alternative means to estimate SRs. I have constructed SR curves at site 590 (**Fig. 5F1**) using both approaches and the revised age datums. With a stepped curve, LSRs increase from 2.7 cm/ky at 11.8 Ma to a maximum of 7.1 cm/ky at 5.3 Ma, remain high until 3.8 Ma, and then drop from 6.6 cm/ky to 3.6 cm/ky (**Fig. 5F1**). Alternatively, with a “best-fit” fourth-order polynomial curve, SRs increase from 3.4 cm/ky at 11.8 Ma to 6.7 cm/ky at 4.9 Ma, and then gradually decline to 1.8 cm/ky at 0.2

Ma (**Fig. 5F1**). Lower Pliocene sediment at site 590 was deposited relatively quickly irrespective of the chosen time scale or age-depth model.

5.4 Samples and Analytical Methods

5.4.1 Preparation

Hole 590B was sampled at ~10 m intervals between 0 and 350 mbsf (cores 1H – 44X) and at ~5 m intervals between 188 and 238 mbsf (cores 21H – 26H). Individual samples are 20 cm^3 sediment "plugs" taken according to standard Ocean Drilling Program (ODP) procedures. Based on my age-depth model (**Fig. 5F1**), these samples are typically about 270 ky apart between 0 and 12 Ma, but about 90 ky apart between 5.6 and 6.6 Ma.

Each sample was split in two. One half was freeze-dried, crushed to a fine powder in a porcelain mortar and pestle, and sub-sampled for whole-rock geochemical analyses. The other half was used to isolate carbonate grains including foraminifera for stable isotope analyses. Sample splits were disaggregated for 5 minutes in 10 % hydrogen peroxide and sieved through 63, 300, 350, and 400 μm teflon meshes with distilled water. These sieved fractions were rinsed with isopropanol and left to dry in air. The fine-grained (<63 μm) fraction was collected in a beaker and allowed to settle for ~24 hours. The beakers were then decanted and the contents were dried in an oven at 60°C for ~24 hours. Six samples of the fine-grained fraction were further separated using a millipore filtration system under suction to obtain a 5 to 25 μm fraction. The purpose of this separation was to isolate nannofossils.

5.4.2 Carbonate

Carbonate concentrations were determined on 49 samples of bulk dry sediment (**Table 5T2**) using the carbonate bomb technique (Müller and Gastner, 1971). Approximately 5 ml of 10 % HCl were reacted in a sealed chamber with 0.2 to 0.3 g of dry, powdered sediment. The volume of gas produced was measured in a graduated burette and converted to carbonate mass using a volume-mass relationship established by analyzing four standards prior to each run of 10 samples. Each sample was analyzed at least twice. Estimated errors in reported carbonate concentration are within 2 % of the measured value.

5.4.3 Major elements and barium

Elemental concentrations were determined in the Advanced Analytical Centre, James Cook University (JCU-AAC) using X-ray fluorescence (XRF) spectrometry. Thirty-two samples of bulk dry sediment (**Table 5T3**) were fused into glass disks using a moldable crucible and analysed for major element oxide concentrations on a Bruker-AXS SRS 3400 spectrometer. Major element concentrations (**Table 5T3**) were obtained through standard comparisons to concentration curves defined by analyses of 20 geological standards. Seven samples of the geological standard "401 MAG3" (a combination of USGS 'MAG-1' and GFS '401') were analysed to evaluate accuracy and precision. Concentrations of all major element oxides were within 1 % of the calculated regression curve and standard deviations were <0.1 %. The sum of all major element oxide concentrations and the loss on ignition (LOI) should be 100 %. For my samples, this sum ranges between 99.6 and 100.3 %. Iron contents are reported as total Fe_2O_3 (Fe_2O_3T) because Fe(II) and Fe(III) were not distinguished.

Barium concentrations were determined using a Siemens SRS-303 XRF spectrometer equipped with an LiF (110) crystal. For each sample, ~4 g of bulk sediment were made into a pressed powdered pellet, and resultant Ba concentrations were determined by standard comparison to predefined concentration curves after correction for Ce interference. Multiple analyses of the MRG-1 (gabbro) and GSD-2 (stream sediment) standards averaged 63 ± 2.7 and 179 ± 8.2 ppm (1σ) compared to certified values of 61 and 185 ppm.

5.4.4 Stable isotopes

Stable isotope compositions of carbonate were determined in the Department of Geology and Geophysics, University of Adelaide, using a Micromass Optima mass spectrometer equipped with an automated on-line carbonate analyser and common orthophosphoric acid bath. Several carbonate components were analysed, including bulk sediment, bulk fine-grained material, bulk 'nannofossil' material, and extracted planktonic foraminifera. In each case, approximately 200-300 μg were analysed.

Isotopes were measured on specific-sized tests of *Orbulina universa* (>350 μm), *Globigerina bulloides* (300-350 μm), and *Globigerinoides sacculifer* (300-400 μm). These three species of planktonic foraminifera were chosen to examine $\delta^{13}C$ variations

between symbiotic and non-symbiotic species and between surface (<10 m) and subsurface (<300 m) waters. *Orbulina universa* hosts photosymbionts and predominantly lives in surface waters; *Gs. sacculifer* hosts photosymbionts but precipitates a final sac-like chamber at depth; *G. bulloides* does not host photosymbionts and is abundant in both surface and subsurface waters (Bé and Tolderlund, 1971; Bé, 1977; Bé et al., 1981). Size fractions were restricted to minimize $\delta^{13}C$ variations associated with test size (e.g., Ravelo and Fairbanks, 1995).

Similar morphotypes of *O. universa* and *G. bulloides* were selected. However, for *Gs. sacculifer*, two morphotypes, 'with sac' (w) and 'without sac' (w/o), were chosen. Mostly G*s. sacculifer* w/o was extracted because this morphotype more accurately records surface water $\delta^{13}C$ (Spero and Lea, 1993).

Sixteen samples of the NBS19 limestone standard were analysed with other samples to evaluate the accuracy and precision of $\delta^{13}C$ measurements. The mean of these analyses was 1.95 ‰ ± 0.05 ‰ (1σ) compared to the consensus value of 1.95 ‰ (Coplen et al., 1983). Five samples from site 590 (**Table 5T4**) were also analysed twice. These replicate analyses were all within 0.1 ‰.

5.4.5 Scanning electron microscopy

Bulk sediment samples from cores 6H and 30X were examined for primary components. Approximately 0.2 g of wet bulk sediment were placed on a 1 cm diameter stub, coated with gold, and analysed using a Philips scanning electron microscope (SEM) at the JCU-AAC.

5.5 Results

5.5.1 Bulk sediment composition

Biogenic $CaCO_3$ dominates upper Neogene sediment at site 590. Carbonate concentrations vary from 87 to 98 % for bulk sediment (**Table 5T2**; **Fig. 5F2**), in agreement with previous work (Stein and Robert, 1986). Moreover, upper Neogene sediment has CaO between 49.7 and 54.3 %, and LOI between 41.4 and 44.2 % (**Table 5T3**). Because pure calcite renders CaO and LOI concentrations of 56 and 44 %, respectively, my XRF results also suggest between 91.3 and 97.6 % $CaCO_3$. Most of

this $CaCO_3$ is comprised of coccoliths between 3 and 10 μm in diameter (**Fig. 5F3**), although foraminifera tests are common.

The non-carbonate fraction at site 590 consists mostly of aluminosilicate clays. After CaO, the most abundant metal oxides are SiO_2 and Al_2O_3 (**Table 5T3**). However, concentrations of both oxides are relatively low (<5.7 and <1.6 %, respectively) and generally covary ($r^2 = 0.95$) with each other (**Fig. 5F2**). The Si/Al ratio in my samples is ~2.7 g/g (**Table 5T3**), which is typical of smectite clays (e.g., Faure, 1998). Indeed, smectites dominate (40-100 %) the non-carbonate fraction of sediment from the Lord Howe Rise (Stein and Robert, 1986). Biogenic Si tests are conspicuously absent.

5.5.2 Carbonate accumulation

Carbonate mass accumulation rates (MARs) provide one record of export production at site 590 because coccoliths dominate bulk carbonate. These MARs were calculated (g/cm^2-ky) for each sample according to:

$$CaCO_3 \text{ MAR} = \text{weight \% } CaCO_3 \times SR \times DBD \text{ ,} \quad \textbf{(Eq. 1)}$$

where SR is the sedimentation rate (cm/ky) taken from age-depth models (**Fig. 5F1**), and DBD is the dry bulk density (g/cm^3). The DBD was estimated from:

$$DBD = (1- \phi/100) \times \rho \text{ ,} \quad \textbf{(Eq. 2)}$$

where ϕ is the wet porosity of sediment, and ρ is the density of sediment particles (**Table 5T2**). Porosity data for my samples were extrapolated from the nearest sample analyzed for physical properties (Morin, 1986). The particle density is approximately 2.7 g/cm^3, given that the sediment is almost entirely carbonate.

Both the stepped and polynomial SR curves were used to calculate $CaCO_3$ MARs (**Fig. 5F4**). With the stepped LSR curve, $CaCO_3$ MARs vary between 3 and 4 g/cm^2-ky older than 9 Ma, 4 and 4.6 g/cm^2-ky between 9 and ~7 Ma, and >5 g/cm^2-ky from ~7 to 3.8 Ma. MARs are highest (~7 g/cm^2-ky) between 5 and 4.3 Ma. Younger than 3.8 Ma, MARs are generally <3 g/cm^2-ky. The polynomial SR curve gives a similar, though smoothed, trend. In this case, $CaCO_3$ MARs average ~3.6 g/cm^2-ky between 12 and 9 Ma, gradually increase to a maximum of 6.7 g/cm^2-ky at 4.9 Ma, and gradually decrease to a minimum of 1.5 g/cm^2-ky at 0.2 Ma. Carbonate MARs were anomalously high at site 590 in the earliest Pliocene.

As stressed by several authors (e.g., Dickens and Owen, 1994; Farrell et al., 1995; Filippelli and Delaney, 1995; Murray et al., 1995), calculated MARs effectively mimic the SR curve in uniform sediment sections with similar physical properties, such as site 590. Incorrect SR curves (e.g., through poorly placed age datums) will therefore lead to inaccurate MARs. This potential problem can be evaluated by normalising the component of interest to one with a different sedimentary behaviour (e.g., Murray et al., 1993; Dickens and Owen, 1994). In the case of $CaCO_3$ or other biological proxies, Ti is an ideal normalising element because, in many open-ocean environments, Ti is dominantly hosted in aluminosilicate phases, added through aeolian processes, and generally immobile after deposition (Goldberg and Arrhenius, 1958; Murray et al., 1993; Murray and Leinen, 1996). At site 590, Ca/Ti ratios are <2200 g/g between 10.8 and 9 Ma, increase to >3200 g/g by 8.3 Ma, and then oscillate between 6600 and 2000 g/g until 6.2 Ma. A peak in Ca/Ti of 3350 g/g, occurring between 6.2 and 5.3 Ma, is followed by an overall decline until 0.5 Ma. Both the $CaCO_3$ MARs and Ca/Ti ratios are elevated in the latest Miocene, although peak $CaCO_3$ MARs occur in the earliest Pliocene when Ca/Ti ratios are relatively low (**Fig. 5F4**).

5.5.3 Barium and aluminium deposition

Barium and Al records probably also track past changes in export production at site 590. Marine barite ($BaSO_4$) forms in microenvironments when organic matter decomposes in the water column following uptake of dissolved Ba^{2+} (Dehairs et al., 1980; Bishop, 1988). As a consequence, Ba fluxes to the seafloor can relate to surface productivity, especially in pelagic sediments dominated by biogenic components (e.g., Goldberg and Arrhenius, 1958; Chow and Goldberg, 1960; Dymond, 1981; Dymond et al., 1992; Dickens and Owen, 1996; Schroeder et al., 1997). Dissolved Al^{3+} is scavenged from seawater by biogenic particles (Orians and Bruland, 1986; Moran and Moore, 1988a,b; Murray et al., 1993). Although aluminosilicate accumulation dominates the total Al flux to the seafloor in many environments, the scavenged component may comprise a significant portion in locations with low total Al (Murray et al., 1993; Murray and Leinen, 1996).

The accumulation of Ba and Al with respect to Ti generally declines from the late Miocene to the Pleistocene (**Fig. 5F4**). The Ba/Ti ratio varies between 0.5 and 1.4 g/g from 10.8 to 6.5 Ma, peaking at 6.5 Ma. Afterwards, Ba/Ti ratios are <0.7 g/g, decreasing to 0.2 g/g at 0.5 Ma. The Al/Ti ratio varies between 15 and 36 g/g from 10.8

to 6.5 Ma, and then drops to between 13 and 23 g/g from 6.5 to 0.5 Ma. Downcore trends in both records covary to a certain extent (r^2 = 0.54) with changes in the Ca/Ti record (**Fig. 5F4**).

5.5.4 Stable carbon isotopes

All $\delta^{13}C$ records of carbonate at site 590 display a significant decrease in upper Miocene-lower Pliocene sediment. However, the magnitude and timing of this shift depends on the phase analysed.

Bulk sediment $\delta^{13}C$ ranges between –0.85 and +1.66 ‰, with an overall decline over the past 12 My (**Table 5T5**; **Fig. 5F5**). Except for low values (~0.5 ‰) between 10.2 and 9.5 Ma, $\delta^{13}C$ is relatively high (>0.9 ‰) until about 5 Ma, reaching a maximum of 1.66 ‰ at 5.6 Ma. The minimum $\delta^{13}C$ of bulk sediment occurs at 0.2 Ma after a minor high between 1.5 and 0.5 Ma. Most of the decline in bulk sediment $\delta^{13}C$ (-1.96 ‰) thus occurs between 5.6 and 1.9 Ma. Although the $\delta^{13}C$ of fine-grained and 'nannofossil' material usually exceeds that of bulk sediment, $\delta^{13}C$ varies <0.29 ‰ in any sample analysed for all three components (**Table 5T4**). Thus, as might be expected for coccolith-rich sediment, the $\delta^{13}C$ of bulk sediment at site 590 effectively records the $\delta^{13}C$ of $CaCO_3$ tests from surface waters.

Similar to bulk sediment, the $\delta^{13}C$ of surface-dwelling planktonic foraminifera decreases over the last 12 My. Previous stable isotope work at site 590 (Elmstrom and Kennett, 1986) investigated the $\delta^{13}C$ of *Gs. sacculifer* but did not distinguish between morphotypes. My $\delta^{13}C$ records of *Gs. sacculifer* w and w/o are similar to each other. Moreover, there is no significant difference between the $\delta^{13}C$ records of *Gs. sacculifer* (w, w/o, and mix) and *O. universa*. I therefore discuss all surface-dwelling planktonic foraminiferan records together (**Fig. 5F5**).

The $\delta^{13}C$ of *Gs. sacculifer* and *O. universa* ranges between 0.72 and 2.67 ‰, a range slightly less and about 1 ‰ heavier than for bulk sediment $\delta^{13}C$. Between 11.8 and 8.3 Ma, $\delta^{13}C$ decreases temporarily. At about 8 Ma the record peaks; $\delta^{13}C$ values then fall by nearly 1 ‰ over 0.5 to 1.5 My, depending on which record is examined (**Fig. 5F5**). Thus, the timing of the pronounced shift in the $\delta^{13}C$ of surface-dwelling planktonic foraminifera occurs between 7.8 and 6.4 Ma at site 590, or 0.8 My before

that in bulk sediment. The $\delta^{13}C$ record subsequently shows high-amplitude (1.64 ‰) fluctuations between 6.3 and 5.0 Ma, and relatively constant, lower values afterwards.

The $\delta^{13}C$ record of *G. bulloides* (**Fig. 5F5**) only begins at 6.5 Ma. Its range (–1.10 to 0.49 ‰) is lower than that of bulk carbonate and surface-dwelling planktonic foraminifera, as expected for a planktonic species commonly found in subsurface water. However, the overall trend of this $\delta^{13}C$ record is different from that of surface-dwelling planktonic foraminifera but somewhat similar to that of bulk carbonate.

A benthic foraminiferan $\delta^{13}C$ record has been constructed at site 590 using tests of *C. kullenbergi* (Elmstrom and Kennett, 1986) (**Fig. 5F5**). This record has been discussed previously (Elmstrom and Kennett, 1986; Kennett, 1986), although with a different timescale (Berggren et al., 1985). Using a revised timescale, the $\delta^{13}C$ drops temporarily between 10.8 Ma and 9.3 Ma, reaches a maximum at 8.7 Ma, then declines towards 6.7 Ma. Despite a slight increase ca. 5 Ma, $\delta^{13}C$ values remain relatively low for the remainder of the record.

5.6 Discussion

5.6.1 The timing of enhanced productivity

Bulk sediment carbonate MARs, Ba/Ti ratios, and Al/Ti ratios at site 590 were 2 to 3 times higher during the latest Miocene and earliest Pliocene relative to previous and subsequent time intervals (**Fig. 5F4**). Similar observations have been made at other sites beneath upwelling regions of the Indian and Pacific oceans (e.g., Van Andel et al., 1975; Kennett et al., 1986; Peterson et al., 1992; Berger et al., 1993; Farrell et al., 1995; Dickens and Owen, 1999). Records of $CaCO_3$, Ba, opal, and organic carbon accumulation at ODP site 850 in the eastern Equatorial Pacific (Schroeder et al., 1997) are especially pertinent for comparison. Between 9.0 and 4.0 Ma, on the Berggren et al. (1995a,b) timescale, all of these records show extremely variable accumulation, with rates typically 2 to 3 times higher than during previous and subsequent time intervals. Following other work (e.g., Farrell et al., 1995; Filippelli and Delaney, 1995), Schroeder et al. (1997) linked these elevated late Miocene-early Pliocene biogenic accumulation rates to elevated productivity in the overlying equatorial Pacific surface waters and the “biogenic bloom” phenomenon. The same general explanation is offered for changes in sediment composition at site 590. My records indicate that the biogenic

bloom occurred at the TF between ca. 9 and 3.8 Ma. This is broadly coincident with the timing of enhanced productivity at other upwelling regions in the Indian and Pacific Oceans (Dickens and Owen, 1999).

There is a distinct offset between the timing of maximum $CaCO_3$ MARs and maximum Ca/Ti, Ba/Ti and Al/Ti ratios at site 590. Carbonate MARs are highest between 6 and 4 Ma, whereas the elemental ratios are highest between 9.0 and 6.5 Ma. A similar temporal offset has been documented (although not explained) at ODP site 850 where $CaCO_3$ and Ba MARs are highest between 7 and 5 Ma but Ba/Ti ratios are highest between 9 and 7 Ma (Schroeder et al., 1997) (**Fig. 5F4**). Temporal offsets between productivity proxies during the biogenic bloom interval have been discussed in the literature (Dickens and Owen, 1999). However, these discrepancies were between palaeoproductivity records from different sites and could be explained by lateral movements of elevated surface productivity regions over time (Dickens and Owen, 1999). Disparities between $CaCO_3$ MARs and elemental ratios at the same location must have a different explanation, such as misplaced age datums, variable elemental fluxes, carbonate dissolution, or a change in the carbonate flux relative to the organic carbon flux. The two latter explanations can be excluded because $CaCO_3$ MAR and Ca/Ti variations are temporally offset (**Fig. 5F4**). Either the age model is wrong or the Ti flux changed over time.

Misplaced depths of biostratigraphic datums would lead to erroneous SRs and incorrect MARs. The key datums used to determine SRs in upper Miocene and lower Pliocene sediment at site 590 are the FADs of *Amaurolithus primus* and *Ceratolithus rugosus*, and the LAD of *Reticulofenestra pseudoumbilicus* (**Table 5T1; Fig. 5F1**). Given that these datums were identified in samples spaced ~10 m apart (Kennett et al., 1986), depths of LADs and FADs could be 10 m too high and 10 m too low, respectively. Taking these potential errors into account, SRs could be up to 1.5 cm/ky higher between 5.1 and 3.8 Ma but remain essentially the same between 7.2 and 5.1 Ma (**Fig. 5F6**). A realignment of datums cannot explain the significant time offset between $CaCO_3$ MARs and key elemental ratios.

Changes in the Ti flux can influence Ca/Ti, Ba/Ti, and Al/Ti ratios of bulk sediment. In particular, increases in either the flux or Ti content of terrigenous material would cause all three ratios to decrease, although by different amounts because common aluminosilicate minerals contain relatively little Ca and Ba. After 6.5 Ma, Al/Ti decreases by a factor of 2.5 whilst Ca/Ti and Ba/Ti decrease by a factor of at least four.

Moreover, much of the change stems from fluctuations in Ti and Al contents rather than fluctuations in Ca and Ba contents (**Table 5T3**). Bulk chemistry changes are consistent with a greater input or higher Ti content of terrigenous material since the Pliocene. Stein and Robert (1986) estimated past terrigenous fluxes at site 590 from MARs of carbonate-free sediment (MARTs) and smectite/illite ratios. In the early Pliocene, MARTs increased from less than 0.5 to greater than 1.0 g/cm^2-ky. A sharp decline in smectite/illite ratios during this time may indicate intensified wind-strength and aeolian transport of illite (Stein and Robert, 1986). Increased delivery of Ti after 6.5 Ma best explains the relatively low Ca/Ti, Ba/Ti, and Al/Ti ratios during a time of high $CaCO_3$ MARs.

5.6.2 Carbon Isotopes

Consistent with the sediment chemistry records, certain $\delta^{13}C$ records from site 590 suggest increased productivity during the latest Miocene and earliest Pliocene. The bulk sediment $\delta^{13}C$ record reaches its highest values between 9 and 5 Ma (**Fig. 5F5**). This signal probably reflects variations in surface water $\delta^{13}C$ because coccoliths dominate the bulk sediment (**Fig. 5F3**). A straightforward interpretation of this signal is that enhanced productivity removed greater amounts of ^{12}C from surface waters. Such a change in carbon cycling should also affect the gradient between surface and intermediate water $\delta^{13}C$. I have calculated this gradient over time at site 590 by comparing coeval planktonic and benthic foraminiferan $\delta^{13}C$ records (Elmstrom and Kennett, 1986). The $\Delta\delta^{13}C$ (planktonic-benthic) record ranges between –0.27 and 1.60 ‰ but is generally highest between 8.4 and 5.3Ma (**Fig. 5F5**). The steepened gradient in the latest Miocene and earliest Pliocene supports enhanced productivity during this time.

However, distinct temporal offsets between the different $\delta^{13}C$ records significantly complicate relationships between carbon isotopes and productivity at site 590. In particular, a decrease of ~1 ‰ in the $\delta^{13}C$ of surface-dwelling planktonic foraminifera occurs ~2 My before a similar decrease in bulk carbonate (**Fig. 5F5**). A similar offset exists at ODP site 704 in the Southern Ocean (Mead et al. 1991), the only other site with comparable bulk carbonate and foraminiferan $\delta^{13}C$ records. I offer two general explanations for the discrepancy between nannofossil and planktonic foraminifera $\delta^{13}C$ records at site 590.

First, either the $\delta^{13}C$ record of bulk sediment or surface-dwelling planktonic foraminifera includes carbonate precipitated out of isotopic equilibrium with ambient seawater. Environmental parameters (e.g., alkalinity, temperature, irradiance) and physiological processes, or 'vital effects', can shift the $\delta^{18}O$ and $\delta^{13}C$ of coccoliths and planktonic foraminifera from +1 ‰ to –2.5 ‰ relative to expected equilibrium values (e.g., Anderson and Cole, 1975; Vergnaud-Grazzini, 1976; Kahn, 1979; Dudley et al., 1980; Goodney et al., 1980; Dudley and Nelson, 1994; Spero et al., 1997; Bemis et al., 2000). Despite these effects on isotope fractionation, several coccolithophore species and *O. universa* accurately track changes in seawater $\delta^{13}C$ over time (Dudley et al., 1986; Williams et al., 1977; Spero, 1992), suggesting that disequilibrium fractionation, if any, remains relatively constant for individual species. A change in environmental conditions or in the relative abundances of coccolithophorid species with different vital effects could cause discrepancies between $\delta^{13}C$ records of bulk nannofossils and surface-dwelling planktonic foraminifera (Paull and Thierstein, 1987; Dudley and Nelson, 1994). The first possibility does not adequately explain why different species of benthic and planktonic foraminifera record roughly coincident negative shifts in $\delta^{13}C$ ca. 7 Ma. The second possibility is plausible because the coccolithophorid assemblage at site 590 changes in the early Pliocene (**Fig. 5F7**; Lohman, 1986), coincident with the marked negative excursion in bulk sediment $\delta^{13}C$ (**Fig. 5F5**).

An alternative and more straightforward explanation for differences in "mixed layer" $\delta^{13}C$ records is that nannofossils and surface-dwelling planktonic foraminifera precipitate their tests at different water depths. In upwelling areas, most coccolithophores occur at the sea-surface (Hagino et al., 2000). The $\delta^{13}C$ of coccoliths should therefore relate to surface water $\delta^{13}C$ (Anderson and Steinmetz, 1981; Dudley and Nelson, 1989). On the other hand, although certain planktonic foraminifera are often classified as "surface-dwellers", these species are not precluded from deeper habitats (Bé and Tolderlund, 1971; Bé, 1977). I have analysed *Gs. sacculifer* (w) and (w/o) in the same sample and find minimal offset (<0.15 ‰) between the two morphotypes. This may indicate a similar $\delta^{13}C$ composition of seawater over the depth at which the morphotypes precipitated their tests. Given the coherent $\delta^{13}C$ records of *O. universa* and *Gs. sacculifer*, it is possible that the tests of these species have precipitated $\delta^{13}C$ over a larger depth range than the coccolithophores. Indeed, Kahn and Williams (1981) suggested that precipitation of foraminifera tests is not restricted to the depth

interval where the highest total standing crop occurs. In this case, temporal offsets between different $\delta^{13}C$ records might be viewed as a series of changes in the carbon isotope gradient of the water column.

5.6.3 Palaeoeanography at the Tasman Front

The $\delta^{13}C$ records of bulk carbonate and foraminifera at site 590 probably track changes in $\delta^{13}C$ at different water depths. These depths would include: the surface, a shallow mixed layer (nominally ≤10 m), and deep intermediate water (nominally ≤1300 m). By combining these changes in $\delta^{13}C$ with sediment proxies for productivity, I can develop a coherent picture for paleoceanographic changes at the TF (**Fig. 5F8**).

Between 9.5 and 8 Ma, $CaCO_3$ MARs rose, minor peaks in Ba/Ti and Al/Ti ratios occurred, and the $\delta^{13}C$ of bulk carbonate and planktonic foraminifera increased slightly (**Figs. 5F4, 5F5**). All of these observations support escalating primary production and excess removal of ^{12}C from surface waters. From 8.0 to 6.5 Ma, $CaCO_3$ MARs rose, the Ca/Ti, Ba/Ti, and Al/Ti ratios reached maximum values, and the $\delta^{13}C$ of planktonic and benthic foraminifera dropped significantly (**Figs. 5F4, 5F5**). The $\delta^{13}C$ of 'subsurface' planktonic foraminifera is also relatively low. The steep $\delta^{13}C$ gradient during this time compares to that in modern frontal regions with significant upwelling and elevated surface productivity (Kroopnick, 1985). The overall depletion in the $\delta^{13}C$ profiles may indicate a global decrease in the $\delta^{13}C$ of seawater. However, if this is the case, coccolithophores must have been isolated from the rest of the water column by a shallow thermocline (or another kind of pycnocline) because there is only a very slight decrease in bulk carbonate $\delta^{13}C$. Collectively, all lines of evidence suggest increased upwelling and primary production at the TF, a view entirely consistent with changes in microfossil assemblages (Elmstrom and Kennett, 1986). Between 6.5 and 5 Ma, the $\delta^{13}C$ of bulk carbonate decreased very slightly while that of planktonic (surface and subsurface) and benthic foraminifera increased. As a result, the $\delta^{13}C$ gradient weakened, implying a decrease in primary productivity or a loss in the density stratification of the water column. Given that this period coincides with maximum $CaCO_3$ MARs and apparently increased fluxes of wind-blown material, upwelling at the TF may have intensified. This scenario again agrees with microfossil studies at site 590 (Elmstrom and Kennett, 1986; Kennett and von der Borch, 1986). Between 5 and 3.5 Ma, all $\delta^{13}C$ records decreased, although by varying amounts, suggesting a decrease in the $\delta^{13}C$ of

seawater and in the $\delta^{13}C$ gradient of the water column. At site 590, the latter is probably linked to reduced primary production, given that $CaCO_3$ MARs decline over the same period.

5.6.4 Global nutrient and carbon cycling in the late Neogene

Various sedimentary records indicate that surface water productivity and burial of key nutrients (e.g., P, SiO_2) increased at upwelling zones of the Indian and Pacific Oceans between ca. 9.0 and 3.5 Ma (Dickens and Owen, 1999). Because primary productivity is limited by the availability of nutrients with short (<100 ky) residence times, this observation - the "biogenic bloom" - implies (e.g., Farrell et al., 1995; Dickens and Owen, 1999; Hermoysian and Owen, 2001): (1) an elevated supply of nutrients to the oceans, (2) a redistribution of nutrients within the global ocean, or (3) both.

Two recent papers (Filippelli, 1997; Hermoysian and Owen, 2001) have emphasized that the biogenic bloom signifies an increase in nutrient delivery to the oceans. Although mountain uplift and weathering probably increased during the latest Miocene and earliest Pliocene (e.g., Raymo et al., 1988; Dobson et al., 2001), this explanation ignores compelling evidence for profound changes in global oceanography that would have redistributed nutrients between 8 and 4 Ma. For example, the maximum depth of the carbonate compensation depth (CCD) switched from the Atlantic to the Pacific, suggesting a shift in deep water flow (e.g., Van Andel, 1975; Rea and Leinen, 1985); the West Antarctic ice sheet developed, leading to large-scale production of Antarctic Bottom Water (e.g., Drewry, 1978; Ciesielski et al., 1982); and, the Isthmus of Panama emerged, separating Pacific and Atlantic circulation (e.g., Keigwin, 1982a; Farrell et al., 1995; Haug and Tiedemann, 1998).

My work at site 590 also challenges two key arguments used as support for increased global burial of nutrients. First, Filippelli (1997) has interpreted the high in bulk carbonate $\delta^{13}C$ during the latest Miocene and earliest Pliocene (e.g., **Fig. 5F5**) as representing greater burial of organic matter in the oceans. However, this argument neglects the fact that $\delta^{13}C$ values of both planktonic and benthic foraminifera decrease during this same interval at site 590 (**Fig. 5F5**) and elsewhere (e.g., Vincent et al., 1980, 1985; Berger and Vincent, 1986). Clearly, the entire oceanic carbon pool did not become enriched in ^{13}C as expected by a straightforward increase in the output of

organic carbon. I strongly suggest instead that $\delta^{13}C$ records of different phases diverge during the biogenic bloom because water mass structures have changed (**Fig. 5F8**). Second, Hermoysian and Owen (2001) have calculated late Neogene phosphorus MARs at sites beneath the central Indian Ocean gyre, suggesting that these rates increase during the biogenic bloom. This observation, if correct, provides an interesting argument for a truly global rise in nutrient burial. However, as highlighted in this chapter (**Figs. 5F1, 5F4**) and elsewhere (e.g., Dickens and Owen, 1994), the integrity of MAR records depends strongly upon excellent stratigraphy. Unlike at site 590, the sites chosen beneath the central Indian Ocean gyre have very poor stratigraphic control (Dickens and Owen, 1999).

At present, site 590 is the only location where multiple elemental and isotopic proxies for past productivity have been measured across the biogenic bloom interval. The suite of records at site 590 indicates that distinct shifts in the $\delta^{13}C$ of seawater accompanied the biogenic bloom phenomenon, supporting previous suggestions that the Chron C3AR carbon shift was at least partly associated with elevated primary production (Vincent et al., 1980, 1985). Moreover, at this location, the biogenic bloom can be separated into two components: an early phase characterised by maximum accumulation of Ba, Al, and Ca relative to Ti and a depletion in foraminiferan $\delta^{13}C$ (the Chron C3AR carbon shift); and a late phase characterised by maximum $CaCO_3$ MARs and a depletion in nannofossil $\delta^{13}C$.

5.7 Conclusions

Site 590, beneath the modern TF in the Tasman Sea, contains a thick section of predominantly biogenic carbonate. Sediment deposited between ca. 9 and 3.8 Ma shows abundant evidence for elevated primary productivity, including a 2 to 3 fold escalation in carbonate MARs, a 2 to 3 fold rise in bulk sediment Ca/Ti, Ba/Ti, and Al/Ti ratios, and a significant increase in the $\delta^{13}C$ gradient of the water column. These observations provide compelling evidence for the biogenic bloom at a frontal zone in the southwest Pacific Ocean. However, manifestations of the biogenic bloom at this location are complex because time offsets occur between various proxies for productivity and between $\delta^{13}C$ records of different carbonate phases. First, $CaCO_3$ MARs peak ca. 5 Ma whereas elemental ratios are highest ca. 6.5 Ma. Second, planktonic and benthic

foraminifera record the Chron C3AR carbon shift between 7.8 and 6.4 Ma, and between 8.7 and 6.7 Ma, respectively, but bulk sediment does not show this shift *(sensu stricto)*. Although not stressed in previous literature, these time offsets have been documented in other sediment cores from the Indian and Pacific oceans, suggesting underlying causes. At site 590, elemental ratios normalized to Ti are probably affected after 6 Ma because of a significant increase in terrigenous fluxes.

Discrepancies between the $\delta^{13}C$ records of bulk sediment and surface-dwelling planktonic foraminifera at site 590 can be explained in terms of different depth habitats of coccolithophores and foraminifera, changes in the rate of upwelling at the TF, and compositional variations in the coccolithophorid assemblage. Together, the biogenic bloom and carbon isotope shifts at site 590 are most readily explained by hydrographic change at the TF affecting nutrient cycling and carbon isotope gradients in the water column.

6 The late Miocene-early Pliocene biogenic bloom at the Subtropical Convergence, east of New Zealand

6.1 Introduction

Studies of Upper Neogene sediment from scientific boreholes have often uncovered two phenomena that somehow relate to global changes in marine geochemical cycling. First, the accumulation of biogenic components (e.g., $CaCO_3$, SiO_2, P) increased significantly beneath divergence zones of the Indian and Pacific Oceans ca. 9.0 to 3.5 Ma (based on the timescales of Cande and Kent [1995] and Berggren et al. [1995a,b]). This phenomenon has been referred to as the late Miocene-early Pliocene biogenic bloom (Farrell et al., 1995a; Dickens and Owen, 1999). Second, the $\delta^{13}C$ composition of marine carbonates from all ocean basins decreased by ~0.5-1.0 ‰, and the depletion is commonly observed within or close to magnetic polarity chron C3Ar (6.57-6.94 Ma [Berggren et al., 1995b]). Details of these two events have been discussed in Chapters 2 and 3. An important question now is how the biogenic bloom and carbon shift may be linked.

In Chapter 5, I showed how the two phenomena manifest at Deep Sea Drilling Project (DSDP) site 590, located beneath the Tasman Front in the Tasman Sea (**Fig. 4F1**). A 2 to 3 fold rise in carbonate MARs and ratios of Ca/Ti, Ba/Ti, and Al/Ti in bulk sediment between about 9 and 3.8 Ma was interpreted as increased export production over this time, in agreement with the "biogenic bloom" hypothesis. Over the same time interval, elevated values of $\Delta\delta^{13}C$ and bulk coccolith $\delta^{13}C$, and negative shifts in the $\delta^{13}C$ values of planktonic and benthic foraminifera, suggest that increased biological cycling of ^{12}C coincided with the "Chron C3Ar carbon shift". Hence the two key phenomena appear to have been coupled, perhaps through changes in the rate of upwelling at the Tasman Front (see **chapter 5**).

Interpretations at Site 590 are complicated, however, by temporal discrepancies between palaeoproductivity signals, limited data about the biological oceanography of the Tasman Front, and a lack of comparative records from other areas of the southwest Pacific. Nonetheless DSDP site 590 remains, to date, the only location for which records of palaeoproductivity and $\delta^{13}C$ on multiple carbonate phases have been compiled over the time frame of interest.

One of the most important circumglobal fronts, the Subtropical Convergence (STC), follows Chatham Rise (CR) east of New Zealand (**Fig. 4F1**). Remotely-sensed ocean colour data and *in situ* measurements of chlorophyll *a*, ^{14}C uptake, and carbon biomass, over the southwest Pacific, indicate that biological production is elevated within the STC zone east of New Zealand relative to adjacent water masses (Comiso et al., 1993; Banse and English, 1997; Chang and Gall, 1998; Murphy et al., 2001). Furthermore, knowledge of the modern-day physical and biological oceanography of this area is rapidly accumulating (e.g., NIWA Ocean Ecosystems Program). Several boreholes have been drilled along CR, including ODP site 1125 (42°54.97′S; 178°16.65′W; 1333 m below sea level, mbsl) and DSDP site 594 (45°31.41′S; 174°56.88′E; 1204 mbsl). These sites are particularly intriguing for studies of the biogenic bloom because they are at similar intermediate water depths well above the lysocline, but site 1125 lies beneath the present-day STC whereas Site 594 lies just south of it. Moreover, initial work shows elevated linear sedimentation rates (LSRs) during the late Miocene-early Pliocene at Site 1125 (Carter et al., 1999).

To investigate further the biogenic bloom and its potential coupling to $\delta^{13}C$ excursions, I examined sediment at sites 594 and 1125 with the following four aims: (1) to examine variations in palaeoproductivity in the STC during the late Miocene and early Pliocene, (2) to reconstruct vertical $\delta^{13}C$ gradients at the same location over a similar time interval, (3) to determine whether there is a first order link between variations in palaeoproductivity and vertical $\delta^{13}C$ gradients in the STC during the late Miocene and early Pliocene, and (4) to compare results from the STC and TF (**Chapter 5**) so that the extent of the biogenic bloom in the southwest Pacific can be established. By addressing these unknowns, my study offers fundamental insights to how the global carbon cycle is coupled to the 'biological pump' on geologic timescales.

6.2 Lithologic sections on Chatham Rise and age models

Upper Neogene sediments at Sites 594 and 1125 on CR comprise pelagic and terrigenous components that can be conveniently placed into two lithological units. At site 594, the upper sequence (unit I), of Pliocene to Quaternary age, consists of

alternating pelagic and hemipelagic lithofacies of bluish grey, foraminifera-bearing nannofossil ooze and greenish grey, clay- and silt-bearing nannofossil ooze, respectively (**Fig. 6F1**). The lower lithological unit (II) is mainly a foraminifera-bearing nannofossil ooze of late early Miocene to earliest Pliocene age, whose relative homogeneity contrasts clearly with the interbeds of terrigenous material in younger sediments (Kennett et al., 1986). At site 1125 the sequence is similarly subdivided (**Fig. 6F1)**. The Pliocene-Pleistocene interval (unit I) comprises alternating light grey nannofossil ooze and greenish grey nannofossil-bearing silty clay, whilst the upper Miocene sediments (unit II) are mainly light grey clayey nannofossil chalk (Carter et al., 1999). At both sites there is a marked change in sediment physical properties between units I and II.

The age models constructed for this study are based on magnetostratigraphy and combined nannofossil, foraminifera, and diatom biostratigraphy (**Table 6T1**). In addition, some oxygen isotope stage boundaries have been identified at site 594 and are used here. For both sites, I first listed all the biostratigraphic events and magnetochrons originally identified at sites 594 (Kennett et al., 1986) and 1125 (Carter et al., 1999). I then reassigned new ages to all datums according to the Berggren et al. (1995a,b) timescale, added any extra datums that have been identified at site 594 since the original studies (see **Table 6T1**), plotted all ages and depths, and finally chose the most reliable and smooth-fitting datums (31 from site 594, 42 from site 1125) with which to plot an age-depth curve for each site (**Fig. 6F1**).

At both sites the age model is very well-constrained over the Quaternary-late Pliocene interval, and despite two unconformities at site 594 at ~100 and 150 mbsf (Kennett et al., 1986), ca. 1 and 3 Ma, respectively, LSRs were evidently higher at site 594 (≤100 m/My) than at site 1125 (~25 m/My) over the past 3 My (**Table 6T1, Fig. 6F1**). The early Pliocene to latest Miocene is dated reasonably well at both sites. Over this interval LSRs increased dramatically at site 1125 (≤175 m/My) whilst declining slightly at site 594, where a disconformity at the Miocene/Pliocene boundary (Kennett et al., 1986) prevents accurate LSR estimation. A fourth unconformity at site 594 at ~225 mbsf (ca. 6.5-8 Ma), and the paucity, poor preservation and diachroneity of biostratigraphic markers and events below this depth, hampers confident age assignment of these upper Miocene sediments (see Ciesielski, 1986). Nonetheless, at site 594 LSRs between ~8 and ~12 Ma appear to be of similar magnitude to those of the Pleistocene. By comparison, the site 1125 age model is well-constrained throughout the late

Miocene. Sedimentation rates are relatively low between 5.7 and 8.5 Ma (~32 m/My), and increase slightly in older sediments.

6.3 Samples and Methods

Twenty-four 10 cm^3 "plugs" of sediment were collected from hole 594 between 126 and 269 mbsf (ca. 1.8 to 9.7 Ma) according to standard ODP procedures. Together with three samples from hole 594A (**Table 6T2**), in compensation for intervals poorly recovered in hole 594, the sample resolution is ~0.3 My. Following the same procedure, hole 1125B was sampled for 20 cm^3 aliquots between 5 and 548 mbsf (ca. 0.3 to 10.9 Ma). The lowest sampling resolution over this interval (49 samples) is ~0.2 My, whereas between 236 and 351 mbsf (~5.4 to 5.7 Ma) the 114 samples yield a higher sampling resolution of <0.003 My (**Table 6T2**).

Portions of all samples were freeze-dried to remove pore water, and crushed in a porcelain mortar and pestle to homogenize sediment, whilst the remaining 10 cm^3 wet samples from site 1125 were disaggregated overnight in 10 % hydrogen peroxide and then sieved with distilled water through a 125 μm Teflon mesh. The >125 μm fraction was rinsed with isopropanol, left to air-dry, and then dry-sieved through 250, 300, and 350 μm Teflon meshes.

All sediment samples were analysed for carbonate content (**Table 6T2**) using the carbonate bomb technique (Müller and Gastner, 1971). Approximately 0.3 g of dried and powdered sediment were reacted in a sealed chamber with 5 mL of 10 % HCl. The volume of gas produced was converted to carbonate content according to a mass-volume equation determined by repeated analyses of four standards. A new equation was calculated prior to each run of 10 samples, and every sample was analysed at least twice. Reported carbonate contents have an accuracy and precision of <2 % .

Ten samples from site 594 and 32 samples from site 1125 were analysed for major element content using X-ray fluorescence (XRF) spectrometry at the Advanced Analytical Centre, James Cook University (JCU-AAC). Thirty two samples from site 590 were also analysed (see methodology in **Chapter 5**). Repeat analyses yielded concentrations of all major element oxides that were within 1 % of the calculated regression curve, with a standard deviation of < 0.1 %. The sum of all major element oxide concentrations and the loss on ignition (LOI) should be 100 %; the range of this sum was 98.1-99.8 % and 99.4-101.3 % for samples from sites 594 and 1125,

respectively. Iron contents are reported as total Fe_2O_3 (Fe_2O_3T) (**Table 6T2**) because Fe(II) and Fe(III) were not distinguished.

The stable carbon and oxygen isotopic composition of bulk sediment (sites 594 and 1125) and of planktonic and benthic foraminifera from 74 samples from site 1125 (**Table 6T3**), was determined in the Department of Geology and Geophysics, University of Adelaide (see methodology in **Chapter 5**). Well-preserved tests of *Orbulina universa*, *Globigerina bulloides*, and *Uvigerina* spp. were selected from the >350, 300-350 μm, and 250-350 μm sieved size fractions, respectively. Repeat and duplicate analyses of bulk sediment and foraminiferan samples yielded a reproducibility (± 1σ) of 0.06 ‰ for $\delta^{13}C$ and 0.10 ‰ for $\delta^{18}O$ (**Table 6T4**); all isotope results are reported in standard delta notation relative to PDB, and have not been corrected for species departures from equilibrium (see Spero, 1992).

6.4 Results

6.4.1 Sediment composition

Upper Neogene sediments at site 594 are predominantly $CaCO_3$ (**Table 6T2, Fig. 6F2**). Between 9.7 and 1.8 Ma, carbonate content varies between 62 and 91 % and averages >80 %. In general, there is a slight overall decrease in $CaCO_3$ content through time, punctuated by a peak at 6.1-5.9 Ma, and three lows at 8.4, 5.5-5.2, and 3.4 Ma. There are no previous (e.g., shipboard) $CaCO_3$ data for Neogene sediments from site 594 with which to compare my results, and analyses of carbonate content in late Quaternary sediments from site 594 (Nelson et al., 1993; Kowalski and Meyers, 1997) yield values lower (10-60 %) than mine. However, results from XRF analyses indicate that $CaCO_3$ contents are similar to those determined by the bomb method (**Table 6T2**). The sum of LOI and CaO is 76-89 %, and this should be close to the amount of $CaCO_3$. The CaO content also shows reasonable correlation ($r^2 = 0.59$) with the amount of $CaCO_3$.

At site 1125, $CaCO_3$ is a significant but more variable component of Upper Neogene (and Quaternary) sediments (**Table 6T2, Fig. 6F3)**. In contrast to the record at site 594, contents generally increase over the past 11 My. Maxima in $CaCO_3$ content occur at ~5.7 and 0.3 Ma (71 %), and these are offset by distinct minima at 10.3 (22 %), 5.4 (23 %), and 1.2 Ma (42 %). These results fit well with predicted carbonate contents,

based on shipboard color reflectance analysis of site 1125 sediments (Millwood et al., 2004). My $CaCO_3$ concentrations also compare well with XRF analyses of CaO content (**Table 6T2**); the sum of LOI and CaO is 31-75 %, and there is excellent correlation between CaO and $CaCO_3$ ($r^2 = 0.96$).

Previous work at sites 594 and 1125 indicates that clay minerals (e.g., smectite, illite) dominate the non-carbonate fraction of Upper Neogene sediment on Chatham Rise (Robert et al., 1986; Winkler and Dullo, 2004). This is supported by XRF analyses of my samples (**Table 6T2, Fig 6F4**). At site 594, the most abundant metal oxides after CaO are SiO_2 (6-24 %), Al_2O_3 (0.7-4.9 %), and Fe_2O_3T (0.3-1.7 %); at site 1125, they are also SiO_2 (16-50 %), Al_2O_3 (4-10 %), and Fe_2O_3T (1.8-2.8 %). Concentrations of SiO_2 and Al_2O_3 covary with each other ($r^2 = 0.97$ and 0.90 at sites 594 and 1125, respectively), but inversely with CaO (**Table 6T2, Fig 6F4**). At site 594, Si/Al averages 6.4 in the late Miocene and 4.3 in younger samples, whereas at site 1125 this ratio is fairly constant over time (~3.5). These ratios compare well with those for Si/Al in deep-sea clays (Martin and Whitfield, 1983), suggesting the presence of aluminosilcate clays in Chatham Rise sediments.

6.4.2 Carbonate accumulation

Calcium carbonate mass accumulation rates (MARs) were calculated for Upper Neogene sediment at sites 594 and 1125 according to the procedure outlined in chapter 5 (**section 5.5.2**). The density data needed for these calculations were extrapolated from bulk density measurements of the nearest sample analysed for physical properties (Kennett et al., 1986; Carter et al., 1999). Carbonate MARs are <7 g/cm^2-ky at both sites throughout most of the time intervals examined (**Figs. 6F2, 6F3; Table 6T5**). However, a period of significantly elevated MARs (≤42 g/cm^2-ky) is observed at site 1125 between 5.7 and 4.8 Ma and centred at ~5.5 Ma. Maximum $CaCO_3$ MARs at site 594 are recorded at 9.7 and 3.4 Ma (approximately 14 and 11 g/cm^2-ky, respectively), and are substantially lower in magnitude than that recorded at site 1125.

Because MARs are dependent on the density, linear sedimentation rate (LSR), and carbonate content of sediment samples, changes in MARs may be related to changes in each of these variables. In general, at both sites 594 and 1125, variance in sediment bulk density and carbonate content is relatively minor compared to the

variance in LSRs (Kennett et al., 1986; Carter et al., 1999; **Table 6T5**), so changes in carbonate MARs are most likely caused by changes in LSRs. The reliability of calculated LSRs depends on the accuracy of the age-depth curve. The age model at site 1125 is very well-constrained (section 6.2 above) so LSR values are probably reliable and thus dictate variations in MARs. One possible exception to this rule, however, is in core sample 26X4: 91-96 (5.381 Ma), which contains significantly lower than average carbonate for this site. At site 594, the poorly-constrained chronostratigraphy of the late Miocene precludes the calculation of high-resolution LSRs, so the reliability of LSRs (and hence MARs) needs to be checked (see below).

In natural environments, the elements Ca and Ti are predominantly found in carbonate and aluminosilicate components, respectively; the Ca/Ti ratio in a sediment sample should reflect relative changes in the accumulation rates of these components (e.g., Murray et al., 1993). The Ca/Ti record for site 1125 spans the time interval from 7.5 to 3.8 Ma and ranges between 48 and 204 g/g (**Fig. 6F3, Table 6T5**). Maxima at 5.56 and 5.48 Ma are followed by a minimum at 5.38; this represents a fourfold decline in Ca/Ti ratios over 0.05 My, in agreement with $CaCO_3$ MARs for the same time interval. Thus there is robust evidence for a major peak in carbonate accumulation at 5.5 Ma at site 1125.

The Ca/Ti record for site 594 is rather crude: 9 samples between 1.8 and 8.4 Ma, whose Ca/Ti values range between 148 and 1273 g/g (**Fig. 6F3**, **Table 6T2**). These ratios are significantly higher in the latest Miocene (624-1273 g/g) compared to the Pliocene-Pleistocene (148-549 g/g). The Ca/Ti and $CaCO_3$ MAR records for site 594 therefore appear to be roughly in agreement ca. 8 Ma, and inversely correlated at 6 Ma (high Ca/Ti, low $CaCO_3$ MARs) and 3 Ma (low Ca/Ti, high $CaCO_3$ MARs). There are two possible explanations for these differences: (a) Ca/Ti ratios reflect changes in either the flux or Ti content of the aluminosilicate influx to site 594, (b) $CaCO_3$ MARs reflect an incorrect age model for site 594. Site 594 is proximal to the Bounty Trough, a submarine conduit for aluminosilicate-rich terrigenous material from the South Island of New Zealand; thus, explanation *(a)* is highly plausible.

Re-examinining the chronostratigraphy of site 594 ca. 3 and 6 Ma (**section 6.2** above; Kennett et al., 1986), it is clear that the age model's accuracy is weakened by an unconformity at ~150 mbsf (ca. 3 Ma) but strengthened by magnetostratigraphy between 5.89 and 6.87 Ma (C3An and C3An.2n).

I have re-examined the age model for site 594 because biostratigraphic analyses of Upper Miocene sediments at this site revealed some inconsistencies (see Ciesielski, 1986). Over the key interval of 201-223 mbsf (5.23-6.57 Ma), the age model for site 594 is constrained by magnetostratigraphy. I assume here that magnetochron boundaries in sediment from site 594 were correctly identified and dated by Barton and Bloemendal (1986), hence I am confident that the age model is reliable for this interval in particular. Note that the unconformity at 223 mbsf causes a gap in the sediment records between approximately 6.5 and 8.2 Ma. Below this depth I consider the age model to be robust too, in spite of fewer potential age-depth calibration points, because I have chosen diatom and nannofossil events of minimal diachroneity and whose depth placements are chronologically consistent.

I therefore suggest that carbonate accumulation at site 594 is indicated more reliably by $CaCO_3$ MARs (derived from LSRs) at 6 Ma, and by Ca/Ti ratios at 3 Ma. Interpreted together, these two records imply that carbonate accumulation at site 594 was relatively low throughout the latest Miocene and Pliocene.

6.4.3 Carbon isotopes

Bulk sediment

At site 594, bulk sediment $\delta^{13}C$ values decline by ~2.8 ‰ across the late Neogene, from 2.54 ‰ at 10.5 Ma to –0.23 ‰ at 1.8 Ma (**Fig. 6F5, Table 6T3**). This decrease in $\delta^{13}C$ occurs mainly in three steps: from 10.5 to 6.5 Ma (-1.5 ‰), from 5.0 to 3.6 Ma (-1.7 ‰), and from 2.6 to 1.8 Ma (-1.5 ‰). However, relatively elevated $\delta^{13}C$ values (1.3-2.0 ‰) punctuate the record between 6.3 and 5.0 Ma.

All stable isotope records for site 1125 cover a longer time interval than those for site 594. At site 1125 there is little net decline (~0.3 ‰) in bulk sediment $\delta^{13}C$ between 10.9 and 0.3 Ma, although two intervals of negative $\delta^{13}C$ shifts are observed (**Fig. 6F5; Table 6T4**). First, between 10.8 and 9.4 Ma, bulk sediment $\delta^{13}C$ falls by 1.3 ‰; subsequent gradual enrichment in ^{13}C through the late Miocene culminates at 5.7-5.4 Ma with a peak of 1.6 ‰. Second, between 5.4 and 3.6 Ma, there is a substantial (1.8 ‰), saw-toothed decline in $\delta^{13}C$. Following the minimum (-0.17 ‰) at 3.6 Ma, the record varies slightly about relatively low values (around 0.3 ‰) until 1.2 Ma; from 1.2 to 0.4 Ma, the record increases to 1.35 ‰.

It is perhaps surprising that bulk carbonate sediments from the northern (site 1125) and southern (site 594) slopes of Chatham Rise record slightly different variations in $\delta^{13}C$ over the past 10 My (**Fig. 6F5**). The two records are broadly consistent between 6.5 and ~2 Ma, and diverge between 10 and 8 Ma. Such disparities represent either (a) real differences between bulk sediment $\delta^{13}C$ at these sites, or (b) errors in the age models. As discussed previously, I deem the age model for each site to be reliable, and conclude that my records of bulk carbonate $\delta^{13}C$ must reflect both site-specific and larger-scale processes.

Foraminifera (Site 1125 only)

In general, $\delta^{13}C$ values of *Orbulina universa* are lower for the Pliocene-Pleistocene interval (~2.0 ‰) compared to the late Miocene (~2.8 ‰), although this trend is not linear (**Fig. 6F5, Table 6T3**). $\delta^{13}C$ values increase between 10.8 and 6.8 Ma (+0.8 ‰), remain relatively elevated until 5.6 Ma, then fall dramatically between 5.6 and 5.4 Ma (-1.3 ‰). $\delta^{13}C$ values remain low between 5.4 and 4.9 Ma (<1.8 ‰), increase slightly between 4.9 and 4.8 Ma (+0.6 ‰), and then remain relatively uniform to the end of the record at 0.3 Ma.

The $\delta^{13}C$ record of *Globigerina bulloides* decreases overall between 10.1 and 0.3 Ma (2.3 to 0.3 ‰), although the most marked depletion occurs in two steps in the latest Miocene between 7.0 and 5.2 Ma (**Fig. 6F5, Table 6T3**). The first step (-2.1 ‰) is from 7.0 to 5.7 Ma, then after a brief rise $\delta^{13}C$ falls again (–2.5 ‰) between 5.6 and 5.2 Ma. The minimum $\delta^{13}C$ value (-0.8 ‰) is recorded at 0.9 Ma.

Tests of *Uvigerina* spp. also record a net decrease in $\delta^{13}C$ between 10.9 and 0.3 Ma (0.5 to -0.6 ‰; **Fig. 6F5, Table 6T3**). Relatively elevated $\delta^{13}C$ values in the late Miocene decrease significantly between about 7 and 5 Ma in two stages, a similar trend to that of *G. bulloides*. The first negative shift (-0.6 ‰) occurs between 7.0 and 5.7 Ma, and the second (-1.3 ‰) occurs between 5.7 and 4.9 Ma. $\delta^{13}C$ values then recover somewhat to oscillate about –0.5 ‰ from 4.8 to 0.3 Ma.

All three species of foraminifera record a decline in $\delta^{13}C$ from the late Miocene to the Pliocene-Pleistocene. Most of this decline occurs in two distinct negative shifts, the first ca. 7.0-6.5 Ma and the second ca. 5.6-5.2 Ma. This foraminiferan $\delta^{13}C$ trend contrasts with that of the bulk sediment; the latter records only a minor drop in $\delta^{13}C$ ca. 7.0-6.5 Ma and relatively elevated $\delta^{13}C$ values ca. 5.6-5.2 Ma (**Fig. 6F5**). However, in

agreement with foraminiferan $\delta^{13}C$ values, bulk sediment $\delta^{13}C$ values for the Pliocene-Pleistocene are significantly lower than those for the late Miocene, and this decline is characterised by a substantial negative excursion. Most of this excursion occurs after 5.2 Ma, and continues until 3.6 Ma. Therefore, there is a clear offset between the timing and duration of foraminiferan and bulk sediment $\delta^{13}C$ excursions over the past 10 My.

6.4.4 Oxygen isotopes

Bulk sediment

The bulk sediment $\delta^{18}O$ record at site 594 covers the time interval from 10.14 to 1.8 Ma and reveals no obvious longterm trend (**Fig. 6F6**; **Table 6T3**). $\delta^{18}O$ values decrease (-1.0 ‰) between 10.14 and 8.4 Ma, peak slightly at 8.2 Ma, then progressively increase to a maximum of 3.3 ‰ at 5 Ma. $\delta^{18}O$ values then decline (-1.4 ‰) between 5 and 3.6 Ma, and remain fairly uniform (2.4-2.7 ‰) between 3.5 and 1.8 Ma.

The bulk sediment $\delta^{18}O$ record for site 1125 is slightly longer than that for site 594, and it shows a net enrichment between 10.9 Ma (0.9 ‰) and 0.3 Ma (2.9‰; **Fig. 6F6**; **Table 6T3**). $\delta^{18}O$ values remain ≤ 0.9 ‰ between 10.9 and 8.8 Ma, increase slightly to 1.3 ‰ at 7.5 Ma, then peak again (1.6 ‰) at 5.7 Ma. Between 5.7 and 5.3 Ma, $\delta^{18}O$ values fluctuate at about 1-2 ‰, although there are two very low values (0.2, 0.0 ‰) at 5.65 and 5.42 Ma, respectively. A major peak at 4.9 Ma (2.3 ‰) is followed by a decline (-1.4 ‰) between 4.9 and 3.6 Ma, and then $\delta^{18}O$ values rise again (+2 ‰) between 3.5 and 0.3 Ma.

The $\delta^{18}O$ curves for bulk sediment from sites 594 and 1125 appear to be inversely correlated between 10.1 and 8.4 Ma, but correspond well between 6.5 and 1.8 Ma (**Fig. 6F6**). Insufficient datapoints in the site 594 record precludes intersite comparison over a continuous 0-10 My period.

Foraminifera (Site 1125 only)

All species of foraminifera record an increase in $\delta^{18}O$ with progressively younger sediments (**Fig. 6F6**; **Table 6T3**). The $\delta^{18}O$ record of *O. universa* covers the time period of 10.9-0.3 Ma. This species' $\delta^{18}O$ values increase (+1.5 ‰) between 10.9 and 7.3 Ma, dip at 5.8 Ma, and peak at 4.9 Ma (1.3 ‰). $\delta^{18}O$ values then decrease (-0.9 ‰) between 4.9 and 4.0 Ma, and rise steadily towards a maximum (2 ‰) at 0.3 Ma. The

range of $\delta^{18}O$ values recorded by *O. universa* (-0.6 to 2 ‰) is similar to that recorded by the bulk sediment.

G. bulloides records more variable and enriched $\delta^{18}O$ values than *O. universa*, and its record spans from 10.1 to 0.3 Ma (**Fig. 6F6**; **Table 6T3**). $\delta^{18}O$ values decrease (-1.5 ‰) between 10.1 and 9.2 Ma, remain fairly constant between 9 and 7 Ma (0.6-0.9 ‰), and peak significantly at 6.4 Ma (2.6 ‰). Low but variable $\delta^{18}O$ values between 5.6 and 4 Ma (-0.2 to 1.1 ‰) are followed by a maximum (3.7 ‰) at 1.4 Ma.

Uvigerina spp. records both the heaviest $\delta^{18}O$ values (2.3-4.4 ‰) and the greatest longterm enrichment in ^{18}O (+2.1 ‰) compared to the other carbonate phases measured in this study. The record spans the time interval from 10.1 to 0.3 Ma. An initial increase (+0.7 ‰) between 10.1 and 7.4 Ma is followed by an interval of depleted ^{18}O (< 3‰) between 7.4 and 5.2 Ma. A clear peak at 4.9 Ma (3.6 ‰) precedes a second depletion (-1.0 ‰) between 4.8 and 3.6 Ma; the record then increases steadily to 4.4 % at 0.3 Ma.

All $\delta^{18}O$ records for site 1125 - bulk sediment and foraminiferan – are broadly similar (**Fig. 6F6**). Their longterm trend of ^{18}O enrichment in younger samples is interrupted by a distinct trough ca. 5.7-5.6 Ma, a peak at 5 Ma, and a decline between 5 and 4 Ma. These fluctuations are not, however, absolutely isochronous. For example, the '5.7-5.6 Ma trough' occurs at 5.68 Ma (*O. universa*), 5.65 Ma (bulk sediment), 5.63 Ma (*G. bulloides*), and 5.60 Ma (*Uvigerina* spp.). Bulk sediment at site 594 also records relatively lower $\delta^{18}O$ values at 5.9 and 5.5 Ma, a peak at 5 Ma, and a decline between 5 and 4 Ma (**Fig. 6F6**). This broad similarity between all the $\delta^{18}O$ records from sites 594 and 1125 contrasts with the differences observed between the corresponding $\delta^{13}C$ records.

6.5 Discussion

6.5.1 Palaeoproductivity in the Subtropical Convergence, 0-12 Ma

A commonly used proxy for past variations in export productivity at sites which are shallower than the lysocline and located below high productivity zones is the mass accumulation rate (MAR) of carbonate sediment (e.g., Berger et al., 1993). ODP site 1125 underlies the present-day STC, at 1.3 km water depth, hence the record of carbonate MARs here can be interpreted most straightforwardly as a first order

approximation of palaeoproductivity. The dramatic, eight-fold increase in $CaCO_3$ MARs between 5.66 and 5.38 Ma (**Fig. 6F3**) suggests a high-productivity interval within the past 12 My; this pattern is in agreement with previous similar studies (e.g., Berger et al., 1993; Farrell et al., 1995a; Dickens and Owen, 1999). However, as stressed earlier in this work (**chapter 5**), the accuracy of calculated $CaCO_3$ MARs depends most heavily on the calculated LSRs (and hence the age model), and to a lesser extent on the carbonate content of sediment samples. I consider the age-depth model (and hence LSRs) at site 1125 to be highly reliable (see **section 6.2**). Furthermore, Ca/Ti values are independent of LSR calculations (e.g., Murray et al., 1993), and these too are relatively high between 5.66 and 5.38 Ma (**Fig. 6F3**). The late Miocene-early Pliocene peak in both the $CaCO_3$ MAR and Ca/Ti curves coincides with maximum carbonate content (% $CaCO_3$) between 5.66 and 5.38 Ma (**Fig. 6F3**), and visual examination of foraminifera from this site revealed only minor dissolution effects in most late Miocene to recent sediments. Examination of the lithological core log for site 1125 (Carter et al., 1999; **Fig. 6F1**) reveals that the interval in question corresponds to unit IIA, the most pale and nannofossil-rich unit at this site. All these results imply that carbonate production (and hence biological productivity) was significantly elevated between 5.66 and 5.38 Ma in the STC east of New Zealand.

A substantial rise in biological production will increase the cycling of ^{12}C through the water column, leading to enhanced $\delta^{13}C$ gradients between the mixed layer and deeper water masses (e.g., Kroopnick, 1985). Past changes in this gradient can be approximated by comparing the $\delta^{13}C$ values of planktonic and benthic foraminifera from the same sediment sample ($\Delta\delta^{13}C$). This index can then be compared with alternative proxies of palaeoproductivity. Although the $\Delta\delta^{13}C$ record for site 1125 shows no obvious long-term trend, there is a distinct peak at 5.65 Ma which coincides with maxima in the other records discussed here (**Fig. 6F3**). Berger et al. (1993) observed a similar link between records of sedimentation rate and $\Delta\delta^{13}C$ for the past 10 My from the west Equatorial Pacific - both records peaked in the latest Miocene, although the $\Delta\delta^{13}C$ trend was weaker than that of sediment accumulation. These authors interpreted their results as evidence (amongst other sediment proxies) of increased productivity during the latest Miocene. The same explanation would appear to hold for the observations at site 1125.

Ancillary evidence of heightened primary productivity during the latest Miocene in the STC east of New Zealand is from planktonic faunal assemblages (**Fig. 6F3**). Preliminary micropalaeontological analyses of sediment samples from site 1125 have found that diatom species of the genera *Thalassionema* and *Thalassiothrix* were particularly abundant between 6 and 5 Ma (Carter et al., 1999); these species are indicative of enhanced primary productivity and upwelling (Kemp et al., 1995). At ODP site 1123, 450 km east of site 1125, a prominent orbuline abundance spike in the planktonic foraminiferan assemblage during chron C3r (with an interpolated age of 5.66 Ma) has been linked to regional changes in productivity and ocean circulation (Crundwell, pers. comm.). At site 1125, only one core catcher sample (27X CC, ~254 mbsf) within the upper 400 m of sediment cores contains more than 5 % *O. universa* (Carter et al., 1999). This sample dates to ~5.5 Ma, and contains 'abundant' (10-30 %) *N. pachyderma* and *Ga. miotumida* and 'frequent' (5-10 %) *G. bulloides* (Carter et al., 1999). These are cool-water species commonly associated with upwelling conditions (e.g., Bé and Tolderlund, 1971; Thunell and Sautier, 1992; Little et al., 1997; Ivanova et al., 1999). These faunal abundance patterns imply that upwelling intensified within the STC in the latest Miocene, and this scenario is consistent with parallel evidence of increased productivity.

An extended period of enhanced productivity in the waters above site 1125 should be reflected by changes in the benthic foraminiferan assemblage at this site over the interval in question. Late Miocene and early Pliocene sediments from site 1125 are characterised by the subassociations *Globocassidulina subglobosa-Hopkinsina mioindex* and *Alabaminella weddellensis-Abditodentrix pseudothalmanni* (E1, 4.2 Ma; E2, 9.5-2.9 Ma, respectively; Hayward et al., 2002, 2004). High abundances of *G. subglobosa* occur beneath present-day areas of enhanced, continuous food supply (Mackensen et al., 1995), and the Holocene equivalent of the *Alabaminella weddellensis-Abditodentrix pseudothalmanni* subassociation on Chatham Rise is influenced by episodic food supply (Hayward et al., 2002). These benthic faunal changes appear to be further evidence of an increase in surface productivity in the STC in the latest Miocene. There is some discrepancy, however, between the records: Hayward et al. (2004) inferred that food supply to site 1125 continued to increase from the early Pliocene onwards, yet my records indicate decreasing export production over this time. This disparity may reflect a change in the type of organic material supplied to

the benthos at site 1125, such as an increase in the flux of allochthonous over autochthonous material.

Interpretions of past changes in palaeoproductivity in the STC may be improved by examining relevant sediment records from a proximal site just outside the frontal boundary. Deep Sea Drilling Project site 594 - at a similar intermediate water depth to site 1125 - records relatively low carbonate accumulation throughout the latest Miocene and Pliocene (**Fig. 6F3; Section 6.4.2**). Moreover, LSRs at site 594 apprear to be inverse those at site 1125 (**Fig. 6F1**), although hiatuses in sediment cores from site 594 may be skewing the trend of the age-depth curve for this site. Diatom and planktonic foraminiferan assemblages at site 594 show no marked changes coeval with those at site 1125 during the latest Miocene-earliest Pliocene (see Ciesielski, 1986, and Lohmann, 1986), and slightly different benthic foraminiferan associations have been identified at each site over the time interval in question (Hayward et al., 2004). These observations suggest a basic differentiation of trends in palaeoproductivity between waters of the STC and those bordering it. An exception to the aforesaid disparate faunal trends is the abundance of *E. exigua* between 9 and 2.8 Ma in the benthic foraminiferan assemblage at site 594, indicative of a high, pulsed food supply (Hayward et al., 2004). However, the explanation offered for a similar discrepancy between inferred food supply and export production at site 1125 - an increase in the flux of allochthonous over autochthonous material - is likely to hold true for site 594 because it too receives substantial terrigenous inputs from New Zealand.

In summary, there is strong evidence that biological productivity in the STC east of New Zealand was distinctly higher during the latest Miocene-earliest Pliocene, peaking at 5.66-5.38 Ma and therefore lasting for at least 280,000 yrs.

6.5.2 $\delta^{13}C$ shifts in the Subtropical Convergence, 0-12 Ma

Changes in productivity affect the downward transport of ^{12}C in the water column, and should therefore be accompanied by changes in seawater $\delta^{13}C$ at all depths. An appropriate tool for assessing such changes is the suite of $\delta^{13}C$ records from site 1125 sediments. These records all show lower $\delta^{13}C$ values for the early Pliocene

compared to the latest Miocene, and the depletion occurs mainly in two distinct shifts: during chron C3Ar and the early Gilbert.

The "Chron C3Ar carbon shift"

There is a negative excursion in foraminiferan $\delta^{13}C$ values from 6.993 to 6.717 Ma (*G. bulloides* [-1.5 ‰] and *Uvigerina* spp. [-0.8 ‰]), and from 6.826 to 6.413 Ma (*O. universa* [-0.6 ‰]); bulk sediment $\delta^{13}C$ decreases marginally at this time (-0.2 ‰; **Table 6T3**). The timing and magnitude of this depletion suggest that it is a signature of the widely recognised "Chron C3Ar carbon shift". Although the decrease in bulk sediment $\delta^{13}C$ is relatively slight compared to the other carbonate phases, the similar trend of all four records at this time is striking. Significantly, if this observation is correct it means that carbonates precipitated at different depths through the entire water column all record a reduction in $\delta^{13}C$, which in turn implies that the $\delta^{13}C$ composition of the global ocean changed ("external fractionation", Berger and Vincent [1986]).

At site 1125, the magnitude of the Chron C3Ar carbon shift tends to increase with depth of carbonate precipitation. Previous studies of the late Miocene carbon shift similarly found that benthic foraminifera tend to record a larger (more negative) $\delta^{13}C$ excursion compared to planktonic foraminifera from the same core sample (Vincent et al., 1980, 1985, and references therein). This differentiation between "surface" and "subsurface/deep" records of the carbon shift suggests that redistribution of ^{12}C between water masses ("internal fractionation") occurred in addition to external fractionation of seawater $\delta^{13}C$ (see Berger and Vincent, 1986). The seafloor and subsurface depths at sites 590 and 1125 are bathed by Antarctic Intermediate Water (AAIW), so any change in the $\delta^{13}C$ composition of this water mass would be recorded most strongly by carbonates precipitated at these depths. Modern-day abyssal circulation dictates Atlantic-Pacific gradients in $\delta^{13}C$, and these gradients are mirrored at the time of the carbon shift and thereafter (Billups, 2002). Hence previous studies suggested that the carbon shift marks the on-set of the Present-day hydrographic regime (e.g., Bender and Graham, 1981; Keigwin et al., 1987).

If the Chron C3Ar carbon shift is a signal of deepwater changes, benthic foraminifera should record the biggest isotopic excursion. At site 1125, however, this is not the case; *G. bulloides*, rather than *Uvigerina* spp., records the largest depletion in $\delta^{13}C$. There are two possible explanations for this. First, irregular time intervals between

$\delta^{13}C$ datapoints in my *G. bulloides* record ca. 9-6 Ma mean it is difficult to distinguish short-term, high-amplitude $\delta^{13}C$ variations from permanent $\delta^{13}C$ shifts. Second, enhanced rates of production/decomposition affect the vertical distribution of $\delta^{13}C$ in the water column, leading to ^{12}C enrichment at the base of the mixed layer. The habitat depth range for *G. bulloides* includes the entire mixed layer, down to the Deep Chlorophyll Maximum (e.g., Bé and Tolderlund, 1971), so its shell's $\delta^{13}C$ composition may reflect changes in both (local) remineralisation rates and (global) intermediate water circulation patterns. There is a problem with this explanation, however, because the inferred interval of maximum productivity at the STC (5.66-5.38 Ma, see above) post-dates the "Chron C3Ar carbon shift" recorded by *G. bulloides* (6.993 to 6.717 Ma). Therefore, the spacing of datapoints in the $\delta^{13}C$ record for *G. bulloides* is probably distorting the magnitude of its Chron C3Ar shift.

Early Gilbert carbon shift

The depletion in $\delta^{13}C$ over the past 12 My appears to be focussed mainly in two periods. The first is the Chron C3Ar carbon shift (see above). The second stage of the late Miocene to early Pliocene $\delta^{13}C$ depletion begins with a semi-permanent negative shift from 5.386 to 5.379 Ma (**Fig. 6F5, Table 6T3**) recorded by planktonic and benthic foraminifera (*O.universa* [-0.5 ‰], *Uvigerina* spp. [-0.7 ‰]); there are no isochronous $\delta^{13}C$ values for *G. bulloides* over this particular interval. The duration of this isotopic excursion is therefore 6 ky. Although bulk sediment $\delta^{13}C$ also declines over this relatively short time interval (-0.9 ‰), the decrease is temporary and $\delta^{13}C$ values remain relatively elevated until around 5 Ma (**Fig. 6F5**). In contrast, foraminiferan $\delta^{13}C$ values either continue to decline or remain depleted until 4.9 Ma, resulting in a net decrease of 0.7 ‰ (*O.universa*), 0.9 ‰ (*G. bulloides*), and 1.2 ‰ (*Uvigerina* spp.) between 5.4 and 4.9 Ma. The subsequent, substantial decline in bulk sediment $\delta^{13}C$ (1.8 ‰) between 5.1 and 3.6 Ma therefore largely post-dates the foraminiferan $\delta^{13}C$ depletions.

Previous studies of long-term variations in foraminiferan $\delta^{13}C$ reveal no widely documented "early Gilbert carbon shift", which suggests that the results from site 1125 reflect a local $\delta^{13}C$ depletion (see below). Nevertheless, many of the earlier $\delta^{13}C$ studies used relatively poor sampling resolutions, and nearly all revealed distinctly lower $\delta^{13}C$ values in the early Pliocene compared to the late Miocene. Thus, the "early Gilbert carbon shift" may not be confined to ODP site 1125, and may therefore relect global-

scale processes. Interestingly, the >1.5 ‰ $\delta^{13}C$ depletion in bulk Lower Pliocene sediments from site 1125 is seen in bulk sediment $\delta^{13}C$ records from DSDP sites 525 (Shackleton and Hall, 1984), 590 (**Fig. 5F6**) and 594 (**Fig. 6F5**), and ODP site 846 (Shackleton and Hall, 1995). The fact that these are geographically diverse sites corroborates the suggestion that the "early Gilbert carbon shift" reflects a net change in oceanic $\delta^{13}C$. Many marine and terrestrial $\delta^{13}C$ records have documented distinct isotopic excursions during the latest Miocene-earliest Pliocene (e.g., Berger and Vincent, 1986; Quade et al., 1995; Shackleton and Hall, 1995; Bickert et al., 2004; Ghosh et al., 2004), and these have been interpreted as a significant change in the $\delta^{13}C$ composition of the ocean and hence in global carbon cycling. Shackleton (1987) surmised that this change was ultimately related to either the effects of Himalayan uplift and Antarctic glaciation on the accumulation and erosion of organic-rich sediment, or the effects of atmospheric and oceanic oxygen levels on long-term geochemical equilibria.

Bulk calcite and foraminifera offsets

The temporal offsets between negative shifts in the bulk sediment and foraminiferan $\delta^{13}C$ records from site 1125 mirrors results from site 590 (**Fig. 5F5**). Three explanations were suggested in the Tasman Front study (**chapter 5**): (1) different depth habitats of foraminifera and coccolithophores, (2) compositional variations in coccolithophorid assemblages, and (3) changes in water column stratification. Evidence suggests that coccolithophores are likely to precipitate their tests at water depths shallower than so-called "surface-dwelling" planktonic foraminifera, especially in areas of upwelling (Kahn and Williams, 1981; Dudley and Nelson, 1989; Hagino et al., 2000), so point (1) holds true for both sites 590 and 1125. There is no marked change in the composition of the coccolithophorid assemblage at site 1125 at the time of the depletion in bulk sediment $\delta^{13}C$ (Carter et al., 1999), so point (2) is probably not valid here. Thirdly, downcore changes in the microfaunal assemblages at site 1125 imply that upwelling intensified between 6 and 5 Ma, thus point (3) - changes in water column stratification - also holds true at site 1125. Additional support for the latter scenario is the fact that sites 590 and 1125 underlie fronts which are hydrodynamically connected by regional surface currents (see **chapter 4**), and so similar palaeoceanographic conditions may have prevailed at both sites in the past.

A fourth explanation for the disparate bulk sediment and foraminiferan $\delta^{13}C$ shifts at site 1125 is the presence of calcite overgrowths on foraminifera in bulk sediment samples. Such diagenetic 'overprints' cause older sediment to be enriched in remineralised ^{12}C, and thus they are $\delta^{13}C$-depleted. The opposite trend is observed in bulk sediment from site 1125, and microscopic examination of sieved sediment fractions confirmed the absence of diagenetic overgrowth in all samples above core 48X (~10 Ma). Therefore, diagenesis is ruled out as an explanation of the diachronous $\delta^{13}C$ shifts at site 1125.

In summary, offsets between negative $\delta^{13}C$ shifts during the early Gilbert, as recorded by the bulk sediment and foraminifera at site 1125, are explained here by different depth habitats of coccolithophores and foraminifera, and changes in water column stratification during the time interval in question.

Cause of early Gilbert carbon shift in the STC

The observation that carbonates precipitated at different depths in the water column all record a decrease in $\delta^{13}C$ between 5.39 and 5.38 Ma implies that surface and deeper waters overlying site 1125 became relatively enriched in ^{12}C at this time. The lack of any well-documented "early Gilbert carbon shift" in global $\delta^{13}C$ records from marine carbonates suggests that this ^{12}C enrichment was a local phenomenon, so the most obvious explanations are (a) an influx of ^{12}C-rich organic material from the New Zealand continental shelf, and/or (b) a change in rates of upwelling and primary productivity. Both scenarios are supported by a lithological change from pale, nannofossil-rich sediments (unit IIA) to darker, more clay-rich sediments at site 1125 (unit IB; Carter et al., 1999) at approximately 5.5 Ma (**Fig. 6F1**). An increase in the terrigenous supply to site 1125 would dilute the carbonate content of the bulk sediment, thereby lowering $CaCO_3$ MARs and Ca/Ti ratios whilst raising Si/Ti and Al/Ti ratios. Between 5.39 and 5.38 Ma there is a marked decline in $CaCO_3$ content, $CaCO_3$ MARs, and Ca/Ti ratios, with a concommitant rise in Si/Ti and Al/Ti ratios (**Figs. 6F3, 6F4**). A decrease in export productivity would also explain these geochemical changes.

Ancillary evidence for increased terrigenous fluxes to site 1125 during the early Gilbert comes from indicators of enhanced rates of decomposition of organic material on the seafloor. Greater decomposition of sinking organic material results in more

corrosive, oxygen-depleted bottom waters (Kroopnick, 1985). At site 1125, the only sediment samples containing poorly-preserved foraminiferan tests - indicative of carbonate dissolution - are from core 26X4, corresponding to 5.38 Ma. This core also contains the highest abundance of *Uvigerina* spp., a species often associated with dysoxic bottom waters (e.g., Streeter and Shackleton, 1979).

The cause of an increase in terrigenous fluxes to site 1125 at 5.4 Ma may be elucidated by examining the $\delta^{18}O$ records from site 1125. Between 5.39 and 5.38 Ma, carbonates precipitated in the mixed layer (bulk sediment and *O. universa*) record a temporary, but distinct, peak in $\delta^{18}O$ (**Fig. 6F6, Table 6T3**). These heavier $\delta^{18}O$ values imply that site 1125 was temporarily overlaid by colder surface water masses. I speculate that climatic deterioration (global cooling, Antarctic glaciation, and sea-level fall) led to increased weathering of the New Zealand continental shelf and a relative increase in the contribution of colder, subantarctic waters to the STC east of New Zealand. An intensification of the Southland Current and northward leakage of subantarctic water masses across the Chatham Rise during the last glacial maximum has been inferred from stable isotope, lithological, and microfossil records (Nelson et al., 2000), and these authors proposed that a similar circulation system developed during periods of significant glaciation since the latest Miocene. Previous evidence of intermittent cold water pulses north of Chatham Rise is from rare to common occurrences of predominantly sinistral populations of the planktonic foraminifera *N. pachyderma* at intervals within latest Miocene and early Pliocene sections (Vella and Kennett, 1975; Hornibrook, 1976; Hornibrook, 1992).

Bulk sediment from site 594, on the southern slope of Chatham Rise, also records a distinct peak in $\delta^{18}O$ at 5.4 Ma, as well as decreasing carbonate content and Ca/Ti ratios through the Pliocene. Previous work on site 594 sediments (Nelson et al., 1985) concluded that abundant terrigenous material in hemipelagic deposits resulted primarily from greatly increased rates of erosion on the South Island during glacial periods and the rapid transferral of this terrigenous detritus to off-shore areas, where sedimentation rates increased and the carbonate content of bottom sediments was diluted. Thus, I suggest that similar conditions prevailed in the early Golbert at site 594.

6.5.3 The biogenic bloom and $\delta^{13}C$ shifts in the Southwest Pacific

Evidence from ODP site 1125 implies that palaeoproductivity in the STC peaked at 5.66-5.38 Ma, and I interpret this as a signal of the "biogenic bloom" phenomenon. Within the southwest Pacific region, there is evidence from DSDP site 590 for the biogenic bloom at the Tasman Front also, dated to 9-3.8 Ma and peaking ca. 5 Ma (**Chapter 5**). There is therefore broad agreement in the timing of enhanced palaeoproductivity at these two oceanic fronts, although the STC probably experienced a greater rise in primary productivity over a shorter time interval compared to the TF (cf. **Figs. 5F6** and **6F3**). Changes in palaeoproductivity in the TF in the latest Miocene-earliest Pliocene have been associated with $\delta^{13}C$ shifts recorded by foraminifera and by bulk sediments from DSDP site 590 (**Chapter 5**), and all these changes have been linked to strengthened surface currents and wind stress. Foraminifera and bulk sediments from site 1125 also record distinct $\delta^{13}C$ shifts within the latest Miocene-earliest Pliocene, and these too can be attributed - at least in part - to hydrographic changes in the STC.

However, the inferred period of maximum palaeoproductivity in the STC begins at least 700 ky after the end of the "Chron C3Ar carbon shift" here. Conversely, the end of this biogenic bloom period coincides with the "early Gilbert carbon shift". Gaining an understanding of such associations - between the timing of enhanced palaeoproductivity and $\delta^{13}C$ variations - is further complicated by temporal offsets between $\delta^{13}C$ records from different carbonate phases at both sites 590 and 1125. I therefore suggest that both local and global-scale mechanisms provide a first-order link between the Chron C3Ar carbon shift, the biogenic bloom, and the early Gilbert carbon shift, because it is these mechanisms which strongly determine nutrient avaiablity – and therefore carbon cycling – at ocean fronts.

It has been suggested that the biogenic bloom may reflect a movement of high-productivity zones, rather than an increase in productivity within a eutrophic region. The Tasman Front may have migrated latitudinally in the past, so I cannot be sure whether the manifestation of the biogenic bloom at this front related to an increased supply or redistribution of nutrients. However, the alignment of the STC with Chatham Rise, east of New Zealand, is possibly the only location where the position of a major global front has been more or less fixed (within a few degrees) over time, owing to bathymetric constraint. Hence I propose that the biogenic bloom interval recorded at site 1125 represents an increase in the availability of nutrients within the STC, rather than a

relocation of a 'high-nutrient' zone. The rise in nutrient concentrations within the mixed layer probably originated, at least partly, from strengthened upwelling in the vicinity of Chatham Rise as a result of stronger oceanic/atmospheric circulation, and this can ultimately be related to Antarctic glaciation.

6.6 Conclusion

Sediments from site 1125, beneath the modern-day STC, show evidence of elevated primary productivity between 5.66 and 5.38 Ma. This includes an eight-fold increase in $CaCO_3$ MARs, higher $\Delta\delta^{13}C$ values, and changes in the diatom and planktonic and benthic foraminiferan assemblages. These observations have been interpreted as evidence of the biogenic bloom in the STC. Overlapping this interval, there is a large depletion in the $\delta^{13}C$ values of bulk sediment and foraminifera, although this mainly occurs in two distinct isotopic shifts. Foraminifera record the "Chron C3Ar carbon shift" at slightly different times within the interval 7.0-6.4 Ma, and the magnitude of the shift varies between –0.6 and –1.5 ‰. Bulk sediment $\delta^{13}C$ declines minimally at this time. Foraminifera record a second shift (≤1.2 ‰) at 5.39-5.38 Ma and 5.3-4.9, which more or less precedes a dramatic decline in bulk sediment $\delta^{13}C$ (1.7 ‰) between 5.1 and 3.6 Ma. The cause of this second $\delta^{13}C$ shift, during the early Gilbert, probably reflects increasing terrigenous fluxes to Chatham Rise, although coeval decreases in upwelling and productivity in the STC may also be invoked.

A comparison of the results from sites 1125 and 590 suggests that the timing of the biogenic bloom and $\delta^{13}C$ shifts in the STC and TF is broadly in agreement. Equally, there are similar offsets between the bulk sediment and foraminiferan $\delta^{13}C$ records at these sites. Temporal discrepancies between the $\delta^{13}C$ curves for carbonates precipitated at different depths in the water column are interpreted here to reflect hydrographic changes in the STC and TF, combined with differential depths of $\delta^{13}C$ fractionation by foraminifera and coccolithophores. Ultimately, therefore, the biogenic bloom and concommitant $\delta^{13}C$ changes in the southwest Pacific resulted from increased nutrient availability in frontal zones, which in turn was a consequence of climate-driven ocean circulation change.

7 Outcome of this research

7.1 Major conclusions

Sediment records from sites 590 and 1125 strongly imply that the biogenic bloom manifested in the southwest Pacific, with palaeoproductivty peaking ca. 5 Ma in the TF and between 5.66 and 5.38 Ma in the STC. In addition, bulk sediments and foraminifera at both sites record marked shifts in $\delta^{13}C$ which overlap in time with the inferred changes in primary productivity. First, planktic and benthic foraminifera record the Chron C3AR carbon shift between 7.8 and 6.4 Ma at site 590, and between 7.0 and 6.4 Ma at site 1125. Then, bulk sediment $\delta^{13}C$ decreases by nearly 2 ‰ between 5.6 and 1.9 Ma at site 590, and between 5.0 and 3.6 Ma at site 1125. Together, the biogenic bloom and carbon isotope shifts at sites 590 and 1125 are most readily explained by hydrographic change at the TF and STC affecting nutrient cycling and carbon isotope gradients in the water column.

The major depletion in bulk sediment $\delta^{13}C$ during the early Pliocene, documented in this study of the Southwest Pacific region, has also been observed in bulk sediments from the South Atlantic and East Equatorial Pacific. Furthermore, the timing and magnitude of this excursion is not reflected in foraminiferan $\delta^{13}C$ records. I tentatively suggest that differential depths of $\delta^{13}C$ fractionation by foraminifera and coccolithophores, coupled to water column dynamics, may explain this common trend in bulk sediment $\delta^{13}C$ records for the early Pliocene.

7.2 Problems encountered

The identification of any limitations, weaknesses, or setbacks in the practical implementation of this study is useful as a learning tool for future work. Here I note the main problems encountered in the course of this study which affected my results most significantly.

(i) Too few samples were taken from sites 590 and 594 for XRF analyses, so my Ca/Ti, Si/Ti, and Al/Ti records for these sites are rather crude and are therefore subject to ambiguous interpretation.

(ii) The initial age-depth model for site 1125 (Carter et al., 1999) was refined at a later stage (**Chapter 6**). My sampling strategy was based on the original age-depth model, and as a result of the age revision there are now no samples for the time interval 5.68-6.41 My. This is a critical period in the context of my study because it coincides with, or immediately pre- or post-dates, the biogenic bloom phenomenon and global $\delta^{13}C$ shifts.

(iii) The scarcity of suitably-sized foraminifera for stable isotope analyses in some of my samples from site 1125, as a result of either an inadequate volume of sediment 'plug' (e.g., $CaCO_3$ content is <50 % in over half of the samples from core-barrel 26X), or insufficient numbers of a target species. The consequences of this problem were most significant for plotting a $\Delta\delta^{13}C$ curve, which required reliable $\delta^{13}C$ data from tests of both *O. universa* and *Uvigerina* spp. in the same sample.

(iv) There were numerous delays and setbacks in obtaining my stable isotope data, owing to technical difficulties at the University of Adelaide and to funding restraints (which prevented me from analysing my samples elsewhere).

7.3 Future work

This study has produced new data about biogenic sedimentation and carbon isotope shifts in the southwest Pacific Ocean during the late Neogene, and therefore lays the groundwork for further related investigations on both local and global scales. Some suggestions for such future work are outlined below.

Firstly, an evaluation of downcore changes in planktic faunal assemblages at ODP site 1125 would greatly improve my palaeoceanographic reconstructions of the biogenic bloom in the STC east of New Zealand. Alternatively, the currently available records for site 1125 could be expanded by additional, higher-resolution sampling. This strategy would permit more precise dating of important shifts in the proxy records, and also reveal shorter-term fluctuations in key parameters. It is pertinent to note here that no-one has yet investigated the link between the biogenic bloom and astronomical cycles. Variations in Earth's orbital precession and eccentricity affect seasonal contrasts of insolation. Enhanced seasonal contrasts promote algal blooms, because the combination of hivernal mixing and summertime heating promotes nutrient regeneration to, and subsequent entrapment in, the mixed layer. Oscillations in seasonality on

geologic timescales may therefore be related to trends in global palaeoproductivity. Such a link to the biogenic bloom is not straightforward, however, because this 'bloom' appears to have been a one-off event.

Another avenue of research would be to quantify the impact of the biogenic bloom on global nutrient and carbon cycling, using quantitative biogeochemical models (e.g., Kump and Arthur, 1999). Such work enables deeper understanding about how the carbon cycle is coupled to the 'biological pump' on geologic timescales, and therefore has implications for predictions of future climate change.

A more specific suggestion - within the broad field of biogeochemical modelling - for possible future research stems from the fact that many current models of nutrient cycling rely on fixed "Redfield ratios" for C:N:P (106:16:1), based on Redfield's (1934, 1958) pioneering demonstration that concentrations of the major nutrients (N, P) in seawater change in relation to fixed concentration ratios in organisms. Yet this might not be the case. Rubin et al. (1998) demonstrated that in Antarctic waters C:P and N:P redfield ratios, unlike those for C:N, are not valid, and concluded that the biological cycling of P in the Southern Ocean was not "Redfieldian". It follows that there may be other regions - at present or in the past - where nutrient cycling does not follow the accepted models of biological utilisation (e.g., Takahasi et al., 1985; Watson and Whitfield, 1985). Similarly, the long held view that the availability of N and P limit the biological utilisation of silica, rather than concentrations of dissolved Si itself (e.g., Paashe, 1973; Brewster, 1980), has been challenged more recently by evidence of silicate regulation of primary production (Dugdale et al., 1995; Dugdale and Wilkerson, 1998; Harrison, 2000). Thus, interpretations of past changes in biological productivity in relation to nutrient limitation may be flawed, and this hampers attempts to unravel the dynamics of the biogenic bloom in terms of nutrient cycling.

Understanding how changes in nutrient and carbon cycling are related to excursions in long-term $\delta^{13}C$ records requires accurate interpretation of isotopic signals. It is perhaps surprising, then, that the number of laboratory and field studies on the 'vital effects' and depth of foraminiferan calcite precipitation are relatively few, given the extensive use of foraminiferan $\delta^{13}C$ (and $\delta^{18}O$, etc) records for palaeoceanographic reconstructions. Hence, my final point with respect to future research is that further knowledge of how the stable isotope values of a given calcite-secreting species equate to seawater chemistry, depth of calcification, and disequilibrium fractionation, would

help to resolve ambiguous trends in these records and improve the accuracy of their interpretations.

BIBLIOGRAPHY

Bibliography

Abbott, L. D., 1995. Neogene tectonic reconstruction of the Adelbert-Finisterre New Britain collision, northern Papua New Guinea. *J. South Asian Sci*., 11: 33-51.

Adams, C. G., Benson, R. H., Kidd, R. B., Ryan, W. B. F. and Wright, R. C., 1977. The Messinian salinity crisis and evidence of late Miocene eustatic changes in the world ocean. *Nature*, 269: 383-386.

Anderson, T. F. and Cole, S. A., 1975. The stable isotope geochemistry of marine coccoliths: A preliminary comparison with planktonic foraminifera. *J. Foram. Res*., 5: 188-192.

Anderson, T. F. and Steinmetz, J. C., 1981. Isotopic and biostratigraphical records of calcareous nannofossils in a Pleistocene core. *Nature*, 294: 741-745.

Andrews, J. C., Lawrence, M. W. and Nilsson, C. S., 1980. Observations of the Tasman Front. *J. Phys. Oceanogr*., 10: 1854-1869.

Arnold, E., Leinen, M. and King, J., 1995. Paleoenvironmental variation based on the mineralogy and rock-magnetic properties of sediment from sites 885 and 886. *Proc. ODP., Sci. Res*., 145: 231-245.

Auzende, J.-M., Dickens, G. R., van de Beuque, S., Exon, N. F., François, C., Lafoy, Y. and Voutay, O., 2000. Thinned crust in Southwest Pacific may harbor gas hydrate. *Eos, Trans. Am. Geophys. Union*, 81: 182, 185.

Backman, J. and Raffi, I., 1997. Calibration of Miocene nannofossil events to orbitally tuned cyclostratigraphies from Ceara Rise. *Proc. ODP., Sci. Res*., 154: 83-100.

Backman, J., Duncan, R. A. et al., 1988. *Proc. ODP., Init. Repts*., 115, pp. 1085.

Banse, K. and English, D. C., 1997. Near-surface phytoplankton pigment from the Coastal Zone Colour Scanner in the subantarctic region southeast of New Zealand. *Mar. Ecol. Prog. Ser*., 156: 51-66.

Barton, C. E. and Bloemendal, J., 1986. Paleomagnetism of sediments collected during Leg 90, Southwest Pacific, *Init. Rept. DSDP*, 90: 1273-1316.

Barron, J. A. and Baldauf, J. G., 1989. Tertiary cooling steps and paleoproductivity as reflected by diatoms and biosiliceous sediments. *Life Sciences Research Reports* 44: 341-354

Bé, A. W. H., 1977. An ecological, zoogeographic and taxonomic review of Recent planktonic foraminifera. In: A. T. S. Ramsay (Editor), *Oceanic Micropaleontology*. Academic Press, London, pp. 1-100.

Bé, A. W. H., Caron, D. A. and Anderson, O. R., 1981. Effects of feeding frequency on life processes of the planktonic foraminifer *Globigerinoides sacculifer* in laboratory culture. *J. Mar. Biol. Assoc*., 61: 257-277.

Bé, A. W. H. and Tolderlund, D. S., 1971. Distribution and ecology of living planktonic foraminifera in surface waters of the Atlantic and Indian Oceans. In: B. M. Funnel and W. R. Riedel (Editors), *The Micropaleontology of Oceans*, Cambridge University Press, London, pp. 105-149.

Behrenfeld, M. J. and Falkowski, P. G., 1997. Photosynthetic rates derived from satellite-based chlorophyll concentration. *Limnol. Oceanogr*., 42: 1-20.

Bemis, B. E., Spero, H. J., Lea, D. W. and Bijma, J., 2000. Temperature influence on the carbon isotopic composition of *Globigerina bulloides* and *Orbulina universa* (planktonic foraminifera). *Mar. Micropal*., 38: 213-228.

Bender, M. L. and Keigwin, L. D. Jr., 1979. Speculations about the upper Miocene change in abyssal Pacific dissolved bicarbonate $\delta^{13}C$. *Earth. Planet. Sci. Lett*., 45: 383-393.

Bender, M. L. and Graham, D. W., 1981. On late Miocene abyssal hydrography. *Mar. Micropal*., 6: 451-464.

Berger, W. H., 1977. Carbon dioxide excursions and the deep sea record: aspects of the problem. In, N. R. Anderson and A. Malahoff (Editors), *The Fate of Fossil Fuel CO_2 in the Ocean*. Plenum Press, New York, pp. 505-542.

Berger, W. H. and Winterer, E. L., 1974. Plate stratigraphy and the fluctuating carbonate line. *Spec. Publ. International Assoc. Sedimentol*., 1: 11-48.

Berger, W. H. and Vincent, E., 1986. Deep-sea carbonates: Reading the carbon isotope signal. *Geol Rundsch*, 75: 249-269.

Berger, W. H., Diester-Hass, L. and Killingley, J. S., 1978a. Upwelling off Northwest Africa: the Holocene decrease as seen in carbon isotopes and sedimentological indicators. *Oceanol. Acta*, 1: 3-7.

Berger, W. H., Killingley, J. S. and Vincent, E., 1978b. Stable isotopes in deep-sea carbonates: Box core ERDC-92, West Equatorial Pacific. *Oceanol. Acta*, 1: 203-216.

Berger, W. H., Leckie, R. M., Janecek, T. R., Stax, R. and Takayama, T., 1993. Neogene carbonate sedimentation on Ontong Java Plateau: Highlights and open questions. *Proc. ODP, Sci. Res*., 130: 711-744.

Berggren, W. A. and Haq, B. U., 1976. The Andalusian Stage (Late Miocene): biostratigraphy, biochronology and paleoecology. *Palaeogeog., Palaeoclimatol., Palaeoecol*., 20: 67-129.

Berggren, W. A., Kent, D. V., Flynn, J. J. and Van Couvering, J. A., 1985. Cenozoic geochronology. *Geol. Soc. Am. Bull.*, 96: 211-260.

Berggren, W. A., Hilgen, F. J., Langereis, C. G., Kent, D. V., Obradovich, J. D., Raffi, I., Raymo, M. E. and Shackleton, N. J., 1995a. Late Neogene chronology: New perspectives in high-resolution stratigraphy. *Geol. Soc. Am. Bull.*, 107: 1272-1287.

Berggren, W. A., Kent, D. V., Swisher, C. C. I. and Aubrey, M. -P., 1995b. A revised Cenozoic geochronology and chronostratigraphy. Geochronology time scales and global stratigraphic correlation. *SEPM Spec. Publ.*, 54: 129-212.

Bickert, T., Haug, G. H. and Tiedemann, R., 2004. Late Neogene benthic stable isotope record of Ocean Drilling Program Site 999: Implications for Caribbean paleoceanography, organic carbon burial, and the Messinian Salinity Crisis. *Paleoceanogr.*, 19, PA1023, doi: 10.1029/2002PA000799.

Billups, K., 2002. Late Miocene through early Pliocene deep water circulation and climate change viewed from the sub-Antarctic South Atlantic. *Palaeogeogr. Palaeoclimatol., Palaeoecol.*, 185: 287-307.

Billups, K., Ravelo, C. A. and Zachos, J. C., 1997. Early Pliocene deep-water circulations; stable isotope evidence for enhanced northern component deep water. *Proc. ODP., Sci. Res.*, 154: 319-330.

Bishop, J. K. B., 1988. The barite-opal-organic carbon association in oceanic particulate matter. *Nature*, 331: 341-343.

Blanc, P. L. and Duplessy, J. C., 1982. The deep-water circulation during the Neogene and the impact of the Messinian salinity crisis. *Deep-Sea Res.*, 29: 1391-1414.

Bohrmann, G., Henrich, R. and Thiede, J., 1990. Miocene to Quaternary paleoceanography in the northern North Atlantic; variability in carbonate and biogenic opal accumulation. In: U. Bleil and J. Thiede (Editors), *Geological History of the Polar Oceans: Arctic versus Antarctic*, D. Reidel Publishing Company, Dordrecht-Boston, pp. 647-675.

Boland, F. M. and Hamon, B. V., 1970. The East Australian Current 1965-1968. *Deep-Sea Res.*, 17: 777-794.

Boyle, E. A. and Keigwin, L. 1987. North Atlantic thermohaline circulation during the past 20,000 years linked to high-latitude surface temperature. *Nature*, 330: 35-40.

Bradford-Grieve, J. M., Chang, F. H., Gall, M., Pickmere, S. and Richards, F., 1997. Size-fractionated phytoplankton standing stocks and primary production during austral winter and spring 1993 in the Subtropical Convergence region near New Zealand. *New Zealand J. Mar. Freshwater Res.*, 31: 201-224.

Bradford-Grieve, J. M., Murdoch, R., James, M., Oliver, M. and McLeod, J., 1998. Mesozooplankton biomass, composition, and potential grazing pressure on

phytoplankton during austral winter and spring 1993 in the Subtropical Convergence region near New Zealand. *Deep-Sea Res*., 45: 1709-1737.

Brass, G. W., 1976. The variation of marine $^{87}Sr/^{86}Sr$ ratio during Phanerozoic time: interpretation using a flux model. *Geochim. Cosmochim. Acta*, 40: 721-730.

Brewster, N. A., 1980. Cenozoic biogenic silica sedimentation in the Antarctic Ocean. *Geol. Soc. Am. Bull*., 91: 337-347.

Broecker, W. S., 1971. A kinetic model for the chemical composition of seawater. *Quaternary Res*., 1: 188-207.

Broecker, W. S., 1974. *Chemical Oceanography*. Harcourt Brace Jovanovich, New York, 214 pp.

Broecker, W. S. and Peng, T. H., 1982. *Tracers in the sea*. Lamont-Doherty Geol. Obs., Palisades, New York, 690 pp.

Broecker, W. S., Peteet, D. M. and Rind, D., 1985. Does the ocean-atmosphere system have more than one stable mode of operation? *Nature*, 315: 21-26.

Broecker, W. S. and Woodruff, F., 1992. Discrepancies in the oceanic carbon isotope record for the last fifteen million years? *Geochim. Cosmochim. Acta*, 56: 3259-3264.

Broekhuizen, N., Hadfield, M. and Taylor, A. H., 1998. Seasonal photoadaptation and diatom dynamics in temperate waters. *Mar. Ecol. Prog. Ser*., 175: 227-239.

Cane, M. A. and Molnar, P., 2001. Closing of the Indonesian seaway as a precursor to east African aridification around 3-4 million years ago. *Nature*, 411: 157-162.

Cande, S. C. and Kent, D. V., 1992. A new geomagnetic polarity time scale for the Late Cretaceous and Cenozoic. *J. Geophys. Res*., 97:13,917-13,951.

Cande, S. C. and Kent, D. V., 1995. Revised calibration of the geomagnetic polarity time scale for the Late Cretaceous and Cenozoic. *J. Geophys. Res*., 100: 6093-6095.

Carter, R. M., McCave, I. N., Richter, C., Carter, L., et al., 1999. *Proc. ODP., Init. Repts*., 181 [CD-ROM]. Available from: Ocean Drilling Program, Texas A&M University, College Station, TX 77845-9547, U.S.A.

Chang, F. H. and Gall, M., 1998. Phytoplankton assemblages and photosynthetic pigments during winter and spring in the Subtropical Convergence region near New Zealand. *New Zealand J. Mar. Freshwater Res*., 32: 515-530.

Chester, R., 1990. *Marine Geochemistry*. Unwin Hyman, London, pp. 698.

Chiswell, S. M., 1994. Variability in sea surface temperature around New Zealand from AVHRR images. *New Zealand J. Mar. Freshwater Res*., 28: 179-192.

Chiswell, S. M., 2001. Eddy energetics in the Subtropical Front over the Chatham Rise, New Zealand. *New Zealand J. Mar. Freshwater Res.*, 35: 1-15.

Chiswell, S. M., Toole, J. and Church, J., 1997. Transports across the Tasman Sea from WOCE repeat sections: the East Australian Current 1990-94. *New Zealand J. Mar. Freshwater Res.*, 31: 469-475.

Chow, T. J. and Goldberg, E. D., 1960. On the marine geochemistry of barium. *Geochim. Cosmochim. Acta*, 20: 192-198.

Ciesielski, P. F., 1986. Middle Miocene to Quaternary diatom biostratigraphy of Deep Sea Drilling Project Site 594, Chatham Rise, Southwest Pacific. *Init. Repts. DSDP*., 90: 863-885.

Ciesielski, P. F. and Weaver, F. M., 1974. Early Pliocene temperature changes in the Antarctic seas. *Geology*, 2: 511-515.

Ciesielski, P. F., Ledbetter, M. T. and Ellwood, B. B., 1982. The development of Antarctic glaciation and the Neogene paleoenvironment of the Maurice Ewing Bank. *Mar. Geol*., 46: 1-51.

Clauzon, G., Suc, J.-P., Gautier, F., Berger, A. and Loutre, M.-F., 1996. Alternate interpretation of the Messinian salinity crisis: Controversy resolved? *Geology*, 24: 363-366.

Coale, K. H., Johnson, K. S., Fitzwater, S. E., Gordon, R. M., Tanner, S., Chavez, S. P., Ferioli, L., Sakamoto, C., Rogers, P., Millero, F., Steinberg, P., Nightingale, P. et al., 1996. A massive phytoplankton bloom induced by an ecosystem-scale iron fertilization experiment in the equatorial Pacific Ocean. *Nature*, 383: 495-501.

Comiso, J. C., McLain, C. R., Sullivan, C. W., Ryan, J. P. and Leonard, C. L., 1993. Coastal zone colour scanner pigment concentrations in the Southern Ocean and relationships to geophysical surface features. *J. Geophys. Res*., 98: 2419-2451.

Coplen, T. -B., Kendall, C., Hopple, J., 1983. Comparison of stable isotope reference samples. *Nature*, 302: 236-238.

Curry, K. I. and Hunter, K. A., 1998. Surface water carbon dioxide in the waters associated with the subtropical convergence, east of New Zealand. *Deep-Sea Res., I*, 45: 1765-1777.

Curry, W. B., Shackleton, N. J., Richter, C., et al., 1995. Leg 154 synthesis. *Proc. ODP., Init. Repts.*, 154: 421-442.

Dercourt, J., Ricou, L. and Vrielynck, E., 1992. *Atlas: Tethys Paleoenvironmental Maps*. Gauthier-Villars, Paris, pp.307.

Dehairs, F., Chesselet, R. and Jedwab, J., 1980. Discrete suspended particles of barite and the barium cycle in the open ocean. *Earth Planet. Sci. Lett*., 49: 528-550.

Delaney, M. L. and Filippelli, G. M., 1994. An apparent contradiction in the role of phosphorus in Cenozoic chemical mass balances for the world ocean. *Paleoceanogr*., 9: 513-527.

Dickens, G. R. and Owen, R. M., 1994. Late Miocene-early Pliocene manganese reduction in the central Indian Ocean: Expansion of the intermediate water oxygen minimum zone. *Paleoceanogr*., 9: 169-181.

Dickens, G. R. and Owen, R. M., 1996. Sediment geochemical evidence for an early-middle Gilbert (early Pliocene) productivity peak in the North Pacific Red Clay Province. *Mar. Micropal*., 27: 107-120.

Dickens, G. R. and Barron, J. A., 1997. A rapidly deposited pennate diatom ooze in Upper Miocene-Lower Pliocene sediment beneath the North Pacific polar front. *Mar. Micropal*., 31: 177-182.

Dickens, G. R. and Owen, R. M., 1999. The latest Miocene-early Pliocene biogenic bloom: A revised Indian Ocean perspective. *Mar. Geol*., 161: 75-91.

Diester-Haass, L., Meyers, P. A. and Vidal, L., 2002. The late Miocene onset of high productivity in the Benguela Current upwelling system as part of a global pattern. *Mar. Geol*., 180: 87-103.

Diester-Haass, L., Meyers, P. A. and Bickert, T., 2004. Carbonate crash and biogenic bloom in the late Miocene: Evidence from ODP Sites 1085, 1086, and 1087 in the Cape Basin, southeast Atlantic Ocean. *Paleoceanogr*., 19, PA1007, doi: 10.1029/2003PA000933, 2004.

Dobson, D. M., Dickens, G. R. and Rea, D. K., 2001. Terrigenous sediment on Ceara Rise; a Cenozoic record of South American orogeny and erosion. *Palaeogeog., Palaeoclimatol., Palaeoecol*., 165: 215-229.

Douglas, R. G. and Savin, S. M., 1973. Oxygen and carbon isotope analyses of Cretaceous and Tertiary foraminifera from the Central North Pacific. *Init. Repts. DSDP*., 17: 591-605.

Douglas, R. G. and Savin, S. M., 1973. Oxygen and carbon isotope analyses of Tertiary and Cretaceous microfossils from Shatsky Rise and other sites in the North Pacific Ocean. *Init. Repts. DSDP*., 32: 509-520.

Drewry, D. J., 1978. Aspects of the early evolution of West Antarctic ice. In: E. M. Van Zinderen Bakker (Editor), *Antarctic Glacial History and World Palaeoenvironments*. A. A. Balkema, Rotterdam, pp. 25-32.

Dudley, W. C. and Nelson, C. S., 1989. Quaternary surface-water isotope signal from calcareous nannofossils at DSDP Site 593, Southern Tasman Sea. *Mar. Micropal*., 13: 353-373.

Dudley, W. C. and Nelson, C. S., 1994. The influence of non-equilibrium isotope fractionation on the Quaternary calcareous nannofossil stable isotope signal in the southwest Pacific Ocean, DSDP Site 594. *Mar. Micropal*., 24: 3-27.

Dudley, W. C., Duplessy, J. C., Blackwelder, P. L., Brand, L. E. and Guillard, R. R. L., 1980. Coccoliths in Pleistocene-Holocene nannofossil assemblages. *Nature*, 285: 222-223.

Dudley, W. C., Blackwelder, P., Brand, L. and Duplessy, J. -C., 1986. Stable isotopic composition of coccoliths. *Mar. Micropal*., 10: 1-8.

Dugdale, R. C. and Wilkerson, F. P., 1998. Silicate regulation of new production in the equatorial Pacific upwelling. *Nature*, 391: 270-273.

Dugdale, R. C., Wilkerson, F. P. and Minas, H. J., 1995. The role of a silicate pump in driving new production. *Deep-Sea Res.*, 42: 697-719.

Duque-Carol., H., 1990. Neogene stratigraphy, paleoceanography and paleobiogeography in the northwest South America and the evolution of the Panama seaway. *Palaeogeogr. Palaeoclimatol. Palaeoecol.*, 77: 203-234.

Dymond, J., 1981. Geochemistry of Nazca Plate surface sediments: an evaluation of hydrothermal, biogenic, detrital, and hydrogenous sources. In: L. D. Kulm, W. J. Schweller, R. A. Prince, D. Laverne, J. Dymond, E. J. Dasch, D. M. Hussong and R. Roderick (Editors), *Nazca Plate: Crustal Formation and Andean Convergence*. Geol. Soc. Am. Mem., 154, pp. 133-174.

Dymond, J., Suess, E. and Lyle, M., 1992. Barium in deep-sea sediment: A geochemical proxy for paleoproductivity. *Paleoceanogr*., 7: 163-181.

Edmond, J. M., 1992. Himalayan tectonics, weathering processes, and the strontium isotope record of marine limestones. *Science*, 258: 1594-1597.

Elderfield, H., 1986. Strontium isotope stratigraphy. *Palaeogeogr., Palaeoclimatol., Palaeoecol*., 57: 71-90.

Elmstrom, K. M. and Kennett, J. P., 1986. Late Neogene paleoceanographic evolution of site 590: Southwest Pacific. In: J. P. Kennett and C. C. von der Borch (Editors), *Init. Repts. DSDP*, 90, Part 2, pp. 1361-1381.

Emery, W. J. and Meincke, J., 1986. Global water masses: summary and review. *Oceanol. Acta*, 9: 383-391.

Farrell, J. W., Raffi, I., Janecek, T. R., Murray, D. W., Levitan, M., Delaney, M., Dadey, K. A., Emeis, K.-C., Lyle, M., Flores, J.-A. and Hovan, S., 1995a. Late Neogene sedimentation patterns in the eastern equatorial Pacific. *Proc. ODP, Sci. Res*., 138: 717-756.

Farrell, J. W., Clemens, S. C. and Gromet, L. P., 1995b. Improved chronostratigraphic reference curve of late Neogene seawater $^{87}Sr/^{86}Sr$. *Geology*, 23: 403-406.

Faure, G., 1998. *Principles and Applications of Geochemistry*. Prentice-Hall, 600 pp.

Fenner, J., Carter, L. and Stewart, R., 1992. Late Quaternary paleoclimatic and paleoceanographic change over northern Chatham Rise, New Zealand. *Mar. Geol*., 108: 383-404.

Filippelli, G. M., 1997. Intensification of the Asian monsoon and a chemical weathering event in the late Miocene-early Pliocene: Implications for late Neogene climate change. *Geology*, 25: 27-30.

Filippelli, G. M. and Delaney, M. L., 1995. Phosphorus geochemistry and accumulation rates in the eastern equatorial Pacific Ocean: results from leg 138. *Proc. ODP, Sci. Res*., 138: 757-767.

Fischer, A. G. and Arthur, M. A., 1977. Secular variations in the pelagic realm. In, H. E. Cook and P. Enos (Editors), *Deep Water Carbonate Environments*. Soc. Econ. Paleontol. Mineral., Spec. Publ., 25: 19-50.

Froelich, P. N., Bender, M. L. and Heath, G. R., 1977. Phosphorus accumulation rates in metalliferous sediments on the East Pacific Rise. *Earth Planet. Sci. Lett*., 34: 351-359.

Froelich, P. N., Malone, P. N., Hodell, D. A., Ciesislski, P. F., Warnke, D. A., Westall, F., Hailwood, E. A., Nobes, D. C., Fenner, J., Mienert, J., Mwenifumbo, C. J. and Müller, D. W., 1991. Biogenic opal and carbonate accumulation rates in the subantarctic South Atlantic: The late Neogene of Meteor Rise Site 704. *Proc. ODP., Sci. Res*., 114: 515-550.

Gaina, C., Müller, D. R., Royer, J. -Y., Stock, J., Hardebeck, J. L. and Symonds, P., 1998. The tectonic history of the Tasman Sea; a puzzle with 13 pieces. *J. Geophys. Res*., 103: 12,413-12,433.

Gartner, S., Jr., 1992. Miocene nannofossil chronology in the North Atlantic, DSDP Site 608. *Mar. Micropal*., 18: 307-331.

Gersonde, R. and Bárcena, M.A., 1998. Revision of the late Pliocene-Pleistocene diatom biostratigraphy for the northern belt of the Southern Ocean. *Micropaleontol*., 44: 1-15.

Gersonde, R., Hodell, D. A., Blum, P., et al., 1999. *Proc. ODP, Init. Repts*., 177 [CD-ROM]. Available from: Ocean Drilling Program, Texas A&M University, College Station, TX 77845-9547, U.S.A.

Ghosh, P., Padia, J. T. and Mohindra, R., 2004. Stable isotopic studies of Palaeosol sediment from upper Siwalik of Himachal Himalaya; evidence for high monsoonal intensity during late Miocene? *Palaeogeog., Palaeoclimatol., Palaeoecol*., 206: 103-114.

Godfrey, J. S., Cresswell, G. R., Golding, T. J. and Pearce, A. F., 1980. The separation of the East Australian Current. *J. Phys. Oceanogr*., 10: 430-440.

Goodney, D. E., Margolis, S. V., Dudley, W. C., Kroopnick, P. and Williams, D. F., 1980. Oxygen and carbon isotopes of recent calcareous nannofossils as paleoceanographic indicators. *Mar. Micropal*. 5: 31-42.

Goldberg, E. D. and Arrhenius, G. O. S., 1958. Chemistry of pelagic sediments. *Geochim. Cosmochim. Acta*, 13: 153-212.

Gupta, A. K. and Thomas, E., 1999. Latest Miocene - Pleistocene productivity and deep-sea ventilation in the northwestern Indian Ocean (Deep Sea Drilling Project Site 219). *Paleoceanogr*., 14: 62-73.

Hagino, K., Okada, H. and Matsuoka, H., 2000. Spatial dynamics of coccolithophores in the Equatorial Western-Central Pacific Ocean. *Mar. Micropal*., 39: 53-72.

Hamilton, W., 1979. Tectonics of the Indonesian region. *U.S. Geol. Survey Prof. Paper*, 1078, U.S. Gov. Print. Office, Washington, D. C., pp. 345.

Haq, B. U., Worsley, T. R., Burckle, L. H., Douglas, R. G., Keigwin Jr., L., D., Opdyke, N. D., Savin, S., M., Sommer II, M., A., Vincent, E. and Woodruff, F., 1980. Late Miocene marine carbon-isotopic shift and synchroneity of some phytoplanktonic biostratigraphic events. *Geology*, 8: 427-431.

Haq, B. U., Hardenbol, J. and Hardenbol, J., 1987. Chronology of fluctuating sea level since the Triassic. *Science*, 235: 1136-1167.

Harrison, K. G., 2000. Role of increased marine silica input on paleo-pCO_2 levels. *Paleoceanogr*., 15: 292-298.

Haug, G. H. and Tiedemann, R., 1998. Effect of the formation of the Isthmus of Panama on Atlantic Ocean thermohaline circulation. *Nature*, 393: 673-676.

Haug, G. H., Maslin, M. A., Sarnthein, M., Tiedemann, R. and Stax, R., 1995. Evolution of Northwest Pacific sedimentation patterns since 6 Ma: site 882. *Proc. ODP., Sci. Res.*, 145: 293-314.

Haug, G. H., Tiedemann, R., Zahn, R. and Ravelo, A. C., 2001. Role of Panama uplift on oceanic freshwater balance. *Geology*, 29: 207-210.

Hay, W. W., 1996. Tectonics and climate. *Geol Rundsch*, 85: 409-437.

Hayes, D. E. and Ringis, J., 1973. Seafloor spreading in the Tasman Sea. *Nature*, 243: 454-458.

Hayward, B. W. H., Neil, H., Carter, R., Grenfell, H. R., and Hayward, J. J., 2002. Depth distribution of Recent deep-sea benthic foraminifera east of New Zealand, and their potential for improving paleobathymetric assessments of Neogene microfaunas. *New Zealand J. Geol. Geophys*., 44: 555-587.

Hayward, B. W. H., Grenfell, H. R., Rowan, C. and Hayward, J. J., 2004. Benthic foraminiferal proxy evidence for the Neogene palaeoceanographic history of the Southwest Pacific, east of New Zealand. *Mar. Geol.*, 205: 147-184.

Heath, R. A., 1985. A review of the physical oceanography of the seas around New Zealand - 1982. *New Zealand J. Mar. Freshwater Res.*, 19: 79-124.

Hermelin, J. O. R., 1992. Variations in the benthic foraminiferal fauna of the Arabian Sea: a response to changes in upwelling intensity? In, C. P. Summerhayes, W. L. Prell and Emeis, K.-C. (Editors), *Upwelling Systems: Evolution since the Early Miocene*. Geol. Soc. Spec. Publ., London, 64: 151-166.

Hermoyian, C. S. and Owen, R. M., 2001. Late Miocene - early Pliocene biogenic bloom: Evidence from low-productivity regions of the Indian and Atlantic Oceans. *Paleoceanogr.*, 16: 95-100.

Herguera, J. C. and Berger, W. A., 1991. Paleoproductivity from benthic foraminifera abundance: Glacial to postglacial change in the west-equatorial Pacific. *Geology*, 19: 1173-1176.

Hess, J., Bender, M. and Schilling, J.-G., 1986. Seawater $^{87}Sr/^{86}Sr$ evolution from Cretaceous to Present. *Science*, 231: 979-984.

Hill, K. C. and Gleadow, A. J. W., 1989. Uplift and thermal history of the Papuan fold belt, Papua New Guinea: apatite fission track analysis. *Austr. J. Earth Sci.*, 36: 515-539.

Hillenbrand, C.-D. and Fuetterer, D. K., 2002. Neogene to Quaternary deposition of opal on the continental rise west of the Antarctic Peninsula, ODP Leg 178, sites 1095, 1096, and 1101. *Proc. ODP., Sci. Res.*, 178 [CD-Rom]. Available from: Ocean Drilling Program, Texas A&M University, College Station, TX 77845-9547, U.S.A.

Hodell, D. A. and Kennett, J. P., 1986. Late Miocene-early Pliocene stratigraphy and paleoceanography of the South Atlantic and southwest Pacific Oceans: a synthesis. *Paleoceanogr.*, 1: 285-311.

Hodell, D. A. and Warnke, D. A., 1991. Climatic evolution of the Southern Ocean during the Pliocene Epoch from 4.8 to 2.6 million years ago. *Quat. Sci. Rev.*, 10: 205-214.

Hodell, D. A., Elmstrom, K. M. and Kennett, J. P., 1986. Latest Miocene benthic $\delta^{18}O$ changes, global ice volume, sea level and the 'Messinian salinity crisis'. *Nature*, 320: 411-414.

Hodell, D. A., Mueller, P. A., McKenzie, J. A. and Mead, G. A., 1989. Strontium isotope stratigraphy and geochemistry of the late Neogene Ocean. *Earth. Planet. Sci. Lett.*, 92: 165-178.

Hodell, D. A., Benson, R. H., Kent, D. V., Boersma, A. and Racic-El Bied, K., 1994. Magnetostratigraphic, biostratigraphic, and stable isotope stratigraphy of an upper Miocene drill core from the Sale Briqueterie (northwestern Morocco): A high resolution chronology for the Messinian stage. *Paleoceanogr.*, 9: 835-855.

Hodell, D. A., Curtis, J. H., Sierro, F. J. and Raymo, M. E., 2001. Correlation of late Miocene to early Pliocene sequences between the Mediterranean and North Atlantic. *Paleoceanogr.*, 16: 164-178.

Hodell, D. A., gersonde, R. and Blum, P., 2002. Leg 177 synthesis: Insights into Southern Ocean paleoceanography on tectonic to millenial timescales. *Proc. ODP., Sci. Res.*, 177: 1-54.

Hornibrook, N. de B., 1976. *Globorotalia truncatulinoides* and the Pliocene-Pleistocene boundary in northern Hawkes Bay, New Zealand. In: Y. Takayanagi and T. Saito (editors), *Progress in micropaleontology*, American Museum of Natural History, NY., pp. 83-102.

Hornibrook, N. de B., 1992. New Zealand Cenozoic marine paleoclimates; a review based on the distribution of some shallow water and terrestrial biota. In: R. Tsuchi and J. C. Ingle, Jr. (Editors), *Pacific Neogene; environment, evolution, and events*, Univ. Tokyo Press, Tokyo, pp. 83-106.

Hornibrook, N. de B. and Jenkins, D. G., 1994. DSDP 594, Chatham Rise, New Zealand - Late Neogene planktonic foraminiferal biostratigraphy revisited. *J. Micropal.*, 13: 93-101.

Hovan, S. A., 1995. Late Cenozoic atmospheric circulation intensity and climatic history recorded by eolian deposition in the eastern Equatorial Pacific Ocean, Leg 138. *Proc. ODP., Sci. Res.*, 138: 615-625.

Howard-Williams, C., Davies-Colley, R. and Vincent, W. F., 1995. Optical properties of the coastal and oceanic waters off South Island, New Zealand: regional variation. *New Zealand J. Mar. Freshwater Res.*, 29: 589-602.

Hsü, K. J., Cita, M. B. and Ryan, W. B. F., 1973. The origin of the Mediterranean evaporites. *Init. Repts. DSDP.*, 13: 1203-1231.

Hsü, K. J. and Shipboard Scientific Party, 1978. History of the Mediterranean Salinity Crisis. *Init. Repts. DSDP.*, 42: 1053-1077.

Ivanova, E. M., Conan, S. M. H., Peeters, F. J. C. and Troelstra, S. R., 1999. Living *Neogloboquadrina pachyderma* sin and its distribution in the sediments from Oman and Somalia upwelling areas. *Marine Micropal.*, 36: 91-107.

Jenkins, D. G. and Srinivasan, M. S., 1986. Cenozoic planktonic foraminifers from the equator to the subantarctic of the Southwest Pacific. *Init. Repts. DSDP*, 90: 795-834.

Kahn, M. I., 1979. Non-equilibrium oxygen and carbon isotopic fractionation in tests of living planktonic foraminifera. *Oceanol. Acta*, 2: 195-208.

Kahn, M. I. and Williams, D. F., 1981. Oxygen and carbon isotopic composition of living planktonic foraminifera from the northeast Pacific Ocean. *Palaeogeogr., Palaeoclimatol., Palaeoecol*., 33: 47-69.

Kawagata, S., 2001. Tasman front shifts and associated paleoceanogrphic changes during the last 250,000 years: foraminiferal evidence from the Lord Howe Rise. *Marine Micropal*., 41: 167-191.

Kawahata, H., 2002. Shifts in oceanic and atmospheric boundaries in the Tasman Sea (Southwest Pacific) during the Late Pleistocene: evidence from organic carbon and lithogenic fluxes. *Palaeogeogr., Palaeoclimatol., Palaeoecol*., 184: 225-249.

Keigwin Jr., L. D., 1979. Late Cenozoic stable isotope stratigraphy and paleoceanography of DSDP sites from the east equatorial and central north Pacific Ocean. *Earth. Planet. Sci. Lett*., 45: 361-382.

Keigwin Jr., L. D., 1982a. Isotope paleoceanography of the Caribbean and east Pacific: role of Panama uplift in late Neogene time. *Science*, 217: 350-353.

Keigwin Jr., L. D., 1982b. Neogene planktonic foraminifers from Deep Sea Drilling Project Sites 502 and 503. *Init. Repts. DSDP*., 68: 269-288.

Keigwin Jr., L. D., 1982c. Stable isotope stratigraphy and paleoceanography of sites 502 and 503. *Init. Repts. DSDP*., 68: 445-453.

Keigwin Jr., L. D. and Shackleton, N. J., 1980. Uppermost Miocene carbon isotope stratigraphy of a piston core in the equatorial Pacific. *Nature*, 284: 613-614.

Keigwin Jr., L. D., Aubrey, M.-P. and Kent, D. V., 1987. North Atlantic late Miocene stable isotope stratigraphy, biostratigraphy and magnetostratigraphy. *Init. Repts. DSDP*, 94: 935-963.

Keller, G., 1981. Miocene biochronology and paleoceanography of the North Pacific. *Mar. Micropal*., 6: 535-551.

Keller, G., 1985. Depth stratification of planktonic foraminifers in the Miocene ocean. In: J. P. Kennett (Editor), *The Miocene ocean; paleoceanography and biogeography*, Mem. Geol. Soc. Am., 163: 177-195.

Keller, G., Zenker, C. E. and Stone, S. M., 1989. Late Neogene history of the Pacific-Caribbean gateway. *J. South Am. Earth Sci*., 2: 73-108.

Kemp, A. E. S. and Baldauf, J. G., 1993. Vast Neogene laminated diatom mat deposits from the eastern equatorial Pacific Ocean. *Nature*, 362: 141-144.

Kemp, A. E. S., Baldauf, J. G. and Pearce, R. B., 1995. Origins and paleoceanographic significance of laminated diatom ooze from the eastern equatorial Pacific Ocean (Leg 138). *Proc. ODP., Sci. Res.*, 128: 641-645.

Kennett, J. P., 1986. Miocene to early Pliocene oxygen and carbon isotope stratigraphy of the Southwest Pacific, DSDP Leg 90. *Init. Repts. DSDP*, 90: 1383-1411.

Kennett, J. P., 1995. A review of polar climatic evolution during the Neogene, based on the marine sediment record. In: E. Vrba et al. (Editors), *Paleoclimate and Evolution With Emphasis on Human Origins*, Yale Univ. Press, New York, pp. 49-64.

Kennett, J. P. and von der Borch, C. C., 1986. Southwest Pacific Cenozoic paleoceanography. *Init. Repts. DSDP*, 90: 1493-1517.

Kennett, J. P., Keller, G. and Srinivasan, M. S., 1985. Miocene planktonic foraminiferal biogeography and paleoceanographic development of the Indo-Pacific. In: J. Kennett (Editor), *The Miocene Ocean: paleoceanography and biogeography*, Geol. Soc. Am. Mem., 163: 197-236.

Kennett, J. P., von der Borch, C. C. et al., 1986. *Initial Reports of DSDP*, 90, Part 1. U.S. Government Printing Office, Washington, 744 pp.

Kent, D. V., 1999. Orbital tuning of geomagnetic polarity timescales. *Phil. Trans. R. Soc. Lond*. A., 357: 1995-2007.

Kowalski, E. A. and Meyers, P. A., 1997. Glacial-interglacial variations in Quaternary production of marine organic matter at DSDP Site 594, Chatham Rise, southeastern New Zealand margin. *Mar. Geol.*, 140: 249-263.

Kroenke, L. W., Berger, W. H., Janecek, T. R., et al., 1991. *Proc. ODP., Init. Repts.*, 130, College Station, Texas.

Kroon, D., Steens, T. and Troelstra, S. R., 1991. Onset of monsoonal related upwelling in the western Arabian Sea as revealed by planktonic foraminifers. *Proc. ODP., Sci. Res.*, 117: 257-263.

Kroopnick, P. M., Margolis, S. V. and Wong, C. S., 1977. $\delta^{13}C$ variations in marine carbonate sediments as indicators of the CO_2 balance between the atmosphere and oceans. In: N. R. Anderson and A. Malahoff (Editors), *The Fate of Fossil Fuel CO_2 in the ocean*. Plenum Press, New York, p-p??

Kroopnick, P. M., 1985. The distribution of ^{13}C of ΣCO_2 in the world oceans. *Deep-Sea Res.*, 32: 57-84.

Kump, L. R. and Arthur, M. A., 1999. Interpreting carbon-isotope excursions: carbonates and organic matter. *Chem. Geol.*, 161:181-198.

Kurihara, K. and Kennett, J. P., 1992. Paleoceanographic significance of Neogene benthic foraminiferal changes in a Southwest Pacific bathyal depth transect. *Mar. Micropal.*, 19: 181-199.

Kwiek, P. B. and Ravelo, A. C., 1999. Pacific Ocean intermediate and deep water circulation during the Pliocene. *Palaeogeog., Palaeoclimatol., Palaeoecol.*, 154: 191-217.

Larsen, H. C., Saunders, A. D., Clift, P. B., Beget, J., Wei, W. and Spezzaferri, S., 1994. Seven million years of glaciation in Greenland. *Science*, 264: 952-955.

Lazarus, D., Spencer-Cervato, C., Pianka-Biolzi, M., Beckmann, J. P., von Salis, K., Hilbrecht, H. and Thierstein, H., 1992. *Revised Chronology of Neogene DSDP Holes from the World Ocean*. Ocean Drilling Program Technical Note 24, Texas A&M University, College Station.

Leinen, M., 1979. Biogenic silica accumulation in the central equatorial Pacific and its implications for Cenozoic paleoceanography. *Geol. Soc. Am. Bull.*, 90: 1310-1376.

Leinen, M., Cwienk, D., Heath, G. R., Biscaye, P. E., Kolla, V., Thiede, J. and Dauphin, J. P., 1986. Distribution of biogenic silica and quartz in recent deep-sea sediments. *Geology*, 14: 199-203.

Levitus, S., 1982. Climatological Atlas of the World Ocean. *NOAA Prof. Paper*., 13: 1-173.

Lewis, K.B., Bennett, D.J., Herzer, R.H. and von der Borch, C.C., 1985. Seismic stratigraphy and structure adjacent to an evolving plate boundary, western Chatham Rise, New Zealand. *Init. Repts. DSDP*, 90: 1325-1337.

Li, J., Wang, R. and Li. B., 2002. Variations of opal accumulation rates and paleoproductivity over the past 12 Ma at ODP Site 1143, southern South China Sea. *Chinese Sci. Bull*., 47: 596-598.

Lilley, F. E. M., Filloux, J. H., Bindoff, N. L., Ferguson, I . J. and Mulhearn, P. J., 1986. Barotropic flow of a warm-core ring from seafloor electric measurements. *J. Geophys. Res*., 91: 12,979-12,984, 13,109.

Little, M. G., Schneider, R. R., Kroon, D., Price, B., Bickert, T. and Wefer, G., 1997. Rapid palaeoceanographic changes in the Benguela upwelling system for the last 160,000 years as indicated by abundances of planktonic foraminifera. *Palaeogeog., Palaeoclimatol., Palaeoecol*., 130: 135-161.

Lohman, W. H., 1986. Calcareous nannoplankton biostratigraphy of the southern Coral Sea, Tasman Sea, and southwestern Pacific Ocean, Deep Sea Drilling Project Leg 90: Neogene and Quaternary. *Init. Repts. DSDP*, 90: 763-793.

Longhurst, A., 1998. *Ecological Geography of the Sea*. Academic Press, San Diego, CA, pp. 398.

Loutit, T. S. and Kennett, J. P., 1979. Application of carbon isotope stratigraphy to late Miocene shallow marine sediments, New Zealand. *Science*, 204: 1196-1199.

Loutit, T. S., Kennett, J. P. and Savin, S. M., 1983. Miocene equatorial and southwest Pacific paleoceanography from stable isotopic evidence. *Mar. Micropal.* 8: 215-233.

Loutit, T. S. and Keigwin, Jr., L. D., 1982. Stable isotopic evidence for latest Miocene sea-level fall in the Mediterranean region. *Nature*, 300: 163-166.

Lyle, M. and Pisias, N. G., 1990. Ocean circulation and atmospheric CO_2 changes; coupled use of models and paleoceanographic data. *Paleoceanogr.*, 5: 15-41.

Lyle, M., Murray, D. W., Finney, B. P., Dymond, J., Robbins, J. M. and Brooksforce, K., 1988. The record of late Pleistocene biogenic sedimentation in the eastern tropical Pacific Ocean. *Paleoceanogr.*, 3: 39-59.

Mackensen, A., Schmiedl, D.K., Harloff, J., Giese, M., 1995. Deep-sea foraminifera in the South Atlantic Ocean: Ecology and assemblage generation. *Micropaleontol.*, 41: 342-358.

Marchesiello, P. and Middleton, J. H., 2000. Modeling the East Australian Current in the Western Tasman Sea. *J. Phys. Oceanogr.*, 30: 2956-2971.

Martin, J. H., Coale, H., Johnson, K. S., Fitzwater, S. E., Gordon, R. M., Tanner, S. J., Hunter, C. N., Elrod, V. A., Nowicki, J. L., Coley, T. L., Barber, R. T., Lindley, S. et al., 1994. Testing the iron hypothesis in ecosystems of the equatorial Pacific Ocean. *Nature*, 371: 123-129.

Martin, J.-M. and Whitfield, M., 1983. The significance of the river input of chemical elements to the ocean. In: C. S. Wong, E. A. Boyle, K. W. Bruland, J. D. Burton and E. D. Goldberg (Editors), *Trace metals in seawater*, Plenum, New York, pp. 265-296.

Martínez, J. I., 1994. Late Pleistocene palaeoceanography of the Tasman Sea: Implications for the dynamics of the warm pool in the western Pacific. *Palaeogeogr., Palaeoclimatol., Palaeoecol.*, 112: 19-62.

Maslin, M. A., Shackleton, N. J. and Pflaumann, U., 1995. Surface water temperature, salinity, and density changes in the northeast Atlantic during the last 45,000 years: Heinrich events, deep water formation, and climatic rebounds. *Paleoceanogr.*, 10: 527-544.

Maslin, M. A., Haug, G. H., Sarnthein, M. and Tiedemann, R., 1996. The progressive intensification of northern hemisphere glaciation as seen from the North Pole. *Geol Rundsch*, 85: 452-465.

Mata, M. M., Tomczak, M., Wijffels, S. and Church, J. A., 2000. East Australian Current volume transports at 30 degrees S; estimates from the World Ocean

Circulation Experiment hydrogeologic sections PR11/P6 and the PCM3 current meter array. *J. Geophys. Res*., 105: 28,509-28,526.

McCartney, M. S., 1977. Subantarctic mode water. In: M. Angel (editor), *A Voyage of Discovery*. Pergamon, Oxford, pp. 103-119.

McClatchie, S., Coombs, R. F., Macaulay, G., 2001. Are there more fish in the front? *NIWA Water and Atmosphere*, 9 (1), 13-16.

Mead, G. A., Hodell, D. A., Müller, D. W. and Ciesielski, P. F., 1991. Fine-fraction carbonate oxygen and carbon isotope results from site 704: implications for movement of the Polar Front during the late Pliocene. *Proc. ODP, Sci. Res*., 114: 437-458.

Mikkelsen, N., 1990. Cenozoic diatom biostratigraphy and paleoceanography of the western equatorial Indian Ocean. *Proc. ODP., Sci. Res*., 115: 411-432.

Miller, K. G. and Fairbanks, R. G., 1983. Evidence for Oligocene-Middle Miocene abyssal circulation changes in the western North Atlantic. *Nature*, 306: 250-253.

Miller, K. G. and Fairbanks, R. G., 1985. Oligocene-Middle Miocene global carbon and abyssal circulation changes. In, E. Sundquist and W. Broecker (Editors), The Carbon Cycle and Atmospheric CO_2: Natural Variations Archaean to Present. *Am. Geophys. Union, Geophys. Monograph*, 32: 469-486.

Miller, K. G., Feigenson, M. D., Wright, J. D. and Clement, B. M., 1991. Miocene isotope reference section, Deep Sea Drilling Project site 608: An evaluation of isotope and biostratigraphic resolution. *Paleoceanogr*., 6: 33-52.

Molnar, P., England, P. and Martinod, J., 1993. Mantle dynamics, uplift of the Tibetan Plateau, and the Indian monsoon. *Rev. Geophys.*, 31: 357-396.

Moody, J. B., Chaboudy, L. R., Jr. and Worsley, T. R., 1988. Pacific pelagic phosphorus accumulation during the last 10 m.y. *Paleoceanogr*., 3: 113-136.

Mora, J., 2003. Variations in the accumulation of marine organic matter and carbonates at Leg 186 sites. *Proc. ODP., Sci. Res*., 186 [CD-ROM]. Available from: Ocean Drilling Program, Texas A&M University, College Station, TX 77845-9547, U.S.A.

Moran, S. B. and Moore, R. M., 1988a. Evidence from mesocosm studies for biological removal of dissolved aluminum from seawater. *Nature*, 335: 706-708.

Moran, S. B. and Moore, R. M., 1988b. Temporal variations in dissolved and particulate aluminum during a spring bloom. *Est. Coast. Shelf Sci*., 27: 205-215.

Morgans, H. E. G., Scott, G. H., Beu, A. G., Graham, I. J., Mumme, T. C., George, W. S. and Strong, C. P., 1996. New Zealand Cenozoic Time Scale (version 11/96). *Inst. Geol. Nucl. Sci., Rep.* 96/38:1–12.

Morin, R. H., 1986. Physical properties of calcareous sediments from the southwest Pacific. *Init. Repts. DSDP*, 90: 1239-1246.

Mudie, P. L., Vernal, A. de. and Head, M. J., 1990. Neogene to Recent palynostratigraphy of circum-Arctic basins: results of ODP Leg 104, Norwegian Sea, Leg 105, Baffin Bay, and DSDP site 611, Irminger Sea. In: U. Bleil and J. Thiede (Editors), *Geological History of the Polar Oceans: Arctic versus Antarctic*, D. Reidel Publishing Company, Dordrecht-Boston, pp. 609-646.

Mulhearn, P. J., 1983. Deep currents of the northern Tasman Sea Basin. *Deep-Sea Res*., 30: 1119-1126.

Mulhearn, P. J., 1987. The Tasman Front: A study using satellite infrared imagery. *J. Phys. Oceanogr.*, 17: 1148-1155.

Mulhearn, P. J., Filloux, F. E. M., Bindoff, N. L. and Ferguson, I. J., 1986. Abyssal currents during the formation and passage of a warm-core ring in the East Australian Current. *Deep-Sea Res*., 33: 1563-1576.

Müller, G. and Gastner, M., 1971. The 'karbonate bomb', a simple device determination of the carbonate content in sediments, soils, and other materials. *Neues Jahr. Mineral*., 10: 446-469.

Müller, D. W., Hodell, D. A. and Ciesielski, P. F., 1991. Late Miocene to earliest Pliocene (9.8 - 4.5 Ma) paleoceanography of the Subantarctic Southeast Atlantic: stable isotopic, sedimentologic, and microfossil evidence. *Proc. ODP, Sci. Res*., 114: 459-474.

Murphy, R. J., Pinkerton, M. H., Richardson, K. M., Bradford-Grieve, J. M. and Boyd, P. W., 2001. Phytoplankton distributions around New Zealand derived from SeaWIFS remotely-sensed ocean colour data. *New Zealand J. Mar. Freshwater Res*., 35: 343-362.

Murray, D. W. and Peterson, L. C., 1997. Biogenic carbonate production and preservation changes between 5 and 10 Ma from the Ceara Rise, western equatorial Atlantic. *Proc. ODP., Sci. Res*., 154: 375-388.

Murray, D. W., Farrell, J. W. and McKenna, V., 1995. Biogenic sedimentation at site 847, eastern equatorial Pacific Ocean, during the past 3 M.Y. *Proc. ODP, Sci. Res*., 138: 429-459.

Murray, R. W. and Leinen, M., 1996. Scavenged excess aluminum and its relationship to bulk titanium in biogenic sediment from the central equatorial Pacific. *Geochim. Cosmochim. Acta*, 60: 3869-3878.

Murray, R. W., Leinen, M. and Isern, A. R., 1993. Biogenic flux of Al to sediment in the central equatorial Pacific Ocean: evidence for increased productivity during glacial periods. *Paleoceanogr*., 8: 651-670.

Musgrave, R. J., 1990. Paleomagnetism and tectonics of Malaita, Solomon Islands. *Tectonics*, 9: 735-759.

Naish, T., Abbott, S., Alloway, B., Beu, A., Carter, R., Edwards, A., Journeaux, T., Kamp, P., Pillans, B., Saul, G. and Woolfe, K., 1998. Astronomical calibration of a southern hemisphere Plio-Pleistocene reference section, Wanganui Basin. *New Zealand Quat. Sci. Rev*., 17: 695–710.

Nees, S. 1997. Late Quaternary paleoceanography of the Tasman Sea: the benthic foraminiferal view. *Palaeogeogr. Palaeoclimatol. Palaeoecol*., 131: 365-389.

Neil, H. L., 1997. *Last Glaciation to present paleoceanographic changes, Subtropical Convergence zone, Chatham Rise, Southwest Pacific Ocean*. D. Phil. Thesis, University of Waikato, Hamilton, New Zealand (unpublished).

Neinhuis, P. H., 1981. Distribution of organic matter in living marine organisms. In: E. K. Duursma and R. Dawson (Editors), *Marine Organic Chemistry*, Elsevier, Amsterdam, pp. 31-69.

Nelson, C. S., 1986. Lithostratigraphy of Deep Sea Drilling Project Leg 90 drill sites in the southwest pacific Ocean: an overview. *Init. Repts. DSDP*, 90: 1471-1491.

Nelson, C. S. and Cooke, P. J., 2001. Overview of history of oceanic front development in the New Zealand sector of the Southern Ocean during the Cenozoic. *New Zealand J. Geol. Geophys*. 44: 535-554.

Nelson, C. S., Hendy, C. H., Jarrett, G. R. and Cuthbertson, A. M., 1985. Near-synchroneity of New Zealand alpine glaciations and Northern Hemisphere continental glaciations during the past 750 kyr. *Nature*, 318: 361-363.

Nelson, C. S., Hendy, C. H., Cuthbertson, A. M. and Jarrett, G. R., 1986. Late Quaternary carbonate and isotope stratigraphy, subantarctic Site 594, Southwest Pacific. *Init. Repts. DSDP*., 90: 1425-1436.

Nelson, C. S., Cooke, P. J., Hendy, C. H. and Cuthbertson, A. M., 1993. Oceanographic and climatic changes over the past 160 000 years at Deep Sea Drilling Project site 594 off southeastern New Zealand, southwest Pacific Ocean. *Paleoceanogr*., 8: 435-458.

Nelson, C. S., Hendy, C. H. and Cuthbertson, A. M., 1994. Oxygen isotope evidence for climate contrasts between Tasman Sea and Southwest Pacific Ocean during the late Quaternary. In: van der Lingen, K. M. Swanson and R. J. Muir (Editors), *Evolution of the Tasman Sea basin*. A. A. Balkema, Rotterdam, Netherlands, pp. 181-196.

Nelson, C. S., Hendy, I. L., Neil, H. L., Hendy, C. H. and Weaver, P. P. E., 2000. Last glacial jetting of cold waters through the Subtropical Convergence zone in the Southwest Pacific off eastern New Zealand, and some geological implications. *Palaeogeog. Palaeoclimatol. Palaeoecol*., 156: 103-121.

Nigrini, C., 1991. Composition and biostratigraphy of radiolarian assemblages from an area of upwelling (Northwestern Arabian Sea, Leg 117). *Proc. ODP., Sci. Res.*, 117: 89-126.

Nodder, S. D. and Northcote, L. C., 2001. Episodic particulate fluxes at southern temperate mid-latitudes (42-45°S) in the Subtropical Front region, east of New Zealand. *Deep-Sea Res.*, 48: 833-864.

Nomura, R., 1991. Ologocene to Pleistocene benthic foraminiferal assemblages at sites 754 and 756, eastern Indian Ocean. *Proc. ODP., Sci. Res.*, 121: 31-76.

Nomura, R., 1995. Paleogene to Neogene deep-sea paleoceanography in the eastern Indian Ocean: benthic foraminifera from ODP Sites 747, 757 and 758. *Micropaleontol.*, 41: 251-290.

Ogg, J., 1998. *Digital time scale databases*. Mesozoic Stratigraphic Laboratory, Dept. of Earth and Atmospheric Sciences, Purdue University, IN.

Orians, K. J. and Bruland, K. W., 1986. The biogeochemistry of aluminum in the Pacific Ocean. *Earth. Planet. Sci. Lett.*, 76: 397-410.

Paashe, E., 1973. Silicon and the ecology of marine plankton diatoms. II. Silicate-uptake kinetics in five diatom species. *Mar. Biol.*, 19: 262-269.

Palmer, M. R. and Elderfield, H., 1985. Sr isotope composition of sea water over the past 75 Myr. *Nature*, 314: 526-528.

Parsons, T. R., 1975. Particulate organic carbon in the sea. In: J. P. Riley and G. Skirrow (Editors), *Chemical Oceanography*, v. 2., Academic Press, London., 365-383.

Parsons. T. R., Takahashi, M. and Hargrave, B., 1984. *Biological Oceanographic Processes* - 3rd ed. Butterworth-Heinemann Ltd, Oxford, UK., 330 pp.

Paull, C. K. and Thierstein, H. R., 1987. Stable isotopic fractionation among particles in Quaternary coccolith-sized deep-sea sediments. *Paleoceanogr.*, 2: 423-429.

Peterson, L. C. and Backman, J., 1990. Late Cenozoic carbonate accumulation and the history of the carbonate compensation depth in the western equatorial Indian Ocean. *Proc. ODP., Sci. Res.*, 115: 467-507.

Peterson, L. C., Murray, D. W., Ehrann, W. U. and Hempel, P., 1992. Cenozoic carbonate accumulation and compensation depth changes in the Indian Ocean. In: R. A. Duncan, D. K. Rea, R. B. Kidd, U. Von Rad and J. K. Weissel (Editors), *Synthesis of Results From Scientific Drilling in the Indian Ocean*, Geophysical Monograph 70. American Geophysical Union, pp. 311-333.

Pierce, J., Weissel, J. et al., 1989. *Proc. ODP., Init. Repts.*, 121, pp. 1000.

Pinet, P. R., 1992. *Oceanography, an introduction to the planet oceanus*. West Publishing Co., MN, United States., 572 pp.

Pisias, N. G. and Leinen, M., 1984. Late Pleistoccene variability of the northwest sector of the Pacific Ocean. In: R. M. Cline and J. D. Hays (Editors), *Investigations of Late Quaternary Paleoceanography and Paleoclimatology*. Mem. Soc. Geol. Am., 145: 375-392.

Pisias, N. G., Mayar, L. A. and Mix, A. C., 1995. Paleoceanography of the eastern Equatorial Pacific during the Neogene; synthesis of Leg 138 drilling results. *Proc. ODP., Sci. Res*., 138: 5-21.

Pollitz, F. F., 1986. Pliocene change in Pacific plate motion. *Nature*, 320: 738-741.

Prell, W. L., Niitsuma, N. et al., 1989. *Proc. ODP., Init. Repts*., 117, pp. 1236.

Prell, W. L. and Kutzbach, J. E., 1992. Sensitivity of the Indian monsoon to forcing parameters and implications for its evolution. *Nature*, 360: 647-652.

Quade, J., Cerling, T. E. and Bowman, J. R., 1989. Development of the Asian monsoon revealed by marked ecologic shift in the latest Miocene of northern Pakistan. *Nature*, 342: 163-166.

Quade, J., Cater, J. M. L., Adam, J. and Harrison, T. M., 1995. Late Miocene environmental change in Nepal and the northern Indian subcontinent: stable isotopic evidence from paleosols. *Geol. Soc. Am. Bull*., 107: 1381-1397.

Raffi, I. and Flores, J.-A., 1995. Pleistocene through Miocene calcareous nannofossils from eastern Equatorial Pacific Ocean (Leg 138). *Proc. ODP., Sci. Res*., 138: 233-286.

Ravelo, A. C. and Fairbanks, R. G., 1995. Carbon isotopic fractionation in multiple species of planktonic foraminifera from core-tops in the tropical Atlantic. *J. Foram. Res*., 25: 53-74.

Raymo, M. E. and Ruddiman, W. F., 1992. Tectonic forcing of late Cenozoic climate. *Nature*, 359: 117-122.

Raymo, M. E., Ruddiman, W. F. and Froelich, P. N., 1988. Influence of late Cenozoic mounain building on ocean geochemical cycles. *Geology*, 16: 649-653

Raymo, M. E., Grant, B., Horowitz, M. and Rau, G. H., 1996. Mid-Pliocene warmth: Stronger greenhouse and stronger conveyor. *Mar. Micropal*., 27: 313-326.

Rea, D. K., 1992. Delivery of Himalayan sediment to the northern Indian Ocean and its relation to global climate, sea level, uplift, and seawater strontium. In: R. Duncan et al. (Editors), Synthesis of results from scientific drilling in the Indian Ocean, *Am. Geophys. Union, Geophys. Monogr*., 70: 387-402.

Rea, D. K. and Leinen, M., 1985. Neogene history of the calcite compensation depth and lysocline in the South Pacific Ocean. *Nature*, 316: 805-807.

Rea, D. K. and Snoeckx, H., 1995. Sediment fluxes in the Gulf of Alaska; paleoceanographic record from Site 887 on the Patton-Murray Seamount Platform. *Proc. ODP., Sci. Res.*, 145: 247-256.

Rea, D. K., Basov, I. A. and Janecek, T. R., 1993. Cenozoic paleoceanography of the North Pacific Ocean; results of ODP Leg 145, the North Pacific Transect. *Eos, Trans. Am. Geophys. Union*, 74: 173.

Rea, D. K., Basov, I. A., Krissek, L. A., et al., 1995. Scientific results of drilling in the North Pacific transect. *Proc. ODP., Sci. Res.*, 145: 577-596.

Redfield, A. C., 1934. On the proportions of organic derivatives in sea water and their relation to the composition of plankton. In: *James Johnstone memorial volume*, Liverpool University Press, pp. 177-192.

Redfield, A. C., 1958. The biological control of chemical factors in the environment. *Am. J. Sci.*, 46: 205-221.

Resig, J. M., 1993. Cenozoic stratigraphy and paleoceanography of biserial planktonic foraminifers, Ontong Java Plateau. *Proc. ODP., Sci. Res.*, 130: 231-244.

Richter, F. M., Rowley, D. B. and DePaolo, D. J., 1992. Sr isotope evolution of seawater: The role of tectonics. *Earth. Planet. Sci. Lett.*, 109: 11-23.

Rind, D. and Chandler, M., 1991. Increased ocean heat transports and warmer climate. *J. Geophys. Res.*, 96: 7437-7461.

Robert, C., Stein, R. and Acquaviva, M., 1986. Cenozoic evolution and significance of clay associations in the New Zealand region of the South Pacific, Deep Sea Drilling Project, Leg 90. *Init. Repts. DSDP.*, 90: 1225-1238.

Robinson, S. G., 1990. Applications for whole-core magnetic susceptibility measurememnts of deep-sea sediments: Leg 115 results. *Proc. ODP., Sci. Res.*, 115: 737-771.

Rubin, S. I., Takahasi, T., Chipman, D. W. and Goddard, J. G., 1998. Primary productivity and nutrient utilization ratios in the Pacific sector of the Southern Ocean based on seasonal changes in seawater chemistry. *Deep-Sea Res.*, 45: 1211-1234.

Ruddiman, W. F., Raymo, M. E., Martinson D. G., Clement, B. M. and Backman, J., 1989. Pleistocene evloution: Northern hemisphere ice sheets and North Atlantic Ocean. *Paleoceanogr*. 4: 353-412.

Sato, T. and Kameo, K., 1996. Pliocene to Quaternary calcareous nannofossil biostratigraphy of the Arctic Ocean, with reference to late Pliocene glaciation. *Proc. ODP., Sci. Res.*, 151: 39-59.

Sato and Takayama, 1992. A stratigraphically significant new speciesof the calcareous nannofossil Reticulofenestra asanoi. In K. Ishizaki and T. Saito, (Editors), *Centenary of Japanese Micropaleontology*, Terra Sci. Publ., Tokyo, pp. 457−460.

Savin, S. M., Douglas, R. G., Keller, G., Killingley, J. S., Shaughnessy, L., Sommer, M. A., Vincent, E., and Woodruff, F., 1981. Miocene benthic foraminiferal isotope records: A synthesis. *Mar. Micropal*. 6: 423-450.

Schmitz, W. R., Jr., 1995. On the interbasin-scale thermohaline circulation. *Rev. Geophys*., 33: 151-173.

Scholle, P. A. and Arthur, M. A., 1980. Carbon isotopic fluctuations in Cretaceous pelagic limestones - potential stratigraphic and petroleum exploration tool. *Am. Assoc. Petrol. Geol. Bull.*, 64: 67-87.

Schroeder, J.O., Murray, R. W., Leinen, M., Pflauum, R. C. and Janecek, T. R., 1997. Barium in equatorial Pacific carbonate sediment: Terriginous, oxide, and biogenic associations. *Paleoceanogr*., 12: 125-146.

Scott, B. D., 1981. Hydrological structure and phytoplankton distribution in the region of a warm-core eddy in the Tasman Sea. *Aust. J. Mar. Freshwater Res*., 32: 479-492.

Scott, G. H., Bishop, S. and Burt, B.J., 1990. Guide to Some Neogene Globorotalids (Foraminiferida) from New Zealand. *New Zealand Geol. Surv. Paleontol. Bull*., 61: 1-135.

Scott, G.H., Nelson, C.S. and Stone, H.H., 1995. Planktic foraminiferal events in early Miocene zones N6 and N7 at southwest Pacific DSDP site 593: relation with climatic changes in oxygen isotope zone Mi1b. *Mar. Micropal*., 25: 29-45.

Seisser, W. G., 1995. Paleoproductivity of the Indian Ocean during the Tertiary Period. *Global. Planet. Change*, 11: 71-88.

Shackleton, N. J. 1987. The carbon isotope record of the Cenozoic: History of organic carbon burial and of oxygen in the ocean and atmosphere. In: J. Brooks and A. J. Fleet (Editors), *Marine Petroleum Source Rocks*. Geol. Soc. London Spec. Pub., 26: 423-434.

Shackleton, N. J. and Kennett, J. P., 1975. Paleotemperature history of the Cenozoic and the initiation of Antarctic glaciation: Oxygen and carbon isotope analyses in DSDP sites 277, 279, and 281. *Init. Repts. DSDP,* 29: 743-755.

Shackleton, N. J. and Cita, M. B., 1979. Oxygen and carbon isotope stratigraphy of benthic foraminifers at site 397: detailed history of climatic change during the late Neogene. *Init. Repts. DSDP*., 21: 433-445.

Shackleton, N. J. and Hall, M. A., 1984. Carbon isotope data from Leg 74 sediments. *Init. Repts. DSDP*., 74: 613-619.

Shackleton, N. J. and Hall, M. A., 1995. Stable isotope records in bulk sediments (Leg 138). *Proc. ODP, Sci. Res*., 138: 797-805.

Shackleton, N. J. and Crowhurst, S., 1997. Sediment fluxes based on an orbitally tuned time scale 5 Ma to 14 Ma, Site 926. *Proc. ODP., Sci. Res.,* 154: 69-82.

Shackleton, N. J. and Hall, M. A., 1997. The late Miocene stable isotope record, Site 926. *Proc. ODP, Sci. Res*., 154: 367-373.

Shackleton, N. J., Hall, M. A. and Boersma, A., 1984. Oxygen and carbon isotope data from Leg 74 foraminifers. *Init. Repts. DSDP*., 74: 599-612.

Shackleton, N. J. and Shipboard Scientific Party, 1984. Accumulation rates in Leg 74 sediments. *Init. Repts. DSDP*., 74: 621-637.

Shackleton, N. J., Crowhurst, S., Hagelburg, T., Pisias, N. G. and Schneider, D. A., 1995. A new late Neogene timescale: Application to Leg 138 sites. *Proc. ODP, Sci. Res*., 138: 73-101.

Snoeckx., H, Rea, D. K., Jones, C. E. and Ingram, B. L., 1995. Eolian and silica deposition in the central North Pacific; results from sites 885/886. *Proc. ODP*., *Sci. Res*., 145: 219-230.

Sokolov, S. and Rintoul, S. R., 2000. Circulation and water masses of the southwest Pacific: WOCE section P11, Papua New Guinea to Tasmania. *J. Mar. Res*., 58: 223-268.

Spero, H. J., 1992. Do planktic foraminifera accurately record shifts in the carbon isotopic composition of seawater ΣCO_2? *Mar. Micropal*., 19: 275-285.

Spero, H. J. and Lea, D. W., 1993. Intraspecific stable isotope variability in the planktic foraminifera *Globigerinoides sacculifer:* results from laboratory experiments. *Mar. Micropal*., 22: 221-234.

Spero, H. J., Bijima, J., Lea, D. W. and Bemis, B. E., 1997. Effect of seawater carbonate concentration on foraminiferal carbon and oxygen isotopes. *Nature*, 390: 497-500.

Srinivasan, M. S. and Sinha, D. K., 1992. Late Neogene planktonic foraminifera events of the Southwest Pacific and Indian Ocean; a comparison. In: R. Tsuchi and J. C. Ingle, Jr. (Editors), *Pacific Neogene; environment, evolution, and events*, Univ. Tokyo Press, Tokyo, pp. 203-220.

Srinivasan, M. S. and Sinha, D. K., 2000. Ocean circulation in the tropical Indo-Pacific during early Pliocene (5.6-4.2 Ma): Paleobiogeographic and isotopic evidence. *Proceedings of the Indian Academy of Science-Earth & Planetary Sciences*, 109: 315-328.

Stanton, B. R., 1979. The Tasman Front. *New Zealand J. Mar. Freshwater Res*., 13: 201-214.

Stanton, B. R., 1981. An oceanographic survey of the Tasman Front. *New Zealand J. Mar. Freshwater Res*., 15: 289-297.

Stax, R. and Stein, R., 1993. Long-term changes in the accumulation of organic carbon in Neogene sediments, Ontong Java Plateau. *Proc. ODP., Sci. Res*., 130: 573-584.

Stein, R. and Robert, C., 1986. Siliclastic sediments at Sites 588, 590, and 591: Neogene and Paleogene evolution in the southwest Pacific and Australian climate. *Init. Repts. DSDP*, 90: 1437-1455.

Stramma, L., Peterson, R. G. and Tomczak, M., 1995. The South Pacific Current. *J. Phys. Oceanogr*., 25: 77-91.

Streeter, S. S. and Shackleton, N. J., 1979. Paleocirculation of the Deep North Atlantic: 150,000-yr record of benthic foraminifera and oxygen-18. *Science* 203: 168-171.

Summerhayes, C. P., Prell, W. L. and Emeis, K.-C., 1992. *Upwelling Systems: Evolution since the Early Miocene*. Geol. Soc. Spec. Publ., London. pp. 519.

Takahasi, T., Broecker, W. S. and Langer, S., 1985. Redfield ratio based on chemical data from isopycnal surfaces. *J. Geophys. Res*., 90: 6907-6924.

Theyer, F., Mayer, L. A., Barron, J. A. and Thomas, E., 1985. The equatorial Pacific high-productivity belt: elements for a synthesis of Deep Sea Drilling Project Leg 85 results. *Init. Repts. DSDP*., 85: 971-985.

Theyer, F., Vincent, E. and Mayer, L. A., 1989. Sedimentation and paleoceanography of the central equatorial Pacific. In: E. L. Winterer, D. M. Hussong and R. W. Decker (Editors), *The Eastern Pacific Ocean and Hawaii*. Geology of North America, Geol. Soc. Am., N: 347-372.

Tappan, H. 1968. Primary production, isotopes, extinctions and the atmosphere. *Palaeogeogr., Palaeoclimatol., Palaeoecol*., 4: 187-210.

Thompson, R. M., 1991. *Gazetteer of seafloor features in the New Zealand region*. Misc. Publ., 104, New Zealand Oceanographic Institute, pp. 64.

Thunell, R. and Sautier, L. R., 1992. Planktonic foraminiferal faunal and stable isotopic indices of upwelling; a sediment trap study in the San Pedro Basin, Southern california Bight. In, C. P. Summerhayes, W. L. Prell and Emeis, K.-C. (Editors), *Upwelling Systems: Evolution since the Early Miocene*. Geol. Soc. Spec. Publ., London, 64: 77-91.

Tilburg, C. E., Hurlburt, H. E., O'Brien, J. J. and Shriver, J. F., 2001. The dynamics of the East Australian Current system: the Tasman Front, the East Auckland Current, and the East Cape Current. *J. Phys. Oceanog*., 31: 2917-2943.

Tomczak, M. and Godfrey, J. S., 1994. *Regional oceanography: an introduction*. Oxford, Pergamon, pp. 422.

Twitchell, S. C., Meyers, P. A. and Diester-Haass, L., 2002. Significance of high C/N ratios in organic-carbon-rich Neogene sediments under the Benguela Current upwelling system. *Org. Geochem.*, 33: 715-722.

Uddstrom, M. J. and Oien, N. A., 1999. On the use of high-resolution satellite data to describe the spatial and temporal variability of sea surface temperatures in the New Zealand region. *J. Geophys. Res.*, 104: 20,729-20,751.

Vail, P. R. and Hardenbol, J., 1979. Sea-level changes during the Tertiary. *Oceanus*, 22: 71-79.

Van Andel, T. H., 1975. Mesozoic/Cenozoic calcite compensation depth and the global distribution of calcareous sediments. *Earth. Planet. Sci. Lett.*, 26: 187-194.

Van Andel, T. H., Heath, G. R. and Moore Jr., T. C., 1975. Cenozoic history and paleoceanography of the central equatorial Pacific Ocean: a regional synthesis of Deep Sea Drilling project data. *Geol. Soc. Am. Mem.*, 143, 143 pp.

Vella, P. and Kennett, J. P., 1975. Molluscan fossils and late Neogene paleotemperatures - Comment. *New Zealand J. Geol. Geophys.*, 18: 197-198.

Vergnaud-Grazzini, C., 1976. Non-equilibrium isotopic compositions of shells of planktonic foraminifera in the Mediterranean Sea. *Palaeogeogr., Palaeoclimatol., Palaeoecol.*, 20: 263-276.

Vidal, L., Bickert, T., Wefer, G. and Röhl, U., 2002. Late Miocene stable isotope stratigraphy of SE Atlantic ODP Site 1085: Relation to Messinian events. *Mar. Geol.*, 180: 71-85.

Vincent, E., Killingley, J. S. and Berger, W. H., 1980. The magnetic epoch 6 carbon shift: A change in the ocean's $^{13}C/^{12}C$ ratio 6.2 million years ago. *Mar. Micropal.*, 5: 185-203.

Vincent, E., Killingley, J. S. and Berger, W. H., 1981. Stable isotope composition of benthic foraminifera from the Equatorial Pacific. *Nature*, 289: 639-643.

Vincent, E., Killingley, J. S. and Berger, W. H., 1985. Miocene oxygen and carbon isotope stratigraphy of the tropical Indian Ocean. *Geol. Soc. Am. Mem.*, 163: 103-130.

Warren, B. A., 1970. General circulation in the South Pacific. In: W. S. Wooster (Editor), *Scientific Exploration of the South Pacific*. National Academy of Sciences, Washington, D. C., pp. 33-49.

Watson, A. J. and Whitfield, M., 1985. Composition of particles in the global ocean, *Deep-Sea Res.*, 32: 1023-1039.

Weaver, P. P. E., Carter, L. and Neil, H. L., 1998. Response of surface water masses and circulation to late Quaternary climate change east of New Zealand. *Paleoceanogr*., 13: 70-83.

Wei, K.-Y., 1997. Southward shifting of the Tasman Front at 4.4 Ma (early Pliocene): paleobiogeographic and oxygen isotope evidence. *J. Asian Earth Sci*., 16: 97-106.

Wells, P. E. and Connell, R., 1997. Movement of hydrological fronts and widespread erosional events in the southwestern Tasman Sea during the late Quaternary. *Austral. J. Earth Sci*., 44: 105-112.

Wells, M. L., Vallis, G. K. and Silver, E. A., 1999. Tectonic processes in Papua New Guinea and past productivity in the eastern equatorial Pacific Ocean. *Nature*, 398: 601-604.

Willcox, J. B., Symonds, P. A., Hinz, K. and Bennett, D., 1980. Lord Howe Rise, Tasman Sea - preliminary geophysical results and petroleum prospects. *BMR J. Australian Geol. Geophys*., 5: 225-236.

Williams, D. F., Sommer II, M. A. and Bender, M. L., 1977. Carbon isotopic compositions of Recent planktonic foraminifera of the Indian Ocean. *Earth. Planet. Sci. Lett*., 36: 391-403.

Winkler, A. and Dullo, W.-C., 2004. Miocene to Pleistocene sedimentation pattern on the Chatham Rise, New Zealand. *Proc. ODP., Sci. Res*., 181 [CD-ROM]. Available from: Ocean Drilling Program, Texas A&M University, College Station, TX 77845-9547, U.S.A.

Wood, R.A., Andrews, P.B., Herzer, R.H., et al., 1989. Cretaceous and Cenozoic geology of the Chatham Rise region, South Island, New Zealand. *New Zealand Geol. Basin Stud*., 3: 1-76.

Woodruff, F., 1985. Changes in Miocene deep-sea benthic foraminiferal distribution in the Pacific Ocean: relationship to paleoceanography. *Geol. Soc. Am. Bull*., Mem., 143: 131-175.

Woodruff, F. and Douglas, R. G., 1981. Response of deep-sea benthic foraminifera to Miocene paleoclimatic events, DSDP site 289. *Mar. Micropal*., 6: 617-632.

Wright, I. C. and Vella, P. P., 1988. A New Zealand late Miocene magnetostratigraphy: glacioeustatic and biostratigraphic correlations. *Earth Planet. Sci. Lett*., 87: 193-204.

Wright, J. D. and Miller, K. G., 1996. Control of North Atlantic Deep Water circulation by the Greenland-Scotland Ridge. *Paleoceanogr*., 11: 157-170.

Wright, J. D., Miller, K. G. and Fairbanks, R. G., 1991. Evolution of modern deepwater circulation: evidence from the late Miocene Southern Ocean. *Paleoceanogr*., 6: 275-290.

Zachos, J., Pagani, M., Sloan, L., Thomas, E. and Billups, K., 2001. Trends, Rhythms, and Aberrations in Global Climate 65 Ma to Present. *Science*, 292: 686-693.

Zentara, S. J. and Kamykowski, D., 1981. Geographic variations in the relationship between silicic acid and nitrate in the South Pacific Ocean. *Deep-Sea Res*., 28: 455-465.

APPENDIX 1

TABLES

Table 3T1
DSDP/ODP sites discussed in chapter 3 which show evidence of increased primary productivity during the late Miocene-early Pliocene (see also **Fig. 3F2**).

Evidence	Increased accumulation rates					Faunal abundance changes			Other
Site	$CaCO_3$	C_{org}	BF	Si	P	Diatom	BF	PF	
Pacific									
72-74, 77, 79-83	*(1)*			*(2)*					
289							*(3)*	*(4)*	
572, 573	*(5)*								
588, 590-593	*(6)*						*(6,7)*	*(6)*	
803	*(8)*	*(8)*	*(8)*		*(9)*	*(8)*	*(8)*	*(8)*	
804, 805	*(8)*	*(8)*	*(8)*				*(8)*	*(8)*	
806	*(8)*	*(8)*	*(8)*		*(9)*	*(8)*	*(8)*	*(8)*	
807	*(8)*	*(8)*	*(8)*		*(9)*		*(8)*	*(8)*	
846, 851	*(10)*	*(10)*		*(10)*	*(9)*				*(11)*
849, 850	*(10)*	*(10)*		*(10)*		*(12)*			*(11)*
882-884				*(13)*					
885/886				*(13,14)*		*(15)*			*(16)*
887				*(13,17)*					
1143	*(18)*			*(18)*					
1150, 1151	*(19)*	*(19)*							
Indian									
219							*(20)*		
707, 709, 710	*(21,22)*					*(23)*			*(24)*
721, 722	*(25,22)*					*(26)*	*(27)*		
728	*(25,22)*					*(26)*			
731							*(27)*		
752									*(28)*
754							*(29)*		*(28)*
757					*(30)*		*(31)*		*(28)*
758	*(32,22)*								
Antarctic									
266, 277				*(33)*					
704	*(34)*			*(34)*		*(34)*			
736-746				*(35)*					
1095, 1096, 1101				*(36)*					
Atlantic									
525-528	*(37)*								
926	*(38)*								
1085		*(39,40)*	*(39,40)*				*(39,40)*		
1087	*(40)*	*(40)*	*(40)*						

Abbreviations are as follows: C_{org} = organic carbon; BF = benthic foraminifera; Si = biogenic silica; P = phosphorus; PF = planktonic foraminifera; 'other' = other sediment geochemical proxies (see text and references). Numbered references are (1) Van Andel et al. (1975), (2) Leinen (1979), (3) Woodruff (1985), (4) Keller (1985), Resig (1993), (5) Theyer et al. (1985), (6) Kennett and von der Borch (1986), (7) Kurihara and Kennett (1992), (8) Berger et al. (1993), (9) Delaney and Filippelli (1994), (10) Farrell et al. (1995), (11) Schroeder et al. (1997),

(12) Kemp and Baldauf (1993), (13)Rea et al. (1993; 1995), (14) Snoeckx et al. (1995), (15) Dickens and Barron (1997), (16) Dickens and Owen (1996), (17) Rea and Snoeckx (1995), (18) Li and Wang (2002), (19) Mora (2003), (20) Gupta and Thomas (1999), (21) Peterson and Backman (1990), (22) Dickens and Owen (1999), (23) Mikkelsen (1990), (24) Backman et al. (1988), Robinson (1990), (25) Prell et al. (1989), (26) Nigrini (1991), (27) Hermelin (1992), (28) Dickens and Owen (1994), (29) Nomura (1991), (30) Hermoyian and Owen (2001), (31) Nomura (1995), (32) Seisser (1995), (33) Brewster (1980), (34) Froelich et al. (1991), (35) Barron and Baldauf (1989), (36) Hillenbrand and Fuetterer (2002), (37) Shackleton et al. (1984), (38) Murray and Peterson (1997), (39) Diester-Haass et al. (2002), (40) Diester-Haass et al. (2004)

Table 3T2
Summary of the timing of the biogenic bloom, based on key studies of this event

Study	Region	Biogenic bloom interval (Ma)
Berger et al., 1993	Pacific	8 to ~4.5 [a] (8.8 to ~5 [c])
Farrell et al., 1995	Pacific	6.7 to 4.5 [b]
Dickens and Owen, 1996	Pacific	9.0 to 3.6 [c]
Dickens and Barron, 1997	Pacific	5.9 to 5.0 [b]
Filippelli, 1997	Global	~8 to 4 [d]
Dickens and Owen, 1999	Indo-Pacific	9.0 to 3.5 [b]
Gupta and Thomas, 1999	Indian	5.5 to 4.0 [c]
Hermoyian and Owen, 2001	Indian & Atlantic	5.5 to ~4 [c]
Diester-Haass et al., 2004	Atlantic	Onset at 6.7 [c]

Ages are based on sediment records calibrated to the following timescales: a = Berggren et al. (1985), b = Shackleton et al. (1995), c = Berggren et al. (1995b), d = Cande and Kent (1992).

Table 4T1
Summary of phytoplankton parameters in subtropical (ST), subtropical convergence (STC), and subantarctic (SA) water masses to the east of New Zealand (all data from 0-10 m water depth)

Water mass	Chlorophyll *a* (mg/m^3)		^{14}C uptake ($mg\ C/m^3d^{-1}$)	Cell carbon biomass ($mg\ C/m^2$)
	(1)	*(2)*	*(1)*	*(2)*
ST	0.13-0.87	0.16-0.47	6.5-68.4	657-669
STC	0.39-3.42	0.54-0.61	27.1-119.6	2599-2953
SA	0.12-0.19	0.10-0.13	2.6-10.7	218-464

Numbered references are: (1) Bradford-Grieve et al. (1997) - data for <200μm fraction, and (2) Chang and Gall (1998).

Table 4T2
Drill site locations used in this study

Site	Latitude	Longitude	Water depth (m)
DSDP 590	31°10.02′S	163°21.51′E	1299
DSDP 594	45°31.41′S	174°56.88′E	1204
ODP 1125	42°54.97′S	178°16.65′W	1333

Table 5T1
Age and depth of datums from holes 590A (*) and 590B used in this study

	Datum	Age (Ma)	Depth (mbsf)	Reference
N	FAD *Emiliania huxleyi*	0.26	3.80	a
N	LAD *Pseudoemiliania lacunosa* †	0.46	6.53	a
M	Base C1n	0.78	11.45	b
M	Top C1r.1n	0.99	15.50	b
M	Base C1r.1n	1.07	17.75	b
N	LAD *Calcidiscus macintyrei* ††	1.59	18.91	a
F	LAD *Globigerinoides fistulosus*	1.60	32.95*	a
M	Top C2n	1.77	33.20*	b
M	Top C2n	1.77	30.65	b
F	LAD *Globigerinoides obliquus extremus*	1.77	59.80*	a
M	Base C2n	1.95	35.75*	b
M	Base C2n	1.95	35.45	b
N	LAD *Discoaster broweri*	1.95	35.83	a
N	LAD *Discoaster pentaradiatus*[1]	2.51	45.43	a
N	LAD *Discoaster surculus*	2.57	46.21	a
F	FAD *Globorotalia truncatulinoides*	2.58	50.20*	a
M	Top C2An.1n	2.58	47.90*	b
M	Top C2An.1n	2.58	45.80	b
M	Base C2An.1n	3.04	62.50*	b
M	Base C2An.1n	3.04	57.65	b
F	LAD *Globorotalia multicamerata*	3.09	40.60*	a
F	LAD *Dentoglobigerina altispira*	3.09	69.40*	a
M	Top C2An.3n	3.33	70.08*	b
M	Top C2An.3n	3.33	60.60	b
F	FAD *Globigerinoides fistulosus*	3.33	59.80*	a
F	FAD *Globorotalia tosaensis*	3.35	80.95*	a
M	Base C2An.3n	3.58	81.20*	b
M	Base C2An.3n	3.58	70.35	b
F	LAD *Pulleniatina primalis*	3.65	80.95*	a
F	FAD *Globorotalia inflata*	3.70	100.15*	c
N	LAD *Reticulofenestra pseudoumbilica*[2]	3.75	87.61	a
N	FAD *Discoaster asymmetricus*	4.13	151.76	d
F	LAD *Globigerina nepenthes*	4.20	112.60*	a
F	LAD *Globorotalia cibaoensis*	4.60	127.00*	b
N	FAD *Ceratolithus rugosus*[3]	5.12	172.51	a
F	FAD *Globorotalia crassaformis* s.s.	5.20	167.35*	e
F	FAD *Globorotalia puncticulata*	5.20	191.35*	c
F	FAD *Globorotalia margaritae*	5.40	194.05*	e, f
N	LAD *Discoaster quinqueramus*	5.60	196.21	b
F	FAD *Globorotalia tumida*	5.60	162.55*	a
F	FAD *Pulleniatina primalis*	6.40	194.05*	b
F	FAD *Globorotalia conomiozea*	7.12	238.85*	b
N	FAD *Amaurolithus primus*[4] ‡	7.20	272.51	b
F	FAD *Globorotalia cibaoensis*	7.80	278.30*	b
N	FAD *Discoaster quinqueramus*	8.60	324.53	b
N	LAD *Discoaster hamatus*[5]	9.40	353.33	b
F	LAD *Globoquadrina dehiscens*	9.90	350.30	c, g

(continued overpage)

(Table 5T1 continued)

	Datum	Age (Ma)	Depth (mbsf)	Reference
F	FAD *Neogloboquadrina acostaensis*	10.90	360.90	b
N	FAD *Discoaster kugleri*[6]	11.80	414.26	b
F	FAD *Globigerina nepenthes*	11.80	398.30	h

Notes: Ages for polarity chrons (M) and for first (FAD) and last (LAD) appearance datums of calcareous nannoplankton (N) and planktonic foraminifera (F) are from (a) Berggren et al. (1995a), (b) Berggren et al. (1995b), (c) Morgans et al. (1996), (d) Shackleton et al. (1995), (e) Scott et al. (1990), (f) Srinivasan and Sinha (1992), (g) Wright and Vella (1988), (h) Ogg et al. (1998). *Pseudoemiliania lacunosa* is now commonly referred to as *Emiliania ovata* (†); similarly, *Cyclococcolithinia macintyrei* = *Calcidiscus macintyrei* (††) and *Ceratolithus primus* = *Amaurolithus primus* (‡). Datums used in the linear sedimentation rate model are numbered.

Table 5T2
Carbonate concentrations and MARs at site 590

Sample (core, section, interval(cm))	Depth (mbsf)	Age_{LSR} (Ma)	Age_{POLY} (Ma)	$CaCO_3$ (%)	MAR_{LSR} $CaCO_3$ ($g/cm^2/ky$)	MAR_{POLY} $CaCO_3$ ($g/cm^2/ky$)
1H 1 130 - 135	1.35	0.07	0.23	90	1.94	1.76
2H 3 75 - 80	5.90	0.33	0.51	87	1.88	1.84
3H 3 74 - 79	15.59	0.86	1.06	87	1.88	2.05
4H 3 62 - 67	25.07	1.39	1.54	90	1.94	2.34
5H 2 60 - 65	33.13	1.83	1.92	89	1.90	2.52
6H 2 40 - 42	42.51	2.35	2.31	89	1.90	2.84
7H 3 60 - 64	53.82	2.76	2.73	89	3.59	3.17
8H 2 95 - 99	62.27	3.01	3.01	90	3.64	3.59
9H 4 111 - 116	75.04	3.38	3.39	91	3.68	4.08
10H 4 64 - 69	84.17	3.65	3.64	90	3.64	4.37
11H 2 120 - 125	91.33	3.81	3.81	90	6.63	4.68
12H 1 134 - 137	99.56	3.94	4.00	89	6.56	5.01
13H 2 80 - 85	110.13	4.11	4.22	91	6.70	5.51
14H 2 80 - 82	119.71	4.27	4.41	95	7.00	6.12
15H 2 100 - 105	129.53	4.43	4.59	95	7.00	6.42
16H 5 90 - 92	143.51	4.65	4.84	95	7.00	6.61
17H 2 100 - 104	148.72	4.74	4.93	96	7.07	6.71
18H 2 75 - 79	158.07	4.89	5.08	96	7.07	6.69
19H 3 75 - 77	169.16	5.07	5.27	96	7.07	6.65
20H 2 75 - 79	177.27	5.22	5.41	96	5.47	6.46
21H 3 76 - 81	188.38	5.45	5.61	95	5.42	6.26
21H 5 76 - 78	191.37	5.51	5.66	98	5.59	6.28
22H 2 77 - 82	196.50	5.62	5.76	96	5.47	6.13
22H 4 78 - 83	199.51	5.68	5.81	96	5.47	5.95
23H 3 77 - 82	207.60	5.85	5.97	96	5.47	5.72
24H 3 75 - 79	217.17	6.05	6.16	95	5.42	5.55
24H 5 75 - 79	220.17	6.11	6.22	96	5.47	5.39
25H 2 75 - 80	225.28	6.22	6.33	97	5.53	5.39
25H 4 75 - 79	228.27	6.28	6.39	95	5.42	5.10
26H 2 75 - 79	234.87	6.42	6.54	98	5.59	5.21
26H 4 75 - 79	237.87	6.48	6.61	95	5.42	4.85
27H 3 85 - 89	246.07	6.65	6.80	96	5.47	4.71
28X 2 75 - 79	252.97	6.79	6.96	95	5.42	4.45
29X 4 72 - 79	264.36	7.03	7.25	97	5.53	4.32
30X 4 74 - 78	273.96	7.24	7.51	97	4.26	4.17
31X 2 72 - 77	280.55	7.42	7.69	98	4.31	4.06
32X 2 74 - 79	290.17	7.68	7.97	96	4.22	3.83
33X 2 52 - 54	299.53	7.94	8.25	96	4.22	3.70
34X 3 79 - 84	310.94	8.25	8.60	94	4.13	3.52
35X 3 70 - 75	320.45	8.50	8.90	94	4.13	3.42
36X 3 83 - 88	330.18	8.77	9.22	93	4.09	3.32
37X 3 70 - 75	339.65	9.03	9.53	91	4.00	3.21
38X 3 72 - 77	349.27	9.29	9.86	92	4.04	3.24
39X 3 72 - 77	358.87	9.62	10.18	94	2.79	3.25
40X 3 72 - 77	368.47	10.00	10.51	94	2.79	3.35
41X 3 72 - 77	378.07	10.37	10.83	92	2.73	3.19
42X 3 75 - 80	387.70	10.75	11.16	90	2.67	3.34

(continued overpage)

(Table 5T2 continued)

Sample (core, section, interval(cm))		Depth (mbsf)	Age_{LSR} (Ma)	Age_{POLY} (Ma)	$CaCO_3$ (%)	MAR_{LSR} $CaCO_3$ ($g/cm^2/ky$)	MAR_{POLY} $CaCO_3$ ($g/cm^2/ky$)
43X 3	83 - 88	397.38	11.14	11.47	93	2.76	3.43
44X 3	85 - 90	407.00	11.51	11.78	91	2.70	-

Notes: mbsf = metres below seafloor. The two sets of ages ($Age_{LSR, POLY}$) have been derived from my age-depth model by applying different curve fitting methods (**Fig. 5F1**). The subscripts 'LSR' and 'POLY' refer to use of the 'stepped' linear sedimentation rate model and the forth order polynomial equation, respectively.

Table 5T3
Elemental concentrations and ratios to Ti of Neogene sediment at site 590

Sample (core, section, interval(cm))	SiO_2 (%)	Al_2O_3 (%)	Fe_2O_3T (%)	CaO (%)	TiO_2 (%)	LOI (%)	Ba (ppm)	Ca/Ti	Ba/Ti	Al/Ti	Si/Al
2H 3 75 - 80	5.70	1.60	0.57	49.84	0.11	41.43	154	559	0.24	13	3.20
4H 3 62 - 67	2.60	0.90	0.31	50.80	0.04	43.40	180	1567	0.78	20	2.59
8H 2 95 - 99	3.70	1.30	0.41	49.70	0.06	42.50	223	1022	0.64	19	2.55
9H 4 111 - 116	2.90	1.00	0.44	52.04	0.07	42.68	220	917	0.54	13	2.60
12H 1 134 - 137	3.70	1.30	0.39	51.19	0.08	42.35	226	789	0.49	15	2.55
15H 2 100 - 105	1.60	0.56	0.28	52.40	0.04	43.50	132	1616	0.57	13	2.56
17H 2 100 - 104	1.10	0.40	0.14	52.90	0.03	43.50	94	2176	0.54	12	2.47
19H 3 75 - 77	1.20	0.40	0.14	54.30	0.02	43.27	142	3350	1.23	18	2.69
21H 3 76 - 81	0.90	0.40	0.12	53.20	0.03	43.80	124	2188	0.71	12	2.02
22H 4 78 - 83	1.20	0.41	0.16	53.20	0.03	43.70	99	2188	0.57	12	2.63
23H 3 77 - 82	1.40	0.47	0.17	52.60	0.03	43.70	191	2163	1.10	14	2.67
24H 3 75 - 79	1.80	0.70	0.23	54.02	0.05	43.01	165	1333	0.57	13	2.31
25H 3 72 - 77	1.13	0.38	0.13	52.85	0.04	44.00	161	1656		9	2.60
26H 2 75 - 79	1.10	0.36	0.12	52.90	0.01	43.70	139	6527	2.40	32	2.74
26H 7 20 25	1.00	0.36	0.09	53.24	0.02	44.00	103	3018		15	2.54
27H 3 85 - 89	1.30	0.44	0.24	53.00	0.03	43.40	136	2180	0.78	13	2.65
28X 2 69 75	1.00	0.34	0.09	53.30	0.02	44.10	119	4230		20	2.52
29X 4 72 - 79	0.80	0.25	0.10	53.60	0.01	43.60	114	6613	1.97	22	2.87
30X 3 72 77	1.14	0.35	0.13	52.80	0.04	44.20	91	1612		8	2.88
31X 3 73 78	1.50	0.45	0.19	53.00	0.03	43.70	156	2338		15	2.94
32X 2 74 - 79	1.80	0.52	0.21	52.50	0.03	43.50	160	2159	0.92	16	3.11
33X 2 52 - 54	1.10	0.30	0.15	53.20	0.02	43.70	173	3282	1.49	13	3.29
33X 3 20 25	2.06	0.63	0.19	52.00	0.04	43.90	184	1720		15	2.91
34X 3 84 86	1.57	0.46	0.09	52.80	0.02	44.00	218	2619		17	3.04
35X 3 70 - 75	2.00	0.59	0.19	52.50	0.02	43.30	212	3239	1.83	26	3.04
36X 1 72 77	2.35	0.71	0.19	51.80	0.04	43.80	251	1713		17	2.92
36X 3 83 - 88	3.60	1.00	0.31	50.70	0.04	42.50	197	1564	0.85	22	3.23
37X 3 68 70	2.81	0.73	0.30	51.10	0.06	43.60	299	1030		11	3.40
38X 3 72 - 77	3.20	0.90	0.73	52.46	0.06	41.69	300	1079	0.86	13	3.19
39X 3 78 80	2.36	0.72	0.27	51.70	0.05	43.70	267	1338		14	2.91
40X 3 77 79	2.76	0.88	0.39	51.70	0.04	43.40	246	1432		18	2.78
41X 3 72 - 77	1.80	0.60	0.25	53.96	0.03	43.16	360	2219	2.07	18	2.69

Notes: elemental ratios to Ti are calculated from oxide-free molar values.

Table 5T4
Carbon isotope data calculated in this study

Sample (core, section, interval(cm))		Depth (mbsf)	Age_{POLY} (Ma)	Bulk sediment (‰)	Bulk Fine (‰)	*Gs. Sacculifer* (w/o) (‰)	*Gs. Sacculifer* (w) (‰)	*O. universa* (‰)	*G. bulloides* (‰)
1H - 1	130 - 135	1.35	0.23	-0.85					-1.10
2H - 3	75 - 80	5.90	0.51	0.56					-0.82
Replicate									*-0.91*
3H - 3	74 - 79	15.59	1.06	0.72					-0.63
4H - 3	62 - 67	25.07	1.54	0.56					-0.42
5H - 2	60 - 65	33.13	1.92	-0.30	0.33		1.53	2.18	1.29
6H - 2	40 - 42	42.51	2.31	-0.02	0.38	1.60		1.40	-0.63
7H - 3	60 - 64	53.82	2.73	0.26	0.55	1.65	1.77	1.68	-0.24
8H - 2	95 - 99	62.27	3.01	0.24	0.52			1.79	0.00
9H - 4	111 - 116	75.04	3.39	0.72	1.13			1.80	-0.05
10H - 4	64 - 69	84.17	3.64	0.52	0.95			1.58	-0.06
11H - 2	120 - 125	91.33	3.81	0.75	0.85			1.55	-0.50
12H - 1	134 - 137	99.56	4.00	*0.50*	0.58	1.45	*1.52*	1.26	0.40
Replicate				*0.42*			*1.49*		
13H - 2	80 - 85	110.13	4.22	0.52	0.69			1.67	-0.39
14H - 2	80 - 82	119.71	4.41	1.15	2.7	1.96	1.91	1.46	
15H - 2	100 - 105	129.53	4.59	0.76	0.96			1.56	-0.25
16H - 5	90 - 92	143.51	4.84	1.02	1.23			1.59	0.27
17H - 2	100 - 104	148.72	4.93	1.13	1.38			1.70	0.30
18H - 2	75 - 79	158.07	5.08	1.13	1.51	1.68		1.65	
19H - 3	75 - 77	169.16	5.27	1.38	1.61	1.79	1.94	2.19	0.49
Replicate				*1.38*					
20H - 2	75 - 79	177.27	5.41	1.40	1.63	1.92		1.86	
21H - 3	76 - 81	188.38	5.61	1.66	1.78		1.88	1.93	-0.29
21H - 5	76 - 78	191.37	5.66	1.33	1.5	1.86		1.56	

(continued overpage)

(Table 5T4 continued)

Sample (core, section, interval(cm))		Depth (mbsf)	Age_{POLY} (Ma)	Bulk sediment (‰)	Bulk Fine (‰)	*Gs. Sacculifer* (w/o) (‰)	*Gs. Sacculifer* (w) (‰)	*O. universa* (‰)	*G. bulloides* (‰)
22H - 2	77 - 82	196.50	5.76	0.94	1.091	1.79			0.19
Replicate				*0.94*					
22H - 4	78 - 83	199.51	5.81	1.22	1.2	1.71		1.19	-0.02
23H - 3	77 - 82	207.60	5.97	1.45	1.52	1.83		1.48	0.17
24H - 3	75 - 79	217.17	6.16	1.24	1.31	1.73		1.91	0.08
24H - 5	75 - 79	220.17	6.22	1.58	1.38			2.36	
25H - 2	75 - 80	225.28	6.33	1.43	1.44	2.00		1.57	
25H - 4	75 - 79	228.27	6.39	0.97	1.09	1.96		1.11	-0.88
26H - 2	75 - 79	234.87	6.54	1.25	1.19	1.99		1.36	-0.41
26H - 4	75 - 79	237.87	6.61	1.09	1.16	1.55		1.50	
27H - 3	85 - 89	246.07	6.80	1.13	1.28	1.56		1.55	
28X - 2	75 - 79	252.97	6.96	1.42	1.53	2.05	2.03	1.56	
29X - 4	72 - 79	264.36	7.25	1.50	1.65	2.53			
30X - 4	74 - 78	273.96	7.51	1.10	1.35	1.97		1.82	
31X - 2	72 - 77	280.55	7.69	1.33	1.5			1.92	
32X - 2	74 - 79	290.17	7.97	1.36	1.46	2.38		2.40	
33X - 2	52 - 54	299.53	8.25	1.27	1.43	2.39		2.14	
34X - 3	79 - 84	310.94	8.60	0.90					
35X - 3	70 - 75	320.45	8.90	1.26					
36X - 3	83 - 88	330.18	9.22	1.21					
37X - 3	70 - 75	339.65	9.53	0.76					
38X - 3	72 - 77	349.27	9.86	0.56					
39X - 3	72 - 77	358.87	10.18	0.48					
40X - 3	72 - 77	368.47	10.51	0.98					
41X - 3	72 - 77	378.07	10.83	1.22					
42X - 3	75 - 80	387.70	11.16	1.33					

(continued overpage)

(Table 5T4 continued)

Sample (core, section, interval(cm))		Depth (mbsf)	Age_{POLY} (Ma)	Bulk sediment (‰)	Bulk Fine (‰)	*Gs. Sacculifer* (w/o) (‰)	*Gs. Sacculifer* (w) (‰)	*O. universa* (‰)	*G. bulloides* (‰)
43X - 3	83 - 88	397.38	11.47	0.93					
44X - 3	85 - 90	407.00	11.78	1.14					

Notes: *Gs. Sacculifer* (w/o) and (w) refer to 'without sac' and 'with sac', respectively.

Table 5T5
Comparison of $\delta^{13}C$ results for the bulk sediment fractions

Sample (Core, section, interval (cm))	Bulk sediment (‰)	Bulk Fine (<63 μm) (‰)	Bulk nannofossils (5-25 μm) (‰)	$\delta^{13}C$ range (‰)
7H 3 60 - 64	0.26	0.55	0.47	0.29
13H 2 80 - 85	0.52	0.69	0.61	0.17
19H 3 75 - 77	1.38	1.61	1.45	0.23
24H 3 75 - 79	1.24	1.31	1.23	0.08
27H 3 85 - 89	1.13	1.28	1.16	0.15
33X 2 52 - 54	1.27	1.43	1.38	0.16

Notes: The $\delta^{13}C$ range has been calculated as the difference between the maximum and minimum $\delta^{13}C$ values for each sample.

Table 6T1
Age and depth of datums for sites 594 and 1125

Datum			Age	594	1125	References	
			(Ma)	(mbsf)	(mbsf)	Age†	Depth
	St 4/5 boundary	I	0.07	10.50			a
FO	acme *Emiliana huxleyi*	N	0.08		1.56		
	St 5/6 boundary	I	0.13	16.90			a
LO	*Helicosphaera inversa*	N	0.16		4.21	b	
	St 7/8 boundary	I	0.21	26.00			c
FO	*Emiliana huxleyi*	N	0.28		4.56	d	
	St 11/12 boundary	I	0.40	47.00			c
LO	*Pseudomiliania lacunosa*	N	0.46		7.31		
	St 13/14 boundary	I	0.50	59.00			c
btm	C1n	M	0.78		~15		
	St 19/20 boundary	I	0.79	83.00			c
LO	*Reticulofenestra asanoi*	N	0.90		18.31	e	d
top	C1r.1n	M	0.99	99.55	~21		f
re.	*Gephyrocapsa* (medium)	N	1.05		22.54		d
btm	C1r.1n	M	1.07		~23		
LO	*Calcidiscus macintyrei*	N	1.11		23.90		d
top	C1r.2r-1n	M	1.20		~30		
btm	C1r.2r-1n	M	1.21		~31		
LO	*Helicosphaera sellii*	N	1.26		32.83	b	
	Tephra T14	T	1.47	103.80		g	
	Tephra T15	T	1.57	112.00		g	
FO	*Gephyrocapsa* (medium)	N	1.73		37.31		d
top	C2n	M	1.77		~38		
LO	*Rhizosolenia barboi*	D	1.80	124.89		h	i
btm	C2n	M	1.95		~41.5		
LO	*Coscinodiscus kolbei*	D	2.00	132.24			i
LO	*Discoaster brouweri*	N	2.17		44.52		d
	C. kolbei/R. barboi zone	D	2.22	136.74			i
btm	*Globorotalia crassaformis* (d)	F	2.35	139.00			c
	Cosmiodiscus insignis zone	D	2.55	142.25			i
LO	*Reticulofenestra pseudoumbilicus*	N	2.57		51.82		d
top	C2An.1n	M	2.58		~52		
LO	*Discoaster surculus*	N	2.65		54.82		d
FO	*Nitzschia weaveri*	D	2.81	151.44			i
FO	*Globorotalia crassaformis (d)*	F	3.00		61.80	j	
btm	C2An.1n	M	3.04		~70		
top	C2An.2n	M	3.11		~78		
btm	C2An.2n	M	3.22		~80		
top	C2An.3n	M	3.33	153.00	~82		f
btm	C2An.3n	M	3.58	160.03	~89.5		f
LO	*Reticulofenestra pseudoumbilica*	N	3.62	162.53			k
FO	*Globorotalia inflata*	F	3.70		99.80	j,l	
LO	*Globorotalia puncticulata*	F	3.70		99.80	m	
top	C3n.1n	M	4.18	173.13			f
LO	*Mesocena diodon*	D	4.57	180.24			i
LO	*Globorotalia mons*	F	4.80		156.70	m	
LO	*Globorotalia sphericomiozea*	F	5.20	181.10		n	o

(continued overpage)

(Table 6T1 continued)

Datum			Age	594	1125	References	
			(Ma)	(mbsf)	(mbsf)	Age†	Depth
btm	C3n.4n	M	5.23	201.00			f
LO	*Hemidiscus triangularis*	D	5.30		223.71		
FO	*Globorotalia pliozea*	F	5.40		245.20	m	
FO	*Globorotalia mons*	F	5.50		274.00	m	
LO	*Discoaster quinqueramus*	N	5.56		288.30	p	
LO	*Nitzschia miocenica*	D	5.70		331.59		
top	C3An	M	5.89	210.00			f
top	C3An.2n	M	6.27	218.63			f
btm	C3An.2n	M	6.57	223.13			f
FO	*Globorotalia juanai*	F	6.60		348.30	m	
LO	*Minylitha convallis*	N	7.73		379.00	q	
FO	*Fragilariopsis reinholdii*	D	8.10	223.14		r	i
LO	*Bolboforma* aff. *Metzmacheri*	F	8.50		389.40		
FO	*Discoaster quinqueramus*	N	8.60	244.12		s	t
FO	*Minylitha convallis*	N	9.43		427.80	p	
LO	*Discoaster hamatus*	N	9.63	260.03		u,s	t
LO	*Globoquadrina dehiscens*	F	9.90		450.80	j,l	
LO	*Globorotalia panda*	F	10.30		475.00	m,v	
FO	*Discoaster hamatus*	N	10.47	274.72			t
FO	*Discoaster bellus*	N	10.48		512.70	w	
Acme	Kaiti *Globorotalia miotumida* (d)	F	10.85		548.20	v	
LO	*Nitzschia denticuloides*	D	11.67	409.14		r	i
FO	*Denticulopsis dimorpha*	D	12.20	437.94		r	i

Notes: †All ages are from Berggren et al. (1995a,b) unless otherwise stated; all depths for site 594 are reference coded, and those for site 1125 are from Carter et al. (1999). Chronostratigraphic events are annotated as follows: I = oxygen isotope, N = calcareous nannofossil, M = magnetochron, T = tephra, D = diatom, F = foraminifera. Referenced ages and depths are: (a) Nelson et al. (1993), (b) Sato and Kameo (1996), (c) B.W. Haywood, p.c., (d) K.Y. Wei, p.c., (e) Sato and Takayama (1992), (f) Barton and Bloemendal (1986), (g) Nelson et al. (1986), (h) Gersonde and Barcena (1998), (i) Ciesielski (1986), (j) Morgans et al. (1996), (k) Naish et al. (1998), (l) Wright and Vella (1988), (m) Scott et al. (1990), (n) Hornibrook and Jenkins (1994), (o) Jenkins and Srinivasan (1986), (p) Raffi and Flores (1995), (q) Shackleton et al. (1995), (r) Gersonde et al. (1998), (s) Gersonde et al. (1999), (t) Lohman (1986), (u) Backman and Raffi (1997), (v) Scott et al. (1995), (w) Gartner (1992).

Table 6T2
Elemental concentrations at (a) DSDP site 594 and (b) ODP site 1125

(a) 594

Sample		Depth	Age	$CaCO_3$	CaO	SiO_2	Al_2O_3	Fe_2O_3 T	TiO_2	LOI
(core, section, interval(cm))		(mbsf)	(Ma)	(%)	(%)	(%)	(%)	(%)	(%)	(%)
14 H 4	73 - 77	126.37	1.84	76	35.3	23.9	4.90	1.71	0.28	41.46
15 X 3	63 - 65	134.35	2.10	70	37.4	21.4	4.42	1.67	0.23	39.02
16 X 3	52 - 57	143.87	2.60	84	-	-	-	-	-	-
594A 10 X 5	71 - 76	156.66	3.46	62	41.4	15.1	3.46	1.29	0.19	41.57
18 X 1	67 - 71	160.21	3.58	87	-	-	-	-	-	-
19 X 3	68 - 73	172.83	4.16	83	-	-	-	-	-	-
20 X 2	54 - 59	180.79	4.97	80	-	-	-	-	-	-
20 X 4	54 - 59	183.79	5.20	84	-	-	-	-	-	-
20 X 5	63 - 66	185.36	5.21	84	47.0	9.4	1.81	0.64	0.10	32.15
21 X 2	64 - 66	190.46	5.21	86	-	-	-	-	-	-
21 X 4	71 - 75	193.55	5.22	80	-	-	-	-	-	-
21 X 6	70 - 74	196.54	5.22	81	46.0	10.1	1.90	0.63	0.12	39.00
594A 11 X 1	70 - 75	198.65	5.23	68	-	-	-	-	-	-
594A 11 X 3	69 - 74	201.64	5.28	74	-	-	-	-	-	-
594A 11 X 5	69 - 74	204.64	5.50	72	-	-	-	-	-	-
23 X 2	70 - 72	209.72	5.87	91	-	-	-	-	-	-
23 X 4	76 - 78	212.78	6.01	88	49.2	6.3	0.74	0.28	0.05	39.55
23 X 6	74 - 79	215.79	6.14	91	-	-	-	-	-	-
24 X 2	85 - 89	219.49	6.33	81	44.1	10.4	1.42	0.57	0.08	41.13
24 X 4	4 - 77	222.37	6.52	78	-	-	-	-	-	-
24 X 6	68 - 73	225.33	8.15	90	-	-	-	-	-	-
25 X 1	69 - 74	227.44	8.20	91	48.9	5.8	0.81	0.32	0.05	35.03

(continued overpage)

(Table 6T2 continued)

Sample (core, section, interval(cm))		Depth (mbsf)	Age (Ma)	$CaCO_3$ (%)	CaO (%)	SiO_2 (%)	Al_2O_3 (%)	Fe_2O_3 T (%)	TiO_2 (%)	LOI (%)
25 X 3	70 - 75	230.5	8.27	-	-	-	-	-	-	-
25 X 5	69 - 74	233.44	8.35	73	-	-	-	-	-	-
26 X 1	68 - 73	237.03	8.43	82	46.1	10.2	1.43	0.54	0.09	30.91
27 X 3	70 - 75	249.65	8.96	90	49.1	5.7	0.90	0.41	0.06	38.48
28 X 3	69 - 74	259.24	9.58	91	-	-	-	-	-	-
29 X 3	74 - 79	268.89	10.14	89	-	-	-	-	-	-

(b) 1125

Sample (core, section, interval(cm))		Depth (mbsf)	Depth (mcd)	Age (Ma)	$CaCO_3$ (%)	CaO (%)	SiO_2 (%)	Al_2O_3 (%)	Fe_2O_3 T (%)	TiO_2 (%)	LOI (%)
1 H 4	72 - 77	5.27	6.81	0.33	71	-	-	-	-	-	-
2 H 2	45 - 50	10.30	13.35	0.58	59	-	-	-	-	-	-
2 H 6	120 - 125	17.05	20.10	0.85	62	-	-	-	-	-	-
3 H 3	72 - 77	21.57	25.66	1.01	70	-	-	-	-	-	-
3 H 6	115 - 120	26.50	30.59	1.15	42	-	-	-	-	-	-
4 H 3	52 - 57	30.87	35.45	1.21	52	-	-	-	-	-	-
4 H 6	105 - 110	35.90	40.48	1.43	65	-	-	-	-	-	-
5 H 4	75 - 80	42.10	51.26	1.99	70	-	-	-	-	-	-
6 H 5	72 - 77	53.07	63.00	2.61	53	-	-	-	-	-	-
7 H 3	72 - 77	59.57	71.69	2.89	56	-	-	-	-	-	-
8 H 1	72 - 77	66.07	77.27	3.02	54	-	-	-	-	-	-
8 H 6	72 - 77	73.57	84.77	3.07	54	-	-	-	-	-	-
9 H 4	72 - 77	80.07	91.61	3.22	65	-	-	-	-	-	-

10 H 2	72 - 77	86.57	100.24	3.48	63	-	-	-	-	-	-

(continued overpage)

(Table 6T2 continued)

Sample (core, section, interval(cm))		Depth (mbsf)	Depth (mcd)	Age (Ma)	$CaCO_3$ (%)	CaO (%)	SiO_2 (%)	Al_2O_3 (%)	Fe_2O_3 T (%)	TiO_2 (%)	LOI (%)
11 H 1	72 - 77	94.57	108.63	3.64	56	-	-	-	-	-	-
12 H 3	72 - 77	106.5	122.5	3.83	59	33.71	24.2	6.3	2.25	0.33	29.66
13 H 3	72 - 77	116.6	132.7	4.02	60	-	-	-	-	-	-
14 H 3	72 - 77	126.1	143.7	4.21	58	34.1	24.5	5.73	2.26	0.296	30.4
15 H 3	72 - 77	135.6	154.4	4.39	45	24.6	35.6	7.90	2.41	0.317	24.6
16 H 3	72 - 77	145.1	164.3	4.58	55	-	-	-	-	-	-
17 H 3	72 - 77	154.6	174.9	4.76	57	33.1	24.7	5.92	2.47	0.354	31.0
18 H 3	72 - 77	164.1	188.6	4.85	52	31.4	25.9	7.36	2.83	0.390	28.8
19 H 3	72 - 77	173.6	198.8	4.93	60	-	-	-	-	-	-
20 H 3	72 - 77	183.1	209.9	5.00	65	38.1	18.7	4.77	1.79	0.267	34.2
21 X 3	70 - 75	192.6	219.6	5.07	63	38.1	19.2	4.93	1.89	0.250	33.1
22 X 3	70 - 75	201	232*	5.13	64	-	-	-	-	-	-
23 X 3	69 - 74	210.5	241.6	5.20	52	-	-	-	-	-	-
24 X 3	70 - 75	220.2	251.2	5.27	47	27.6	32.3	7.23	2.49	0.331	26.0
25 X 3	69 - 74	229.7	260.8	5.33	46	28.7	30.2	7.70	2.8	0.387	26.8
26 X 1	44 - 49	236.1	267.2	5.36	45	27.1	31.7	7.69	2.78	0.372	26.2
26 X 1	91 - 96	236.6	267.6	5.36	48	-	-	-	-	-	-
26 X 1	140 - 145	237.1	268.1	5.36	50	27.5	30.8	7.75	2.82	0.378	27.1
26 X 2	44 - 49	237.6	268.7	5.36	51	-	-	-	-	-	-
26 X 2	91 - 96	238.1	269.1	5.37	48	28.2	30.8	6.84	2.38	0.328	28.1
26 X 2	140 - 145	238.6	269.6	5.37	47	-	-	-	-	-	-
26 X 3	44 - 49	239.1	270.2	5.37	43	-	-	-	-	-	-

26 X 3	70 - 75	239.4	270.4	5.37	45	-	-	-	-	-	-
26 X 3	91 - 96	239.6	270.6	5.37	40	-	-	-	-	-	-

(continued overpage)

(Table 6T2 continued)

Sample (core, section, interval(cm))		Depth (mbsf)	Depth (mcd)	Age (Ma)	$CaCO_3$ (%)	CaO (%)	SiO_2 (%)	Al_2O_3 (%)	Fe_2O_3 T (%)	TiO_2 (%)	LOI (%)
26 X 3	140 - 145	240.1	271.1	5.38	42	23.8	36.0	8.04	2.65	0.371	24.9
26 X 4	44 - 49	240.6	271.7	5.38	40	-	-	-	-	-	-
26 X 4	91 - 96	241.1	272.1	5.38	23	-	-	-	-	-	-
26 X 4	140 - 145	241.5	272.5	5.38	67	-	-	-	-	-	-
26 X 5	45 - 50	242.1	273.2	5.39	69	-	-	-	-	-	-
26 X 5	92 - 97	242.6	273.6	5.39	63	37.0	21.3	5.60	2.02	0.278	32.2
26 X 5	140 - 145	243.1	274.1	5.39	64	-	-	-	-	-	-
26 X 6	44 - 49	243.6	274.7	5.39	64	36.5	21.3	5.07	1.78	0.234	32.2
26 X 6	90 - 95	244.1	275.1	5.39	59	-	-	-	-	-	-
26 X 6	140 - 145	244.6	275.6	5.40	58	32.7	25.6	6.18	2.23	0.294	30.3
27 X 1	45 - 50	245.7	276.8	5.40	61	36.1	22.8	5.81	2.17	0.298	30.9
27 X 1	92 - 97	246.2	277.2	5.40	60	-	-	-	-	-	-
27 X 1	140 - 145	246.7	277.7	5.41	62	36.9	20.0	4.87	2.35	0.247	32.3
27 X 2	44 - 49	247.2	278.3	5.41	66	-	-	-	-	-	-
27 X 2	90 - 95	247.7	278.7	5.41	67	39.1	18.1	4.84	1.8	0.252	33.4
27 X 2	140 - 145	248.2	279.2	5.41	70	-	-	-	-	-	-
27 X 3	45 - 50	248.7	279.8	5.41	70	-	-	-	-	-	-
27 X 3	70 - 75	249	280	5.41	64	-	-	-	-	-	-
27 X 3	90 - 95	249.2	280.2	5.41	65	-	-	-	-	-	-
27 X 3	140 - 145	249.7	280.7	5.42	64	-	-	-	-	-	-
27 X 4	43 - 48	250.2	281.3	5.42	69	-	-	-	-	-	-

27 X 4	88 - 93	250.6	281.7	5.42	60	-	-	-	-	-	-
27 X 4	133 - 138	251.1	282.2	5.42	70	-	-	-	-	-	-
27 X 5	44 - 49	251.7	282.8	5.42	66	-	-	-	-	-	-

(continued overpage)

(Table 6T2 continued)

Sample (core, section, interval(cm))		Depth (mbsf)	Depth (mcd)	Age (Ma)	$CaCO_3$ (%)	CaO (%)	SiO_2 (%)	Al_2O_3 (%)	Fe_2O_3 T (%)	TiO_2 (%)	LOI (%)
27 X 5	90 - 95	252.2	283.2	5.42	63	-	-	-	-	-	-
27 X 5	140 - 145	252.7	283.7	5.43	70	40.1	16.4	4.66	1.76	0.241	34.5
27 X 6	44 - 49	253.2	284.3	5.43	60	-	-	-	-	-	-
27 X 6	87 - 92	253.6	284.7	5.43	65	-	-	-	-	-	-
28 X 1	45 - 50	255.3	286.4	5.44	68	-	-	-	-	-	-
28 X 1	90 - 95	255.8	286.8	5.44	65	-	-	-	-	-	-
28 X 1	140 - 145	256.3	287.3	5.44	64	-	-	-	-	-	-
28 X 2	44 - 49	256.8	287.9	5.44	69	-	-	-	-	-	-
28 X 2	91 - 96	257.3	288.3	5.44	59	-	-	-	-	-	-
28 X 2	140 - 145	257.8	288.8	5.44	55	-	-	-	-	-	-
28 X 3	44 - 49	258.3	289.4	5.45	63	36.6	21.2	5.92	2.11	0.291	31.8
28 X 3	70 - 75	258.6	289.6	5.45	62	-	-	-	-	-	-
28 X 3	93 - 98	258.8	289.9	5.45	61	-	-	-	-	-	-
28 X 3	140 - 145	259.3	290.3	5.45	66	-	-	-	-	-	-
28 X 4	44 - 49	259.8	290.9	5.45	67	-	-	-	-	-	-
28 X 4	90 - 95	260.3	291.3	5.45	60	-	-	-	-	-	-
28 X 4	140 - 145	260.8	291.8	5.45	62	-	-	-	-	-	-
28 X 5	44 - 46	261.3	292.3	5.46	59	-	-	-	-	-	-
28 X 5	90 - 95	261.8	292.8	5.46	59	-	-	-	-	-	-
28 X 5	140 - 145	262.3	293.3	5.46	56	-	-	-	-	-	-

28 X 6	42 - 45	262.8	293.8	5.46	65	37.4	20.1	5.17	1.85	0.262	32.3
28 X 6	90 - 95	263.3	294.3	5.46	62	-	-	-	-	-	-
28 X 6	140 - 145	263.8	294.8	5.46	61	-	-	-	-	-	-
29 X 3	66 - 71	268.1	299.2	5.48	68	-	-	-	-	-	-

(continued overpage)

(Table 6T2 continued)

Sample (core, section, interval(cm))		Depth (mbsf)	Depth (mcd)	Age (Ma)	$CaCO_3$ (%)	CaO (%)	SiO_2 (%)	Al_2O_3 (%)	Fe_2O_3 T (%)	TiO_2 (%)	LOI (%)
30 X 3	70 - 75	277.9	308.9	5.52	66	37.6	20.7	5.28	1.93	0.271	32.5
31 X 3	80 - 85	287.5	318.5	5.56	69	40.1	18.1	4.47	1.61	0.234	34.0
32 X 1	47 - 50	293.8	324.9	5.58	61	36.0	21.8	6.08	2.16	0.292	31.7
32 X 1	90 - 95	294.3	325.3	5.58	61	-	-	-	-	-	-
32 X 1	140 - 145	294.8	325.8	5.58	63	35.9	22.0	5.91	2.16	0.277	31.9
32 X 2	44 - 49	295.3	326.4	5.58	62	-	-	-	-	-	-
32 X 2	90 - 95	295.8	326.8	5.58	67	38.4	19.4	4.91	1.99	0.250	33.0
32 X 2	140 - 143	296.2	327.3	5.59	68	-	-	-	-	-	-
32 X 3	43 - 48	296.8	327.9	5.59	68	-	-	-	-	-	-
32 X 3	70 - 75	297.1	328.1	5.59	67	-	-	-	-	-	-
32 X 3	90 - 95	297.3	328.3	5.59	63	-	-	-	-	-	-
32 X 3	142 - 146	297.8	328.8	5.59	62	-	-	-	-	-	-
32 X 4	48 - 53	298.3	329.4	5.59	62	-	-	-	-	-	-
32 X 4	90 - 95	298.8	329.8	5.59	60	-	-	-	-	-	-
32 X 4	140 - 145	299.3	330.3	5.60	64	-	-	-	-	-	-
32 X 5	41 - 43	299.7	330.8	5.60	63	-	-	-	-	-	-
32 X 5	90 - 95	300.3	331.3	5.60	61	-	-	-	-	-	-
32 X 5	140 - 145	300.8	331.8	5.60	63	-	-	-	-	-	-
32 X 6	42 - 47	301.3	332.3	5.60	60	34.2	24.5	6.15	2.16	0.302	30.7

32 X 6	90 - 95	301.8	332.8	5.60	64	-	-	-	-	-	-
32 X 6	140 - 145	302.3	333.3	5.61	67	-	-	-	-	-	-
33 X 1	45 - 50	303.5	334.6	5.61	63	-	-	-	-	-	-
33 X 1	90 - 95	304	335	5.61	67	-	-	-	-	-	-
33 X 1	140 - 145	304.5	335.5	5.61	57	-	-	-	-	-	-

(continued overpage)

(Table 6T2 continued)

Sample (core, section, interval(cm))		Depth (mbsf)	Depth (mcd)	Age (Ma)	$CaCO_3$ (%)	CaO (%)	SiO_2 (%)	Al_2O_3 (%)	Fe_2O_3 T (%)	TiO_2 (%)	LOI (%)
33 X 2	44 - 49	305	336.1	5.61	59	-	-	-	-	-	-
33 X 2	90 - 95	305.5	336.5	5.62	54	-	-	-	-	-	-
33 X 2	140 - 145	306	337	5.62	57	-	-	-	-	-	-
33 X 3	43 - 48	306.5	337.6	5.62	62	-	-	-	-	-	-
33 X 3	69 - 74	306.7	337.8	5.62	62	-	-	-	-	-	-
33 X 3	90 - 93	306.9	338	5.62	61	36.3	21.9	5.65	1.92	0.281	32.2
33 X 3	140 - 145	307.5	338.5	5.62	62	-	-	-	-	-	-
33 X 4	44 - 49	308	339.1	5.62	62	-	-	-	-	-	-
33 X 4	90 - 95	308.5	339.5	5.63	58	-	-	-	-	-	-
33 X 4	132 - 137	308.9	339.9	5.63	57	-	-	-	-	-	-
33 X 5	48 - 47	309.5	340.5	5.63	55	-	-	-	-	-	-
33 X 5	90 - 95	310	341	5.63	54	-	-	-	-	-	-
33 X 5	141 - 146	310.5	341.5	5.63	51	-	-	-	-	-	-
33 X 6	48 - 53	311	342.1	5.63	54	-	-	-	-	-	-
33 X 6	90 - 95	311.5	342.5	5.63	55	-	-	-	-	-	-
33 X 6	140 - 145	312	343	5.64	58	32.3	25.9	6.89	2.37	0.330	29.5
34 X 1	47 - 52	313.1	344.2	5.64	59	-	-	-	-	-	-
34 X 1	90 - 95	313.6	344.6	5.64	58	-	-	-	-	-	-

34 X 1	142 - 147	314.1	345.1	5.64	64	-	-	-	-	-	-
34 X 2	45 - 50	314.6	345.7	5.65	63	-	-	-	-	-	-
34 X 2	89 - 94	315	346.1	5.65	65	-	-	-	-	-	-
34 X 2	140 - 145	315.6	346.6	5.65	58	-	-	-	-	-	-
34 X 3	45 - 50	316.1	347.2	5.65	64	-	-	-	-	-	-
34 X 3	72 - 77	316.4	347.4	5.65	58	-	-	-	-	-	-

(continued overpage)

(Table 6T2 continued)

Sample (core, section, interval(cm))		Depth (mbsf)	Depth (mcd)	Age (Ma)	$CaCO_3$ (%)	CaO (%)	SiO_2 (%)	Al_2O_3 (%)	Fe_2O_3 T (%)	TiO_2 (%)	LOI (%)
34 X 3	93 - 98	316.6	347.7	5.65	61	-	-	-	-	-	-
34 X 3	140 - 145	317.1	348.1	5.65	60	-	-	-	-	-	-
34 X 4	44 - 49	317.6	348.7	5.65	65	-	-	-	-	-	-
34 X 4	89 - 94	318	349.1	5.66	65	-	-	-	-	-	-
34 X 4	140 - 145	318.6	349.6	5.66	64	-	-	-	-	-	-
34 X 5	44 - 49	319.1	350.2	5.66	64	-	-	-	-	-	-
34 X 5	90 - 95	319.6	350.6	5.66	62	-	-	-	-	-	-
34 X 5	140 - 145	320.1	351.1	5.66	65	-	-	-	-	-	-
34 X 6	45 - 50	320.6	351.7	5.66	71	-	-	-	-	-	-
35 X 3	71 - 76	325.7	356.7	5.68	61	-	-	-	-	-	-
37 X 3	68 - 73	344.8	375.9	6.41	64	37.7	20.0	5.24	1.97	0.264	33.0
38 X 1	72 - 77	351.47	382.54	6.72	56	-	-	-	-	-	-
38 X 3	68 - 73	354.4	385.5	6.83	56	31.3	27.5	7.04	2.37	0.333	28.8
38 X 6	72 - 77	358.97	390.04	6.99	57	-	-	-	-	-	-
39 X 3	68 - 73	364.1	395.2	7.18	55	-	-	-	-	-	-
39 X 6	72 - 77	368.67	399.74	7.35	64	-	-	-	-	-	-
40 X 3	68 - 73	373.8	404.9	7.54	47	-	-	-	-	-	-

43 X 2	72 - 77	401.27	432.34	8.79	51	-	-	-	-	-	-
43 X 5	72 - 77	405.77	436.84	8.90	50	-	-	-	-	-	-
44 X 3	72 - 77	411.69	442.76	9.04	47	-	-	-	-	-	-
45 X 1	72 - 77	419.07	450.14	9.22	52	-	-	-	-	-	-
45 X 5	72 - 77	425.07	456.14	9.36	54	-	-	-	-	-	-
46 X 2	72 - 77	430.17	461.24	9.48	42	-	-	-	-	-	-
46 X 6	72 - 77	436.17	467.24	9.60	41	-	-	-	-	-	-

(continued overpage)

(Table 6T2 continued)

Sample		Depth	Depth	Age	$CaCO_3$	CaO	SiO_2	Al_2O_3	Fe_2O_3 T	TiO_2	LOI
(core, section, interval(cm))		(mbsf)	(mcd)	(Ma)	(%)	(%)	(%)	(%)	(%)	(%)	(%)
48 X 2	72 - 77	449.07	480.14	9.86	41	-	-	-	-	-	-
49 X 4	72 - 77	461.67	492.74	10.08	46	-	-	-	-	-	-
50 X 5	72 - 77	472.77	503.84	10.26	22	-	-	-	-	-	-
54 X 2	72 - 77	506.37	537.44	10.45	49	-	-	-	-	-	-
58 X 4	72 - 77	547.87	578.94	10.85	52	-	-	-	-	-	-

Notes: All samples from sites 594 and 1125 are from holes 594 and 1125B, respectively, unless otherwise stated. Depths are given in ‘metres below seafloor’ (mbsf) and have been calculated to the base of the sample interval; all ages have been calculated according to **Table 6T1** (see also **Fig. 6F1**). ‘Metres composite depth’ (mcd) for site 1125 (cores 1H4-22X2*) are from Carter et al. (1999); the mbsf depth offset between holes 1125A and 1125B at core 22X2 (31.07m) is used to calculate mcd’s for deeper cores.

Table 6T3
Stable carbon and oxygen isotope data (‰ relative to PDB) at (a) DSDP site 594 and (b) ODP site 1125

(a) 594

Sample (core, section, interval(cm))			Depth (mbsf)	Age (Ma)	Bulk sediment $\delta^{13}C$	Bulk sediment $\delta^{18}O$
14 H 4	73 - 77		126.37	1.84	-0.23	2.53
15 X 3	63 - 65		134.35	2.10	0.13	2.69
16 X 3	52 - 57		143.87	2.60	1.26	2.52
594A 10 X 5	71 - 76		156.66	3.46	1.22	2.36
18 X 1	67 - 71		160.21	3.58	0.18	1.86
19 X 3	68 - 73		172.83	4.16	*1.17*	*2.24*
20 X 2	54 - 59		180.79	4.97	*1.88*	*3.37*
20 X 4	54 - 59		183.79	5.20	*1.28*	*2.77*
20 X 5	63 - 66		185.36	5.21	1.71	2.75
21 X 2	64 - 66		190.46	5.21	1.73	2.74
21 X 4	71 - 75		193.55	5.22	*1.49*	*3.10*
21 X 6	70 - 74		196.54	5.22	1.48	2.70
594A 11 X 1	70 - 75		198.65	5.23	1.63	2.93
594A 11 X 3	69 - 74		201.64	5.28	1.77	2.87
594A 11 X 5	69 - 74		204.64	5.50	1.34	2.33
23 X 2	70 - 72		209.72	5.87	1.87	2.16
23 X 4	76 - 78		212.78	6.01	1.99	2.59
23 X 6	74 - 79		215.79	6.15	1.98	2.23
24 X 2	85 - 89		219.49	6.33	1.89	2.69
24 X 4	4 - 77		222.37	6.52	0.99	2.03
24 X 6	68 - 73		225.33	8.15	1.13	1.8
25 X 1	69 - 74		227.44	8.20	1.91	2.12
25 X 3	70 - 75		230.45	8.27	*2.04*	*2.59*
25 X 5	69 - 74		233.44	8.35	1.43	1.92
26 X 1	68 - 73		237.03	8.43	1.32	1.49
27 X 3	70 - 75		249.65	8.96	2.01	2.2
28 X 3	69 - 74		259.24	9.58	2.42	2.52
29 X 3	74 - 79		268.89	10.14	2.54	2.51

((b) continues overpage)

(Table 6T3 continued)

(b) 1125

Sample (core, section, interval(cm))	Depth (mbsf)	Depth (mcd)	Age (Ma)	Bulk sediment		*O. universa*		*G. bulloides*		*Uvigerina spp.*	
				$\delta^{13}C$	$\delta^{18}O$	$\delta^{13}C$	$\delta^{18}O$	$\delta^{13}C$	$\delta^{18}O$	$\delta^{13}C$	$\delta^{18}O$
1 H 4 72 - 77	5.27	6.81	0.326	*1.40*	*2.90*	*2.17*	*1.99*	0.31	2.54	-0.56	4.41
2 H 2 45 - 50	10.30	13.35	0.584	0.63	1.61	1.65	1.16	-0.73	1.17	-0.31	3.70
2 H 6 120 - 125	17.05	20.10	0.854	0.21	2.19	1.68	1.54	-0.82	1.73	-0.41	3.97
3 H 3 72 - 77	21.57	25.66	1.012	1.12	2.01	1.99	1.64	0.30	1.15	*-0.49*	*3.53*
3 H 6 115 - 120	26.50	30.59	1.148	-0.01	1.28	*1.72*	-	-0.55	1.17	-0.66	4.04
4 H 3 52 - 57	30.87	35.45	1.209	0.69	1.55	2.31	1.16	0.05	1.00	-0.52	3.45
4 H 6 105 - 110	35.90	40.48	1.426	0.24	1.34	*1.87*	*1.16*	0.28	3.73	-0.63	3.73
5 H 4 75 - 80	42.10	51.26	1.994	0.28	1.40	2.41	1.21	0.72	1.26	-0.48	3.53
6 H 5 72 - 77	53.07	63.00	2.607	0.56	1.43	*2.11*	*1.21*	0.23	0.89	*-0.66*	*3.19*
7 H 3 72 - 77	59.57	71.69	2.888	0.27	1.09	2.66	0.92	-0.01	0.56	-0.39	2.91
8 H 1 72 - 77	66.07	77.27	3.021	*0.48*	*1.21*	2.21	0.96	*0.08*	*0.71*	-0.63	2.84
8 H 6 72 - 77	73.57	84.77	3.071	0.40	1.10	1.75	0.90	0.34	0.97	-0.50	2.82
9 H 4 72 - 77	80.07	91.61	3.224	0.35	1.13	2.06	0.62	-0.39	0.53	-	-
10 H 2 72 - 77	86.57	100.24	3.482	0.40	0.97	*2.03*	*0.97*	-0.10	0.76	-0.46	2.79
11 H 1 72 - 77	94.57	108.63	3.639	-0.17	0.94	1.99	0.70	0.20	0.25	-0.48	2.65
12 H 3 72 - 77	106.47	122.47	3.829	0.00	1.04	-	-	-	-	-	-
13 H 3 72 - 77	116.57	132.65	4.024	0.35	1.28	2.26	0.47	*-0.46*	*0.08*	*-0.63*	*2.70*
14 H 3 72 - 77	126.07	143.69	4.208	0.29	1.10	*2.30*	*0.82*	0.40†	0.32†	*-0.53*	*2.69*
15 H 3 72 - 77	135.57	154.38	4.392	0.73	1.37	*1.52*	*0.76*	*0.13*	*0.42*	*-0.76*	*3.00*
16 H 3 72 - 77	145.07	164.34	4.575	0.55	1.32	*2.21*	*0.73*	*0.32*	*0.36*	*-0.62*	*2.88*
17 H 3 72 - 77	154.57	174.94	4.759	0.71	1.35	*2.27*	*0.74*	*0.96*	*0.07*	*-0.45*	*2.91*
18 H 3 72 - 77	164.07	188.58	4.855	0.94	2.27	*1.61*	*1.31*	*-0.40*	*1.05*	*-1.37*	*2.86*
19 H 3 72 - 77	173.57	198.83	4.926	0.70	1.55	-	-	-	-	-	-
20 H 3 72 - 77	183.07	209.88	4.997	0.77	1.77	*1.80*	*0.69*	*0.11*	*0.62*	*-0.96*	*3.03*
21 X 3 70 - 75	192.55	219.61	5.067	1.23	1.78	*1.73*	*0.97*	*0.18*	*0.52*	-	-
22 X 3 70 - 75	200.95	232.02	5.130	0.76	1.34	-	-	-	-	-	-

(continued overpage)

(Table 6T3 continued)

Sample (core, section, interval(cm))	Depth (mbsf)	Depth (mcd)	Age (Ma)	Bulk sediment		*O. universa*		*G. bulloides*		*Uvigerina spp.*	
				$\delta^{13}C$	$\delta^{18}O$	$\delta^{13}C$	$\delta^{18}O$	$\delta^{13}C$	$\delta^{18}O$	$\delta^{13}C$	$\delta^{18}O$
23 X 3 69 - 74	210.54	241.61	5.202	*0.60*	*1.48*	*1.68*	*0.94*	*-0.57*	*0.61*	*-1.14*	*2.92*
24 X 3 70 - 75	220.15	251.22	5.273	0.66	1.47	*1.78*	*1.07*	-	-	*-0.95*	*2.75*
25 X 3 69 - 74	229.74	260.81	5.328	1.21	1.55	-	-	-	-	-	-
26 X 1 44 - 49	236.09	267.16	5.358	0.58	0.94	*2.14*	*0.67*	-	-	-	-
26 X 1 91 - 96	236.56	267.63	5.360	0.53	1.09	-	-	-	-	*-0.41*	*2.63*
26 X 1 140 - 145	237.05	268.12	5.362	0.60	0.95	-	-	*-0.30*	*0.15*	*-0.53*	*2.86*
26 X 2 44 - 49	237.59	268.66	5.365	0.63	1.01	1.97	0.93	-	-	-	-
26 X 2 91 - 96	238.06	269.13	5.367	-	*1.12*	1.75	0.98	-	-	-	-
26 X 2 140 - 145	238.55	269.62	5.369	0.73	1.06	1.38	0.86	-	-	-	-
26 X 3 44 - 49	239.09	270.16	5.372	0.78	1.33	2.27	0.96	-	-	*-0.97*	*2.67*
26 X 3 70 - 75	239.35	270.42	5.373	*0.73*	*1.48*	*2.19*	*0.94*	-	-	-	-
26 X 3 91 - 96	239.56	270.63	5.374	0.73	1.453	-	-	-	-	-	-
26 X 3 140 - 145	240.05	271.12	5.376	0.86	1.29	2.14	0.35	-	-	-	-
26 X 4 44 - 49	240.59	271.66	5.379	0.71	1.32	1.83	1.20	-	-	*-0.89*	*2.81*
26 X 4 91 - 96	241.06	272.13	5.381	0.87	1.55	-	-	-	-	-	-
26 X 4 140 - 145	241.45	272.52	5.383	1.16	2.12	2.08	0.99	-	-	*-0.69*	*2.84*
26 X 5 45 - 50	242.1	273.17	5.386	1.59	1.85	*2.30*	-	-	-	-0.19	2.79
26 X 5 92 - 97	242.57	273.64	5.388	1.41	1.65	1.59	0.22	-	-	-	-
26 X 5 140 - 145	243.05	274.12	5.390	1.65	1.72	*2.41*	*0.63*	0.52	0.55	*-0.43*	*2.81*
26 X 6 44 - 49	243.59	274.66	5.393	1.11	1.62	*1.80*	*0.68*	-	-	-	-
26 X 6 90 - 95	244.05	275.12	5.395	1.09	1.75	2.38	0.55	-	-	-0.65	2.6
26 X 6 140 - 145	244.55	275.62	5.397	1.20	1.48	2.20	0.56	0.03	-0.20	-	-
27 X 1 45 - 50	245.7	276.77	5.402	0.85	1.70	2.25	0.44	-	-	-0.57	2.82
27 X 1 92 - 97	246.17	277.24	5.403	1.12	1.51	2.16	0.81	-	-	*-0.40*	*2.86*
27 X 1 140 - 145	246.65	277.72	5.405	0.99	1.53	*1.94*	-	-0.03	0.40	-0.62	2.92
27 X 2 44 - 49	247.19	278.26	5.407	0.73	1.57	2.49	0.70	0.07	0.14	-0.44	2.70
27 X 2 90 - 95	247.65	278.72	5.409	0.76	1.73	1.92	-	-	-	-0.55	2.62

(continued overpage)

(Table 6T3 continued)

Sample (core, section, interval(cm))	Depth (mbsf)	Depth (mcd)	Age (Ma)	Bulk sediment		*O. universa*		*G. bulloides*		*Uvigerina spp.*	
				$\delta^{13}C$	$\delta^{18}O$	$\delta^{13}C$	$\delta^{18}O$	$\delta^{13}C$	$\delta^{18}O$	$\delta^{13}C$	$\delta^{18}O$
27 X 2 140 - 145	248.15	279.22	5.410	0.75	1.91	2.05	0.85	0.20	0.83	*-0.47*	*2.84*
27 X 3 45 - 50	248.7	279.77	5.412	0.66	1.79	-	-	-	-	-	-
27 X 3 70 - 75	248.95	280.02	5.413	0.86	1.72	-	-	-	-	-	-
27 X 3 90 - 95	249.15	280.22	5.414	0.71	1.58	-	-	-	-	-	-
27 X 3 140 - 145	249.65	280.72	5.415	1.16	1.49	-	-	-	-	-	-
27 X 4 43 - 48	250.18	281.25	5.417	1.05	1.55	-	-	-	-	-	-
27 X 4 88 - 93	250.63	281.70	5.419	0.99	1.57	-	-	-	-	-	-
27 X 4 133 - 138	251.08	282.15	5.420	0.82	1.66	-	-	-	-	-	-
27 X 5 44 - 49	251.69	282.76	5.423	0.80	0.01	-	-	-	-	-	-
27 X 5 90 - 95	252.15	283.22	5.424	0.78	1.57	-	-	-	-	-	-
27 X 5 140 - 145	252.65	283.72	5.426	0.83	1.85	-	-	-	-	-	-
27 X 6 44 - 49	253.19	284.26	5.428	0.90	1.99	-	-	-	-	-	-
27 X 6 87 - 92	253.62	284.69	5.429	0.83	1.61	-	-	-	-	-	-
28 X 1 45 - 50	255.3	286.37	5.435	1.08	1.91	-	-	-	-	-	-
28 X 1 90 - 95	255.75	286.82	5.437	1.11	1.81	-	-	-	-	-	-
28 X 1 140 - 145	256.25	287.32	5.438	1.04	1.70	-	-	-	-	-	-
28 X 2 44 - 49	256.79	287.86	5.440	1.08	1.79	-	-	-	-	-	-
28 X 2 91 - 96	257.26	288.33	5.442	1.35	1.89	-	-	-	-	-	-
28 X 2 140 - 145	257.75	288.82	5.444	1.52	1.89	-	-	-	-	-	-
28 X 3 44 - 49	258.29	289.36	5.445	1.55	1.82	-	-	-	-	-	-
28 X 3 70 - 75	258.55	289.62	5.446	1.53	1.82	-	-	-	-	-	-
28 X 3 93 - 98	258.78	289.85	5.447	1.65	1.94	-	-	-	-	-	-
28 X 3 140 - 145	259.25	290.32	5.449	1.11	1.69	-	-	-	-	-	-
28 X 4 44 - 49	259.79	290.86	5.451	1.28	1.82	-	-	-	-	-	-
28 X 4 90 - 95	260.25	291.32	5.452	1.64	1.86	-	-	-	-	-	-
28 X 4 140 - 145	260.75	291.82	5.454	1.46	1.64	-	-	-	-	-	-
28 X 5 44 - 46	261.26	292.33	5.456	1.46	1.76	-	-	-	-	-	-

(continued overpage)

(Table 6T3 continued)

Sample (core, section, interval(cm))	Depth (mbsf)	Depth (mcd)	Age (Ma)	Bulk sediment		*O. universa*		*G. bulloides*		*Uvigerina spp.*	
				$\delta^{13}C$	$\delta^{18}O$	$\delta^{13}C$	$\delta^{18}O$	$\delta^{13}C$	$\delta^{18}O$	$\delta^{13}C$	$\delta^{18}O$
28 X 5 90 - 95	261.75	292.82	5.457	1.47	1.58	-	-	-	-	-	-
28 X 5 140 - 145	262.25	293.32	5.459	1.12	1.54	-	-	-	-	-	-
28 X 6 42 - 45	262.75	293.82	5.461	0.65	1.59	-	-	-	-	-	-
28 X 6 90 - 95	263.25	294.32	5.463	1.00	1.69	-	-	-	-	-	-
28 X 6 140 - 145	263.75	294.82	5.464	1.14	1.49	-	-	-	-	-	-
29 X 3 66 - 71	268.11	299.18	5.480	1.23	1.60	-	-	-	-	-	-
30 X 3 70 - 75	277.85	308.92	5.516	0.91	1.47	2.17	0.64	0.28	0.69	-	-
31 X 3 80 - 85	287.47	318.54	5.557	1.41	1.42	-	-	-	-	-	-
32 X 1 47 - 50	293.8	324.87	5.578	1.34	1.65	-	-	-	-	-	-
32 X 1 90 - 95	294.25	325.32	5.579	*1.47*	*1.68*	*2.53*	*1.25*	1.13	0.83	-	-
32 X 1 140 - 145	294.75	325.82	5.581	1.29	1.96	-	-	1.43	0.77	-	-
32 X 2 44 - 49	295.29	326.36	5.583	1.46	1.57	2.41	0.80	1.30	0.39	-	-
32 X 2 90 - 95	295.75	326.82	5.584	1.42	1.72	-	-	-	-	-	-
32 X 2 140 - 143	296.23	327.30	5.586	1.39	1.60	-	-	-	-	-	-
32 X 3 43 - 48	296.78	327.85	5.587	1.34	1.42	-	-	-	-	-	-
32 X 3 70 - 75	297.05	328.12	5.588	1.31	1.53	-	-	-	-	-	-
32 X 3 90 - 95	297.25	328.32	5.589	1.38	1.58	-	-	-	-	-	-
32 X 3 142 - 146	297.76	328.83	5.591	1.29	1.65	-	-	-	-	-	-
32 X 4 48 - 53	298.33	329.40	5.592	1.14	1.48	-	-	-	-	-	-
32 X 4 90 - 95	298.75	329.82	5.594	1.17	1.41	-	-	-	-	-	-
32 X 4 140 - 145	299.25	330.32	5.595	1.15	1.20	-	-	-	-	-	-
32 X 5 41 - 43	299.73	330.80	5.597	1.24	1.49	2.91	-0.04	0.97	0.09	-	2.53
32 X 5 90 - 95	300.25	331.32	5.599	1.07	1.59	-	-	-	-	-	-
32 X 5 140 - 145	300.75	331.82	5.600	1.07	1.38	-	-	-	-	-	-
32 X 6 42 - 47	301.27	332.34	5.602	1.15	1.42	-	-	-	-	-	-
32 X 6 90 - 95	301.75	332.82	5.603	1.32	1.34	-	-	-	-	-	-
32 X 6 140 - 145	302.25	333.32	5.605	1.31	1.21	-	-	-	-	-	-

(continued overpage)

(Table 6T3 continued)

Sample (core, section, interval(cm))		Depth (mbsf)	Depth (mcd)	Age (Ma)	Bulk sediment		*O. universa*		*G. bulloides*		*Uvigerina spp.*	
					$\delta^{13}C$	$\delta^{18}O$	$\delta^{13}C$	$\delta^{18}O$	$\delta^{13}C$	$\delta^{18}O$	$\delta^{13}C$	$\delta^{18}O$
33 X 1	45 - 50	303.5	334.57	5.609	0.97	1.45	-	-	-	-	-	-
33 X 1	90 - 95	303.95	335.02	5.611	-	-	-	-	-	-	-	-
33 X 1	140 - 145	304.45	335.52	5.612	0.93	1.27	-	-	-	-	-	-
33 X 2	44 - 49	304.99	336.06	5.614	0.93	1.53	2.41	0.57	1.28	0.54	-	-
33 X 2	90 - 95	305.45	336.52	5.615	*1.05*	*1.08*	-	-	-	-	-	-
33 X 2	140 - 145	305.95	337.02	5.617	*1.28*	*1.24*	-	-	-	-	-	-
33 X 3	43 - 48	306.48	337.55	5.619	1.17	1.05	-	-	-	-	-	-
33 X 3	69 - 74	306.74	337.81	5.620	1.16	1.10	-	-	-	-	-	-
33 X 3	90 - 93	306.93	338.00	5.620	1.22	1.14	-	-	-	-	-	-
33 X 3	140 - 145	307.45	338.52	5.622	1.17	1.14	-	-	-	-	-	-
33 X 4	44 - 49	307.99	339.06	5.624	1.20	1.25	-	-	-	-	-	-
33 X 4	90 - 95	308.45	339.52	5.625	1.32	1.40	-	-	-	-	-	-
33 X 4	132 - 137	308.87	339.94	5.627	1.32	1.51	-	-	-	-	-	-
33 X 5	48 - 47	309.47	340.54	5.628	1.17	1.12	2.71	0.59	1.91	0.08	-	-
33 X 5	90 - 95	309.95	341.02	5.630	1.04	1.21	-	-	-	-	-	-
33 X 5	141 - 146	310.46	341.53	5.632	*0.98*	*1.40*	-	-	-	-	-	-
33 X 6	48 - 53	311.03	342.10	5.634	1.09	1.28	-	-	-	-	-	-
33 X 6	90 - 95	311.45	342.52	5.635	1.07	1.42	-	-	-	-	-	-
33 X 6	140 - 145	311.95	343.02	5.636	1.26	1.48	-	-	-	-	-	-
34 X 1	47 - 52	313.12	344.19	5.640	1.02	1.02	-	-	-	-	-	-
34 X 1	90 - 95	313.55	344.62	5.642	1.09	1.16	-	-	-	-	-	-
34 X 1	142 - 147	314.07	345.14	5.643	1.01	1.14	-	-	-	-	-	-
34 X 2	45 - 50	314.6	345.67	5.645	1.07	1.32	*2.66*	*0.76*	0.62	0.64	-0.95	2.64
34 X 2	89 - 94	315.04	346.11	5.646	0.89	1.45	-	-	-	-	-	-
34 X 2	140 - 145	315.55	346.62	5.648	1.08	1.27	-	-	-	-	-	-
34 X 3	45 - 50	316.1	347.17	5.650	1.03	0.18	-	-	-	-	-	-
34 X 3	72 - 77	316.37	347.44	5.651	1.06	0.88	-	-	-	-	-	-

(continued overpage)

(Table 6T3 continued)

Sample (core, section, interval(cm))		Depth (mbsf)	Depth (mcd)	Age (Ma)	Bulk sediment		*O. universa*		*G. bulloides*		*Uvigerina spp.*	
					$\delta^{13}C$	$\delta^{18}O$	$\delta^{13}C$	$\delta^{18}O$	$\delta^{13}C$	$\delta^{18}O$	$\delta^{13}C$	$\delta^{18}O$
34 X 3	93 - 98	316.58	347.65	5.651	1.24	1.42	-	-	-	-	-	-
34 X 3	140 - 145	317.05	348.12	5.653	1.64	1.71	-	-	-	-	-	-
34 X 4	44 - 49	317.59	348.66	5.655	1.24	1.29	-	-	-	-	-	-
34 X 4	89 - 94	318.04	349.11	5.656	1.37	1.31	-	-	-	-	-	-
34 X 4	140 - 145	318.55	349.62	5.658	*1.47*	*1.43*	-	-	-	-	-	-
34 X 5	44 - 49	319.09	350.16	5.660	*1.30*	*1.37*	-	-	-	-	-	-
34 X 5	90 - 95	319.55	350.62	5.661	1.07	1.43	-	-	-	-	-	-
34 X 5	140 - 145	320.05	351.12	5.663	1.10	1.48	2.26	0.90	-	-	*-0.03*	*2.84*
34 X 6	45 - 50	320.6	351.67	5.664	1.25	1.64	-	-	-	-	-	-
35 X 3	71 - 76	325.66	356.73	5.681	0.95	1.11	2.81	0.54	0.38	0.16	-0.70	2.65
37 X 3	68 - 73	344.83	375.90	6.413	1.43	1.24	2.49	0.58	-	-	-0.49	2.55
38 X 1	72 - 77	351.47	382.54	6.717	*1.28*	*0.97*	2.82	0.48	0.93	0.11	*-0.49*	*2.60*
38 X 3	68 - 73	354.43	385.50	6.826	1.17	1.22	3.07	0.89	1.12	0.36	0.19	2.78
38 X 6	72 - 77	358.97	390.04	6.993	*1.52*	*1.07*	3.00	0.57	2.46	1.17	*0.34*	*2.78*
39 X 3	68 - 73	364.13	395.20	7.183	1.40	1.21	2.94	0.89	*0.87*	*0.88*	0.00	2.72
39 X 6	72 - 77	368.67	399.74	7.350	*1.40*	*1.33*	-	-	-	-	0.17	2.98
40 X 3	68 - 73	373.83	404.90	7.540	1.40	1.34	-	-	-	-	-	-
43 X 2	72 - 77	401.27	432.34	8.787	1.10	0.88	-	-	*1.24*	*0.60*	-	-
43 X 5	72 - 77	405.77	436.84	8.896	0.93	0.52	*2.71*	*0.36*	1.48	0.74	-	-
44 X 3	72 - 77	411.69	442.76	9.040	0.94	0.79	*2.50*	*0.62*	1.42	0.61	-	-
45 X 1	72 - 77	419.07	450.14	9.219	1.09	0.65	*2.97*	*0.42*	0.98	-0.34	-	-
45 X 5	72 - 77	425.07	456.14	9.364	0.54	0.49	3.00	0.02	1.95	0.54	-	-
46 X 2	72 - 77	430.17	461.24	9.478	0.40	0.60	*2.75*	*0.38*	1.33	0.63	-0.46	2.49
46 X 6	72 - 77	436.17	467.24	9.601	0.57	0.78	2.42	0.69	-	-	*-0.74*	*2.65*
48 X 2	72 - 77	449.07	480.14	9.865	0.50	0.59	-	-	-	-	-	-
49 X 4	72 - 77	461.67	492.74	10.080	*1.18*	*0.85*	2.64	0.29	2.20	1.17	0.42	2.33
50 X 5	72 - 77	472.77	503.84	10.263	0.94	0.68	3.12	0.49	-	-	-	-

(continued overpage)

(Table 6T3 continued)

Sample (core, section, interval(cm))		Depth (mbsf)	Depth (mcd)	Age (Ma)	Bulk sediment		*O. universa*		*G. bulloides*		*Uvigerina spp.*	
					$\delta^{13}C$	$\delta^{18}O$	$\delta^{13}C$	$\delta^{18}O$	$\delta^{13}C$	$\delta^{18}O$	$\delta^{13}C$	$\delta^{18}O$
54 X 2	72 - 77	506.37	537.44	10.450	1.21	0.93	1.83	0.09	-	-	-	-
58 X 4	72 - 77	547.87	578.94	10.847	1.69	0.87	2.27	-0.61	-	-	0.48	-

Notes: All samples from sites 594 and 1125 are from holes 594 and 1125B, respectively, unless otherwise stated. Depths are given in 'metres below seafloor' (mbsf) and have been calculated to the base of the sample interval; all ages have been calculated according to **Table 6T1** (see also **Fig. 6F1**). 'Metres composite depth' (mcd) for site 1125 (cores 1H4-22X2*) are from Carter et al. (1999); the mbsf depth offset between holes 1125A and 1125B at core 22X2 (31.07m) is used to calculate mcd's for deeper cores. Isotope values in *italics* denote the average of duplicate analyses (see **Table 6T5**). † possible contamination during analyses.

Table 6T4
Statistical summary of the accuracy and precision of the stable carbon and oxygen isotope analyses at sites 594 and 1125

	n	Mean error (‰)		σ (‰)		Range of error (‰)			
		$\delta^{13}C$	$\delta^{18}O$	$\delta^{13}C$	$\delta^{18}O$	$\delta^{13}C_{min}$	$\delta^{13}C_{max}$	$\delta^{18}O_{min}$	$\delta^{18}O_{max}$
Bulk sediment$_{594}$	5	0.08	0.10	0.06	0.10	0.02	0.17	0.02	0.27
Bulk sediment$_{1125}$	15	0.07	0.13	0.05	0.07	0.02	0.19	0.02	0.22
O.universa	23	0.09	0.15	0.06	0.07	0.01	0.20	0.01	0.29
G.bulloides	12	0.12	0.12	0.05	0.09	0.04	0.20	0.02	0.29
Uvigerina spp.	23	0.09	0.15	0.05	0.07	0.01	0.15	0.04	0.24

Notes: Repeat analyses were performed on a number (*n*) of core samples. The average (mean) error, and its standard deviation (σ), is based on the maximum range between repeat values ($\delta^{13}C_{max}$-$\delta^{13}C_{min}$, etc.) for each core sample.

Table 6T5
Carbonate accumulation rates and elemental ratios at (a) DSDP site 594 and (b) ODP site 1125

(a) 594

Sample (core, section, interval(cm))				Depth (mbsf)	Age (Ma)	MAR $CaCO_3$ ($g/cm^2/ky$)	Ca/Ti (g/g)	Si/Ti (g/g)	Al/Ti (g/g)
14	H	4	73 - 77	126.37	1.84	5.03	148	66	15
15	X	3	63 - 65	134.35	2.10	2.60	192	72	17
16	X	3	52 - 57	143.87	2.60	5.13	-	-	-
594A 10	X	5	71 - 76	156.66	3.46	10.89	255	61	16
18	X	1	67 - 71	160.21	3.58	1.78	-	-	-
19	X	3	68 - 73	172.83	4.16	2.82	-	-	-
20	X	2	54 - 59	180.79	4.97	4.36	-	-	-
20	X	4	54 - 59	183.79	5.20	4.71	-	-	-
20	X	5	63 - 66	185.36	5.21	4.82	-	-	-
21	X	2	64 - 66	190.46	5.21	4.82	549	72	16
21	X	4	71 - 75	193.55	5.22	4.66	-	-	-
21	X	6	70 - 74	196.54	5.22	4.77	472	68	14
594A 11	X	1	70 - 75	198.65	5.23	3.98	-	-	-
594A 11	X	3	69 - 74	201.64	5.28	1.86	-	-	-
594A 11	X	5	69 - 74	204.64	5.50	1.76	-	-	-
23	X	2	70 - 72	209.72	5.87	2.18	-	-	-
23	X	4	76 - 78	212.78	6.01	3.56	1273	107	14
23	X	6	74 - 79	215.79	6.14	3.70	-	-	-
24	X	2	85 - 89	219.49	6.33	2.14	657	101	16
24	X	4	4 - 77	222.37	6.52	2.08	-	-	-
24	X	6	68 - 73	225.33	8.15	6.65	-	-	-
25	X	1	69 - 74	227.44	8.20	6.65	1164	90	14
25	X	3	70 - 75	230.45	8.27	6.62	-	-	-
25	X	5	69 - 74	233.44	8.35	5.33	-	-	-
26	X	1	68 - 73	237.03	8.43	5.92	624	90	14
27	X	3	70 - 75	249.65	8.96	2.47	-	-	-
28	X	3	69 - 74	259.24	9.58	2.40	-	-	-
29	X	3	74 - 79	268.89	10.14	13.76	-	-	-

(b) 1125

Sample (core, section, interval(cm))				Depth (mbsf)	Age (Ma)	MAR $CaCO_3$ ($g/cm^2/ky$)	Ca/Ti (g/g)	Si/Ti (g/g)	Al/Ti (g/g)
1	H	4	72 - 77	5.27	0.33	1.8	-	-	-
2	H	2	45 - 50	10.30	0.58	2.3	-	-	-
2	H	6	120 - 125	17.05	0.85	2.8	-	-	-
3	H	3	72 - 77	21.57	1.01	3.0	-	-	-
3	H	6	115 - 120	26.50	1.15	4.7	-	-	-
4	H	3	52 - 57	30.87	1.21	8.6	-	-	-
4	H	6	105 - 110	35.90	1.43	1.0	-	-	-
5	H	4	75 - 80	42.10	1.99	1.7	-	-	-
6	H	5	72 - 77	53.07	2.61	3.6	-	-	-

(continued overpage)

(Table 6T5 continued)

Sample (core, section, interval(cm))		Depth (mbsf)	Age (Ma)	MAR $CaCO_3$ ($g/cm^2/ky$)	Ca/Ti (g/g)	Si/Ti (g/g)	Al/Ti (g/g)
7 H 3	72 - 77	59.57	2.89	1.9	-	-	-
8 H 1	72 - 77	66.07	3.02	19.0	-	-	-
8 H 6	72 - 77	73.57	3.07	10.5	-	-	-
9 H 4	72 - 77	80.07	3.22	2.1	-	-	-
10 H 2	72 - 77	86.57	3.48	3.2	-	-	-
11 H 1	72 - 77	94.57	3.64	8.4	-	-	-
12 H 3	72 - 77	106.47	3.83	5.4	122	57	17
13 H 3	72 - 77	116.57	4.02	5.5	-	-	-
14 H 3	72 - 77	126.07	4.21	5.3	137	64	17
15 H 3	72 - 77	135.57	4.39	4.1	93	87	22
16 H 3	72 - 77	145.07	4.58	5.0	-	-	-
17 H 3	72 - 77	154.57	4.76	5.1	111	54	15
18 H 3	72 - 77	164.07	4.85	12.7	96	52	17
19 H 3	72 - 77	173.57	4.93	14.6	-	-	-
20 H 3	72 - 77	183.07	5.00	15.7	170	55	16
21 X 3	70 - 75	192.55	5.07	14.1	182	60	17
22 X 3	70 - 75	200.95	5.13	14.5	150	58	18
23 X 3	69 - 74	210.54	5.20	11.4	-	-	-
24 X 3	70 - 75	220.15	5.27	10.4	99	76	19
25 X 3	69 - 74	229.74	5.33	16.2	89	61	18
26 X 1	44 - 49	236.09	5.36	16.1	87	66	18
26 X 1	91 - 96	236.56	5.36	17.9	-	-	-
26 X 1	140 - 145	237.05	5.36	18.5	87	63	18
26 X 2	44 - 49	237.59	5.36	18.9	-	-	-
26 X 2	91 - 96	238.06	5.37	16.9	102	73	18
26 X 2	140 - 145	238.55	5.37	16.5	-	-	-
26 X 3	44 - 49	239.09	5.37	15.4	-	-	-
26 X 3	70 - 75	239.35	5.37	16.2	-	-	-
26 X 3	91 - 96	239.56	5.37	13.9	-	-	-
26 X 3	140 - 145	240.05	5.38	15.2	77	75	19
26 X 4	44 - 49	240.59	5.38	14.8	48	103	24
26 X 4	91 - 96	241.06	5.38	8.5	-	-	-
26 X 4	140 - 145	241.45	5.38	25.7	-	-	-
26 X 5	45 - 50	242.1	5.39	26.3	-	-	-
26 X 5	92 - 97	242.57	5.39	23.7	159	60	18
26 X 5	140 - 145	243.05	5.39	24.3	-	-	-
26 X 6	44 - 49	243.59	5.39	24.6	186	71	19
26 X 6	90 - 95	244.05	5.39	23.5	-	-	-
26 X 6	140 - 145	244.55	5.40	22.9	133	68	19
27 X 1	45 - 50	245.7	5.40	29.0	144	59	17
27 X 1	92 - 97	246.17	5.40	28.5	-	-	-
27 X 1	140 - 145	246.65	5.41	29.5	178	63	17
27 X 2	44 - 49	247.19	5.41	31.8	-	-	-

(continued overpage)

(Table 6T5 continued)

Sample (core, section, interval(cm))		Depth (mbsf)	Age (Ma)	MAR $CaCO_3$ ($g/cm^2/ky$)	Ca/Ti (g/g)	Si/Ti (g/g)	Al/Ti (g/g)
27 X 2	90 - 95	247.65	5.41	33.4	185	56	17
27 X 2	140 - 145	248.15	5.41	35.0	-	-	-
27 X 3	45 - 50	248.7	5.41	35.5	-	-	-
27 X 3	70 - 75	248.95	5.41	30.9	-	-	-
27 X 3	90 - 95	249.15	5.41	31.9	-	-	-
27 X 3	140 - 145	249.65	5.42	32.3	-	-	-
27 X 4	43 - 48	250.18	5.42	34.9	-	-	-
27 X 4	88 - 93	250.63	5.42	31.4	-	-	-
27 X 4	133 - 138	251.08	5.42	36.8	-	-	-
27 X 5	44 - 49	251.69	5.42	35.6	-	-	-
27 X 5	90 - 95	252.15	5.42	34.6	-	-	-
27 X 5	140 - 145	252.65	5.43	37.7	198	53	17
27 X 6	44 - 49	253.19	5.43	32.3	-	-	-
27 X 6	87 - 92	253.62	5.43	35.1	-	-	-
28 X 1	45 - 50	255.3	5.44	35.4	-	-	-
28 X 1	90 - 95	255.75	5.44	34.7	-	-	-
28 X 1	140 - 145	256.25	5.44	33.2	-	-	-
28 X 2	44 - 49	256.79	5.44	35.2	-	-	-
28 X 2	91 - 96	257.26	5.44	29.0	-	-	-
28 X 2	140 - 145	257.75	5.44	27.5	-	-	-
28 X 3	44 - 49	258.29	5.45	31.2	150	57	18
28 X 3	70 - 75	258.55	5.45	28.8	-	-	-
28 X 3	93 - 98	258.78	5.45	30.6	-	-	-
28 X 3	140 - 145	259.25	5.45	33.8	-	-	-
28 X 4	44 - 49	259.79	5.45	35.5	-	-	-
28 X 4	90 - 95	260.25	5.45	30.8	-	-	-
28 X 4	140 - 145	260.75	5.45	32.4	-	-	-
28 X 5	44 - 46	261.26	5.46	31.2	-	-	-
28 X 5	90 - 95	261.75	5.46	31.4	-	-	-
28 X 5	140 - 145	262.25	5.46	28.3	-	-	-
28 X 6	42 - 45	262.75	5.46	34.6	170	60	17
28 X 6	90 - 95	263.25	5.46	33.1	-	-	-
28 X 6	140 - 145	263.75	5.46	29.5	123	53	18
29 X 3	66 - 71	268.11	5.48	35.0	158	52	18
30 X 3	70 - 75	277.85	5.52	26.8	166	59	17
31 X 3	80 - 85	287.47	5.56	30.2	204	60	17
32 X 1	47 - 50	293.8	5.58	34.9	147	58	18
32 X 1	90 - 95	294.25	5.58	34.5	-	-	-
32 X 1	140 - 145	294.75	5.58	35.6	154	62	19
32 X 2	44 - 49	295.29	5.58	33.7	-	-	-
32 X 2	90 - 95	295.75	5.58	36.4	183	60	17
32 X 2	140 - 143	296.23	5.59	36.5	-	-	-
32 X 3	43 - 48	296.78	5.59	36.7	-	-	-

(continued overpage)

(Table 6T5 continued)

Sample (core, section, interval(cm))		Depth (mbsf)	Age (Ma)	MAR $CaCO_3$ ($g/cm^2/ky$)	Ca/Ti (g/g)	Si/Ti (g/g)	Al/Ti (g/g)
32 X 3	70 - 75	297.05	5.59	36.1	-	-	-
32 X 3	90 - 95	297.25	5.59	31.8	-	-	-
32 X 3	142 - 146	297.76	5.59	33.8	-	-	-
32 X 4	48 - 53	298.33	5.59	33.9	-	-	-
32 X 4	90 - 95	298.75	5.59	31.8	-	-	-
32 X 4	140 - 145	299.25	5.60	34.5	-	-	-
32 X 5	41 - 43	299.73	5.60	34.5	-	-	-
32 X 5	90 - 95	300.25	5.60	32.9	-	-	-
32 X 5	140 - 145	300.75	5.60	34.2	-	-	-
32 X 6	42 - 47	301.27	5.60	34.3	135	63	18
32 X 6	90 - 95	301.75	5.60	35.8	-	-	-
32 X 6	140 - 145	302.25	5.61	37.1	-	-	-
33 X 1	45 - 50	303.5	5.61	35.6	-	-	-
33 X 1	90 - 95	303.95	5.61	38.4	-	-	-
33 X 1	140 - 145	304.45	5.61	30.8	-	-	-
33 X 2	44 - 49	304.99	5.61	32.0	-	-	-
33 X 2	90 - 95	305.45	5.62	29.1	-	-	-
33 X 2	140 - 145	305.95	5.62	30.0	-	-	-
33 X 3	43 - 48	306.48	5.62	34.1	-	-	-
33 X 3	69 - 74	306.74	5.62	33.6	-	-	-
33 X 3	90 - 93	306.93	5.62	32.6	154	61	18
33 X 3	140 - 145	307.45	5.62	32.8	-	-	-
33 X 4	44 - 49	307.99	5.62	34.7	-	-	-
33 X 4	90 - 95	308.45	5.63	31.1	-	-	-
33 X 4	132 - 137	308.87	5.63	30.7	-	-	-
33 X 5	48 - 47	309.47	5.63	30.1	-	-	-
33 X 5	90 - 95	309.95	5.63	28.9	-	-	-
33 X 5	141 - 146	310.46	5.63	27.6	-	-	-
33 X 6	48 - 53	311.03	5.63	30.0	-	-	-
33 X 6	90 - 95	311.45	5.63	29.3	-	-	-
33 X 6	140 - 145	311.95	5.64	33.0	117	61	18
34 X 1	47 - 52	313.12	5.64	31.2	-	-	-
34 X 1	90 - 95	313.55	5.64	30.9	-	-	-
34 X 1	142 - 147	314.07	5.64	35.1	-	-	-
34 X 2	45 - 50	314.6	5.65	31.8	-	-	-
34 X 2	89 - 94	315.04	5.65	35.1	-	-	-
34 X 2	140 - 145	315.55	5.65	30.8	-	-	-
34 X 3	45 - 50	316.1	5.65	34.2	-	-	-
34 X 3	72 - 77	316.37	5.65	32.8	-	-	-
34 X 3	93 - 98	316.58	5.65	31.9	-	-	-
34 X 3	140 - 145	317.05	5.65	32.9	-	-	-
34 X 4	44 - 49	317.59	5.65	35.1	153	56	18
34 X 4	89 - 94	318.04	5.66	36.4	-	-	-

(continued overpage)

(Table 6T5 continued)

Sample (core, section, interval(cm))	Depth (mbsf)	Age (Ma)	MAR $CaCO_3$ ($g/cm^2/ky$)	Ca/Ti (g/g)	Si/Ti (g/g)	Al/Ti (g/g)
34 X 4 140 - 145	318.55	5.66	35.2	-	-	-
34 X 5 44 - 49	319.09	5.66	36.5	-	-	-
34 X 5 90 - 95	319.55	5.66	36.3	-	-	-
34 X 5 140 - 145	320.05	5.66	38.3	-	-	-
34 X 6 45 - 50	320.6	5.66	42.3	-	-	-
35 X 3 71 - 76	325.66	5.68	33.8	-	-	-
37 X 3 68 - 73	344.83	6.41	2.0	170	59	17
38 X 1 72 - 77	351.47	6.72	2.6	-	-	-
38 X 3 68 - 73	354.43	6.83	2.5	112	64	19
38 X 6 72 - 77	358.97	6.99	2.8	-	-	-
39 X 3 68 - 73	364.13	7.18	2.6	-	-	-
39 X 6 72 - 77	368.67	7.35	3.1	-	-	-
40 X 3 68 - 73	373.83	7.54	2.2	96	75	20
43 X 2 72 - 77	401.27	8.79	3.6	-	-	-
43 X 5 72 - 77	405.77	8.90	3.8	-	-	-
44 X 3 72 - 77	411.69	9.04	3.7	-	-	-
45 X 1 72 - 77	419.07	9.22	3.7	-	-	-
45 X 5 72 - 77	425.07	9.36	4.2	-	-	-
46 X 2 72 - 77	430.17	9.48	3.6	-	-	-
46 X 6 72 - 77	436.17	9.60	3.7	-	-	-
48 X 2 72 - 77	449.07	9.86	3.2	-	-	-
49 X 4 72 - 77	461.67	10.08	4.6	-	-	-
50 X 5 72 - 77	472.77	10.26	2.4	-	-	-
54 X 2 72 - 77	506.37	10.45	18.9	-	-	-
58 X 4 72 - 77	547.87	10.85	10.2	-	-	-

APPENDIX 2

FIGURES

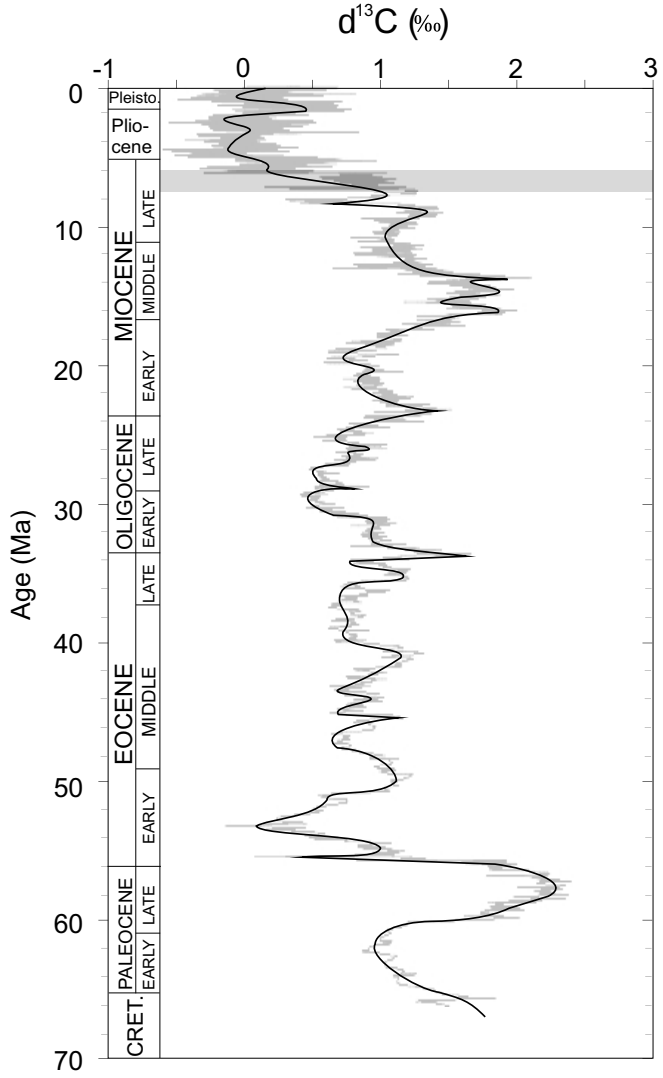

Fig. 2F1 Cenozoic carbon isotope record from global deep-sea sediments. Smooth (—) curve adapted from the multi-record (—) curve in Zachos et al. (2001). Shaded area indicates the time interval of the widely observed late Miocene $\delta^{13}C$ shift.

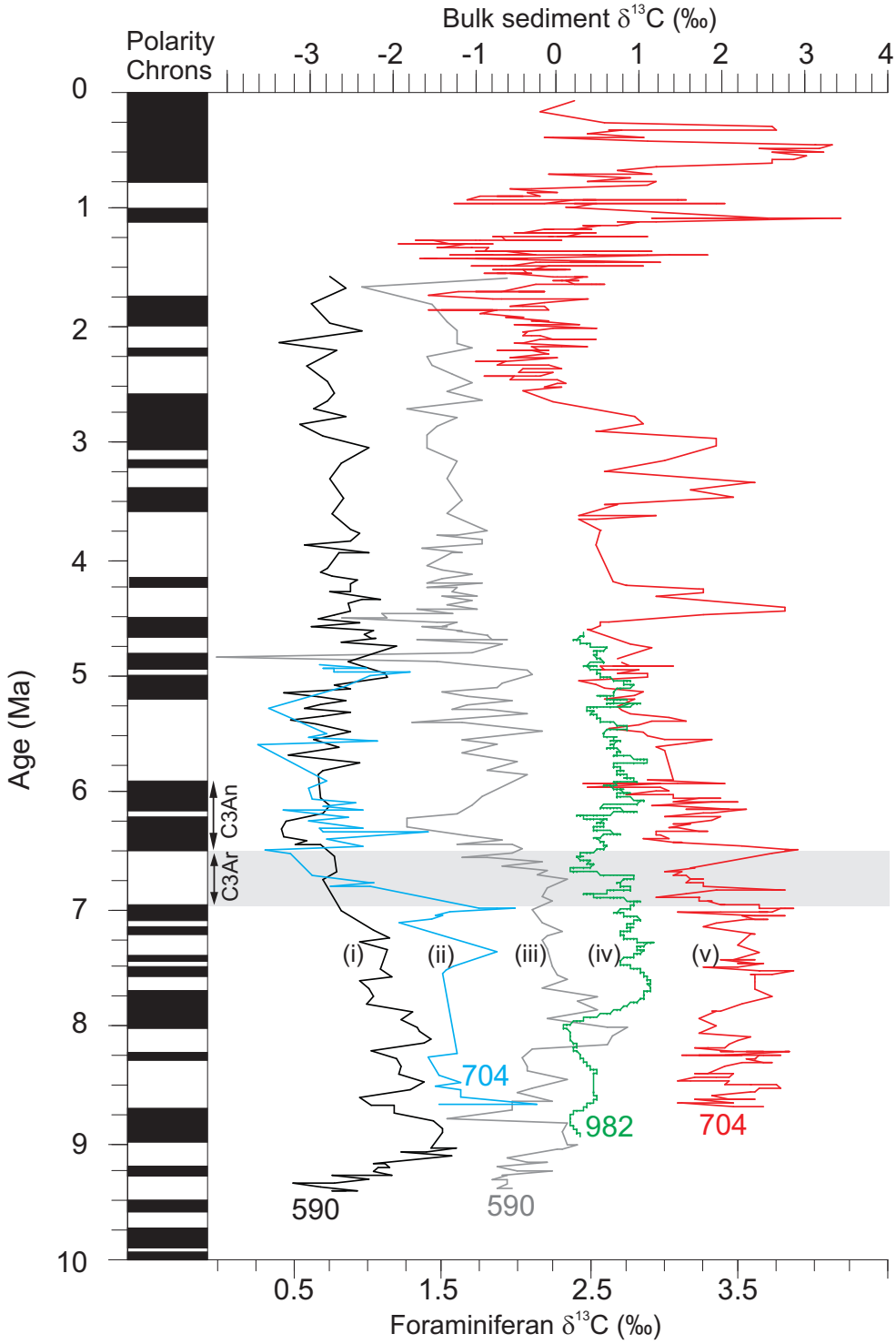

Fig. 2F2 Previously published $\delta^{13}C$ records from the Atlantic and Pacific Oceans, representing a range of carbonate phases and spanning the late Miocene-early Pliocene. Carbonate phases represented are (i) Benthic foraminifera (*Cibicidoides kullenbergi*; Elmstrom and Kennett [1986]), (ii) sub-surface dwelling planktic foraminifera (*Neogloboquadrina pachyderma*; Müller et al. [1991]), (iii) surface dwelling planktic foraminifera (*Globigerinoides sacculifer*, Elmstrom and Kennett [1986]), (iv) bulk sediment (data smoothed into a 21-point moving average trendline; Hodell et al. [2001]), (v) bulk fine fraction (Mead et al., 1991). Ages have been adjusted to the Berggren et al. (1995b) timescale by assigning new ages to the previously established age models for these sites, except for site 982 which relies on astronomically-derived ages.

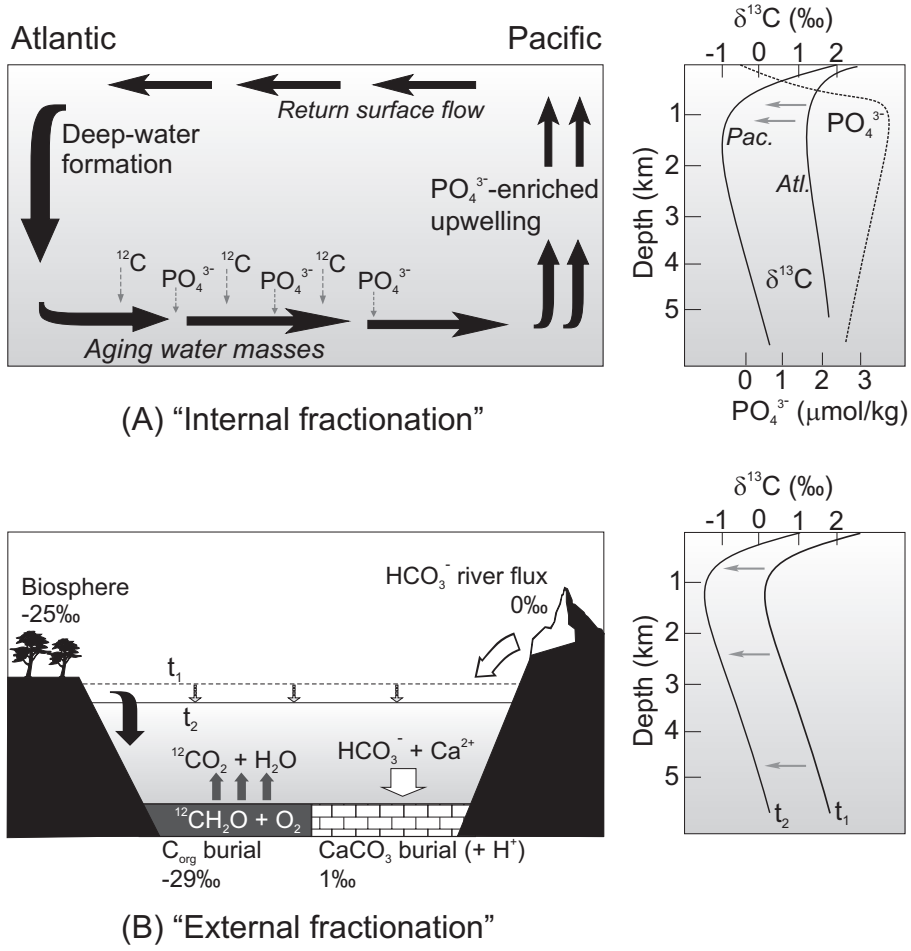

Fig. 2F3 (a) Schematic model of present-day thermohaline circulation, with corresponding vertical profiles of stable carbon isotopes and dissolved phosphate (PO_4^{3-}). Note the depletion in $\delta^{13}C$ (←) between the Atlantic and Pacific Oceans. (Profiles adapted from Kroopnick [1985]). (b) Carbon isotopic composition of key carbon reservoirs and fluxes invoked in the Chron C3Ar carbon shift. A decrease in total dissolved $\delta^{13}C$ over the time interval t_1 to t_2 is illustrated qualitatively in the right-hand cartoon. (See Scholle and Arthur [1980], Kump and Arthur [1999]).

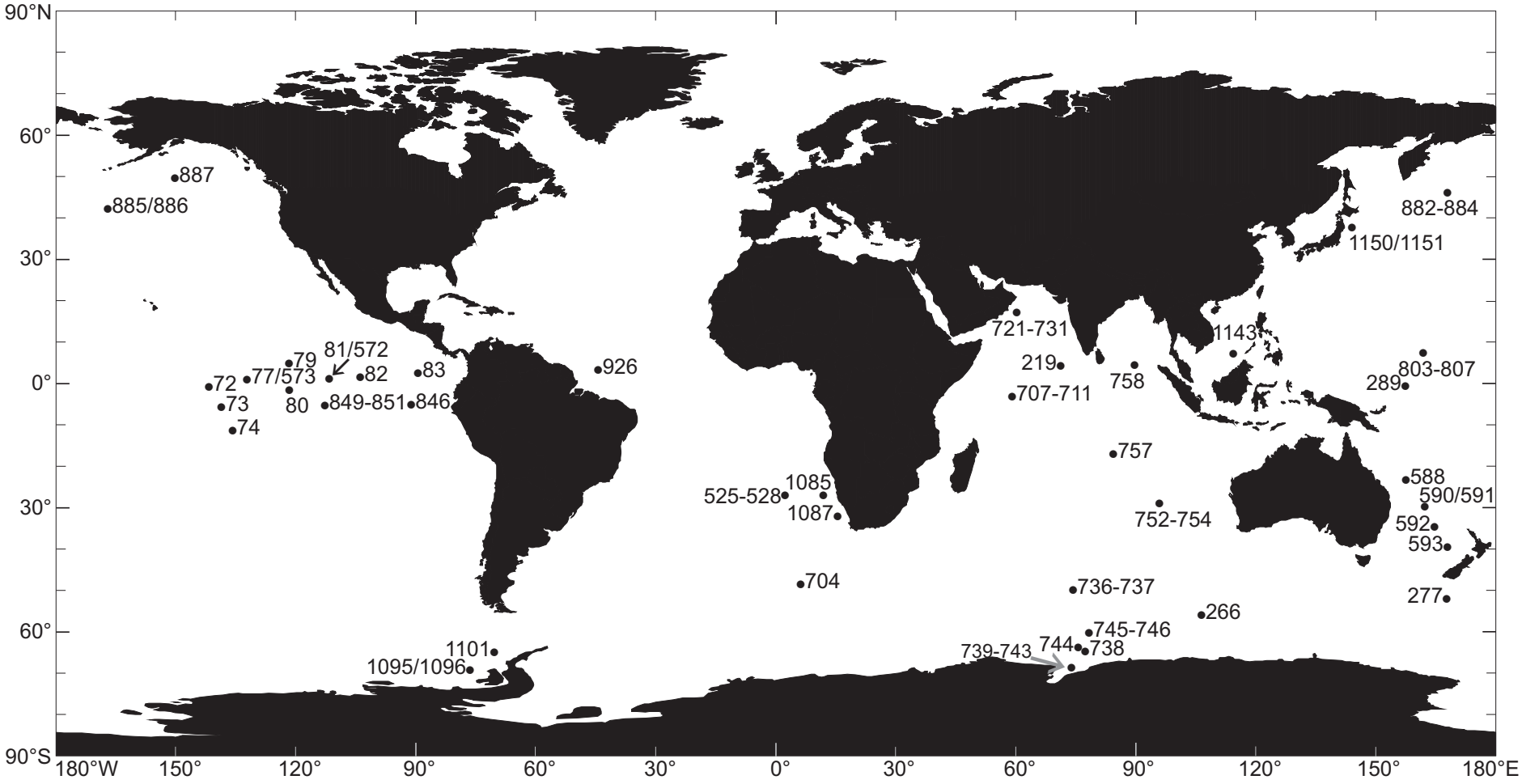

Fig. 3F1 Locations of DSDP and ODP sites discussed in chapter 3

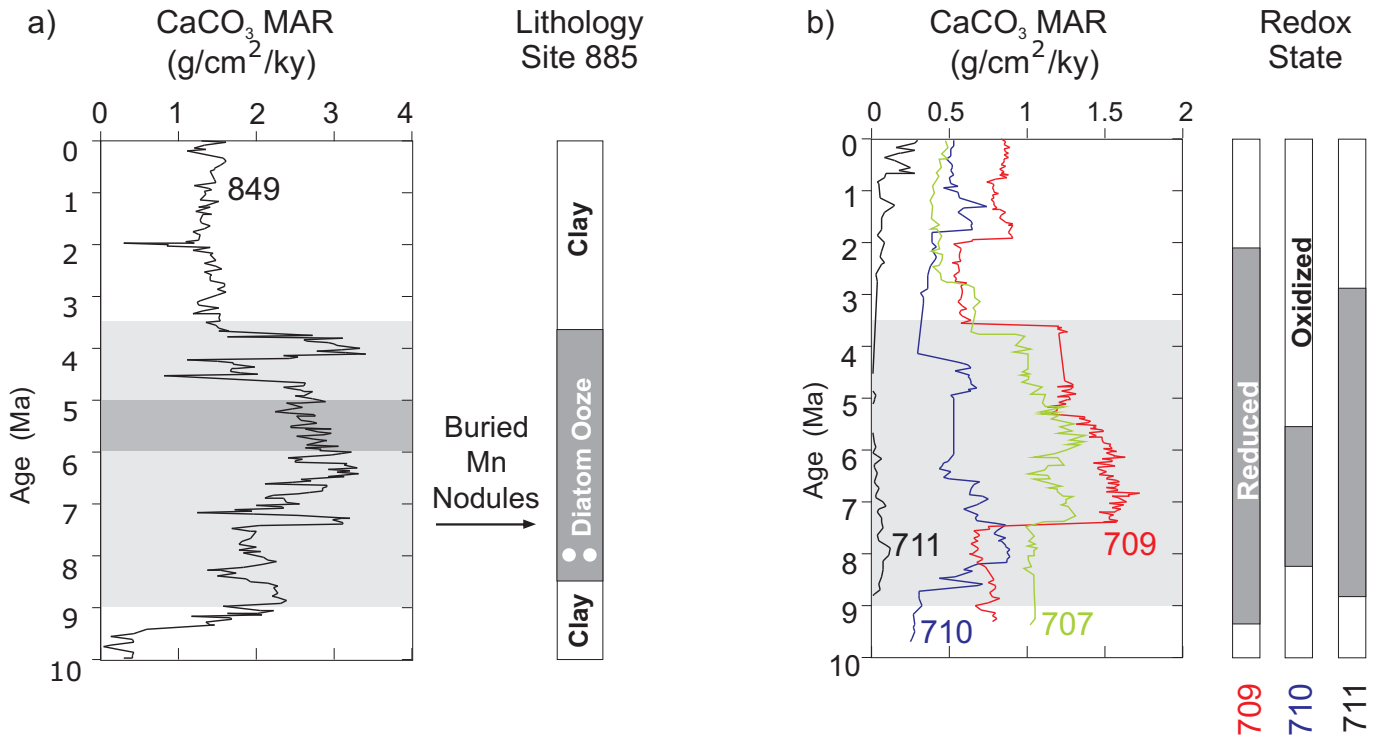

Fig. 3F2 Down-core records of carbonate accumulation and significant lithological changes at (a) ODP sites 849 and 885 in the Pacific Ocean, and (b) ODP sites 707 and 709-711 in the Indian Ocean (from Dickens and Owen [1999]). Ages are based on the Berggren et al. (1995b) timescale.

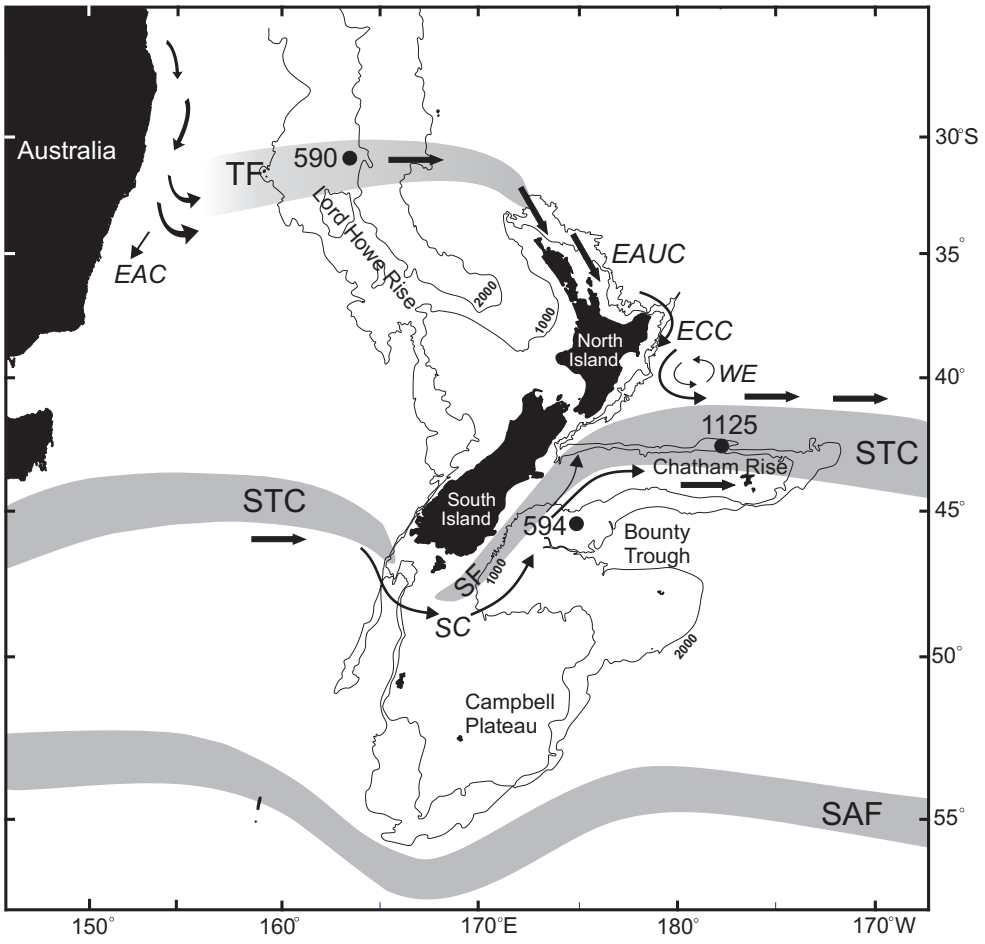

Fig. 4F1 Location map showing hydrography and bathymetry of the New Zealand region of the southwest Pacific Ocean, with positions of DSDP sites 590 and 594, and ODP site 1125. Depth contours are in metres; TF = Tasman Front, STC = Subtropical Convergence, SF = Southland Front, SAF = Subantarctic Front, EAC = East Australian Current, EAUC = East Auckland Current, ECC = East Cape Current, WE = Wairarapa Eddy, SC = Southland Current.

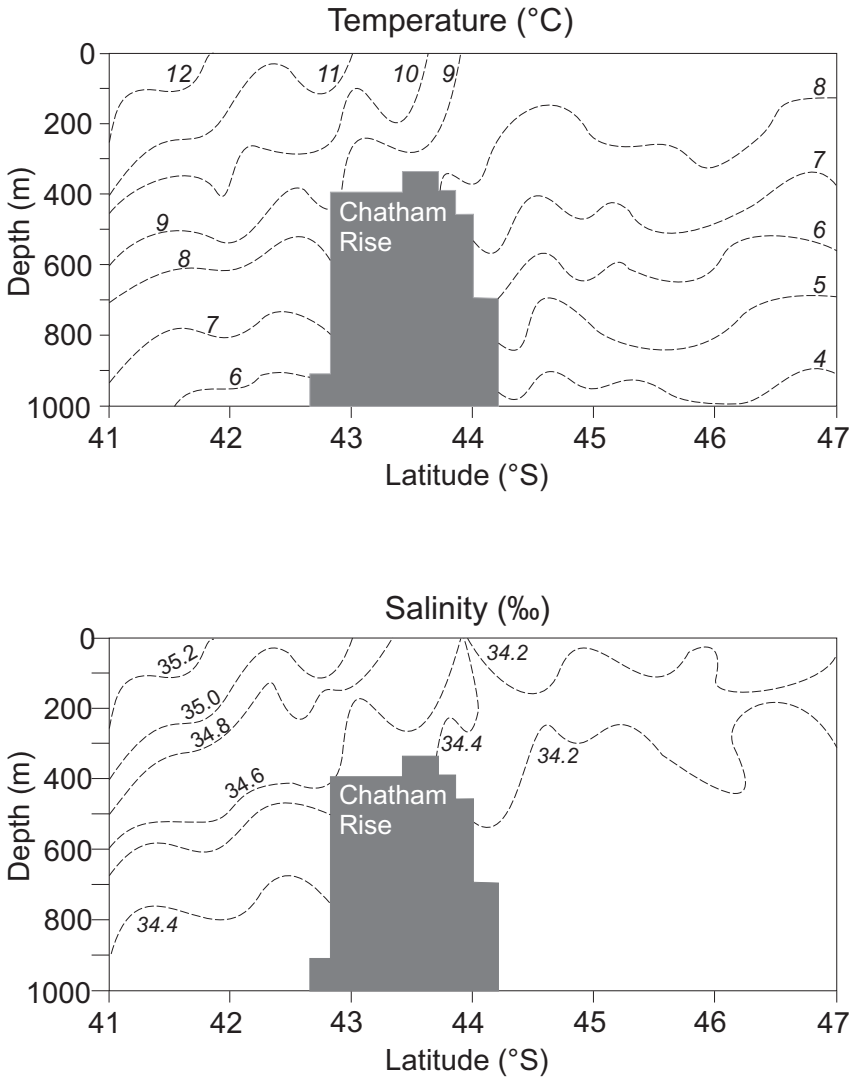

Fig. 4F2 Temperature and salinity transects across the Subtropical Convergence (STC) and Chatham Rise at 178°30′E (adapted from McClatchie et al. [2001]).

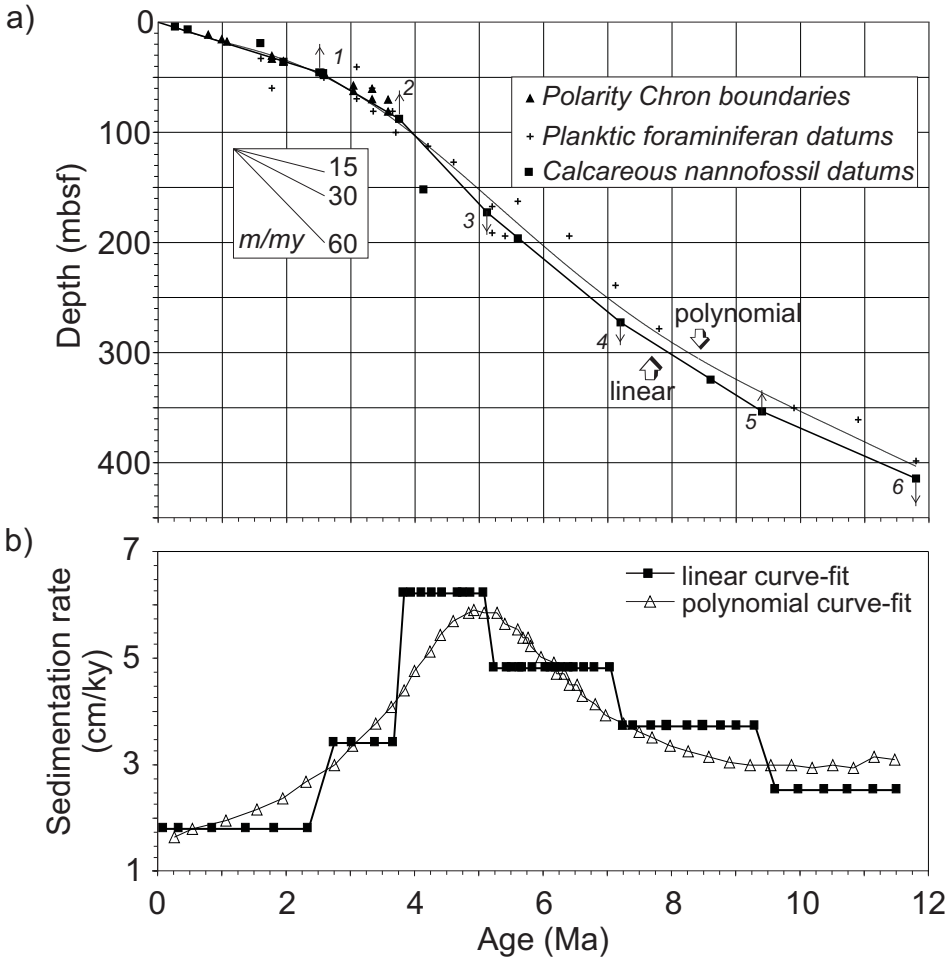

Fig. 5F1 (a) Age-depth model and sedimentation rate (SR) curves for site 590. The linear SR curve is based on the datums numbered 1 to 6 (Table 5T1). The smoothed SR curve was determined by non-linear regression analysis using Engineering Equation Solver (EES) version 4.441, and is described by the polynomial equation: $y = (0.146 + 6.383e\text{-}2)x - (3.473e\text{-}4)x^2 + (1.053e\text{-}6)x^3 - (1.013e\text{-}9)x^4$. (b) Calculated SRs at site 590, using both the linear and polynomial curve-fitting methods.

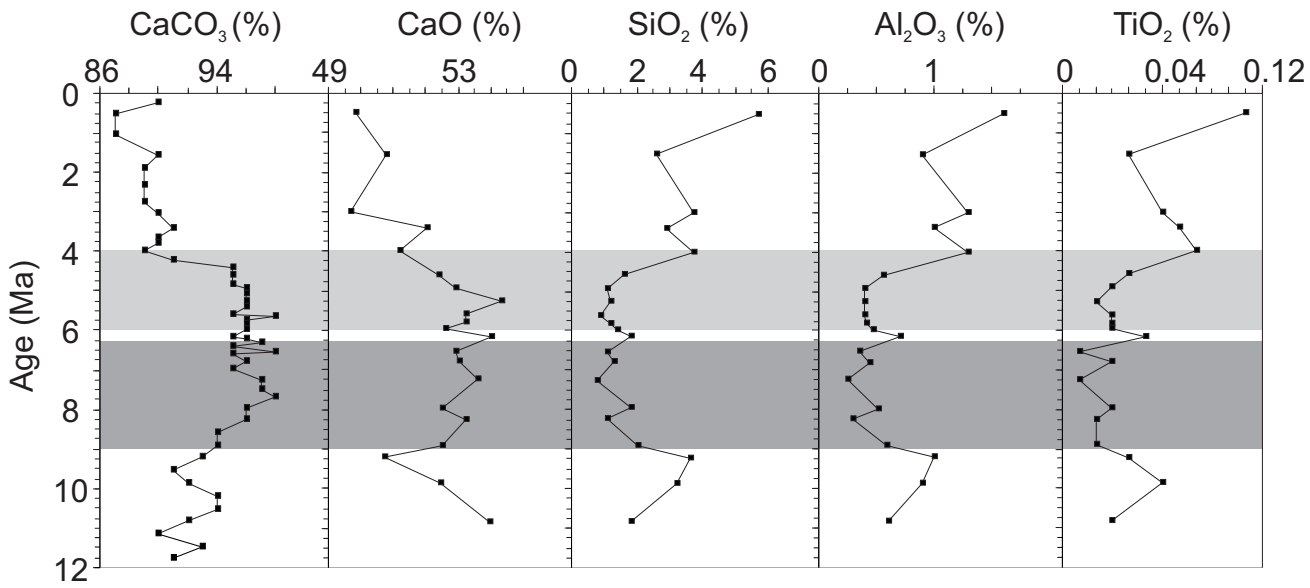

Fig. 5F2 Carbonate and elemental oxide concentrations at site 590. Sample ages are from "AgePOLY", Table 5T2. The two shaded areas indicate time intervals of inferred elevated productivity based on different proxies (see section 5.6).

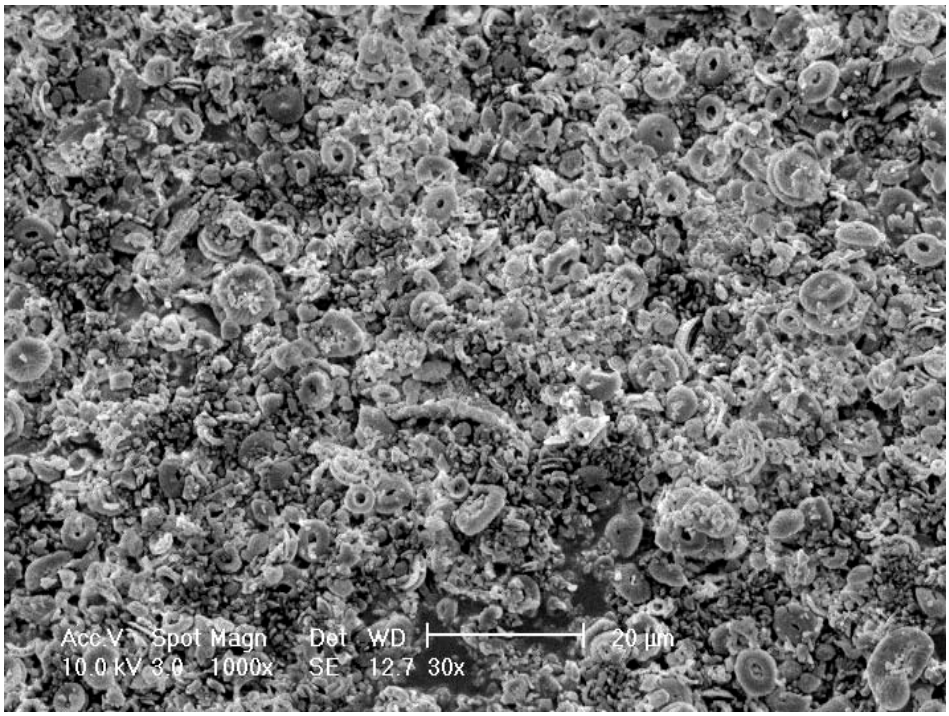

Fig. 5F3 Scanning electron microscope (SEM) photograph of bulk sediment from sample 590B-30X4, 74-78 cm. Note that the sediment is almost entirely composed of coccoliths.

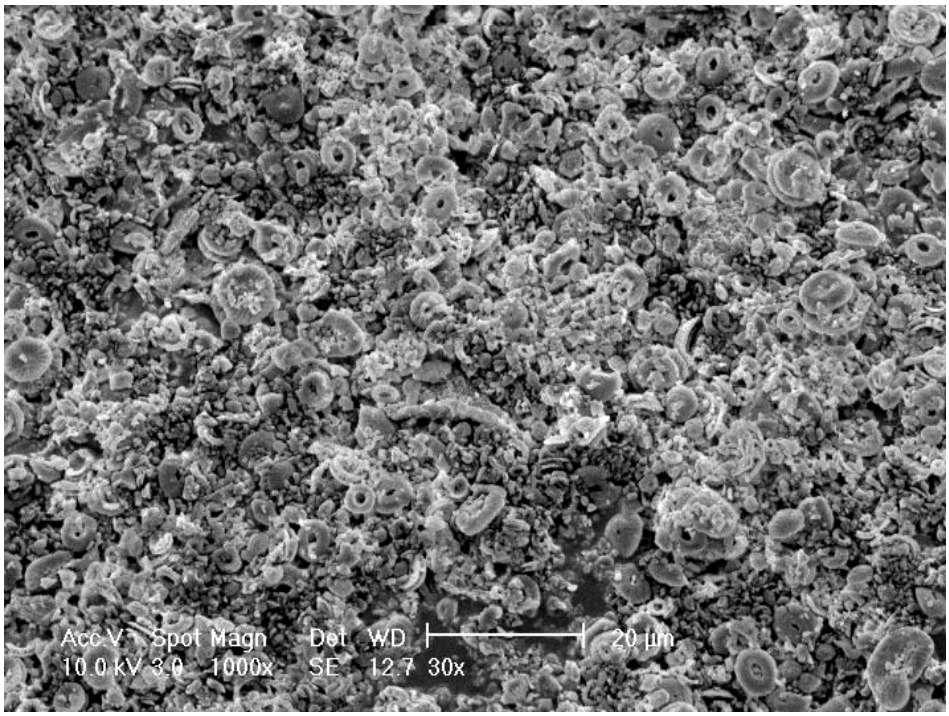

Fig. 5F3 Scanning electron microscope (SEM) photograph of bulk sediment from sample 590B-30X4, 74-78 cm. Note that the sediment is almost entirely composed of coccoliths.

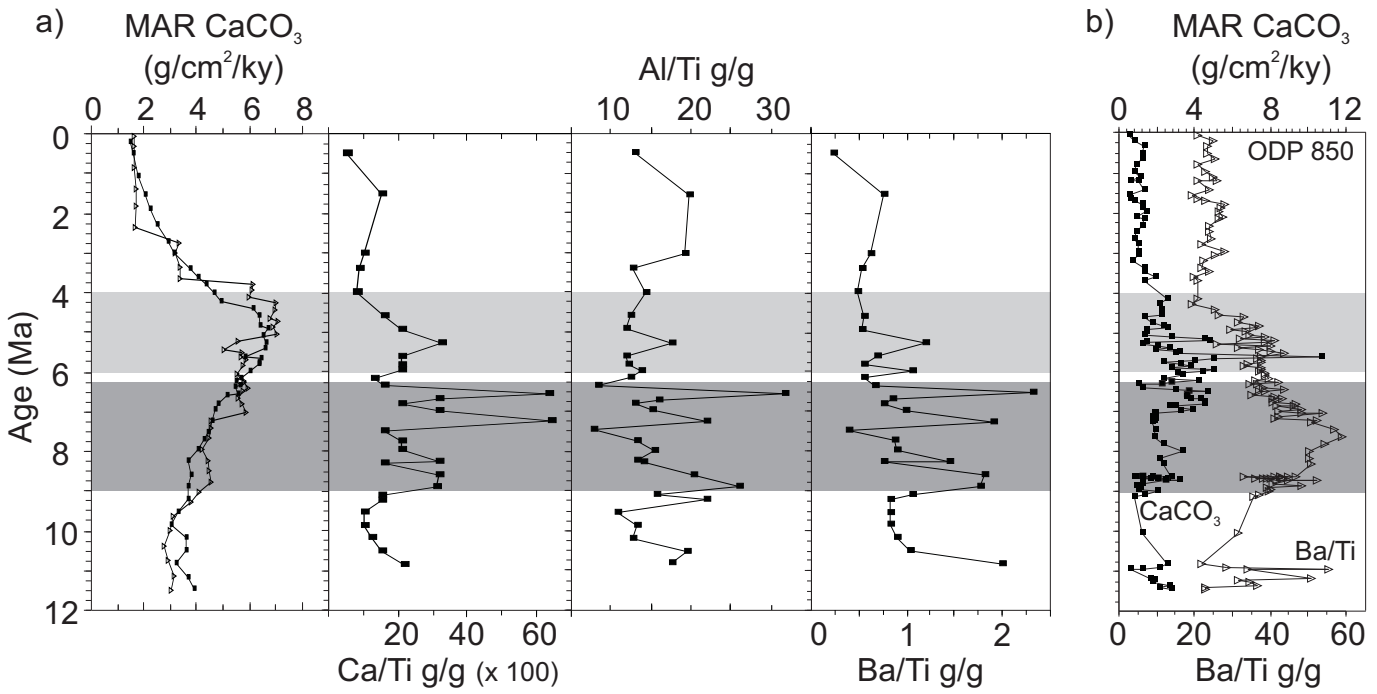

Fig. 5F4 (a) Carbonate MARs and Ca/Ti, Ba/Ti, Al/Ti ratios at site 590. The carbonate MARs have been calculated using LSRs (Δ) and smoothed SRs (■). (b) Carbonate MARs (■) and Ba/Ti ratios (Δ) at ODP site 850 (Schroder et al., 1997). Data have been calibrated to the timescale of Berggren et al. (1995a,b) to permit comparison with site 590 data.

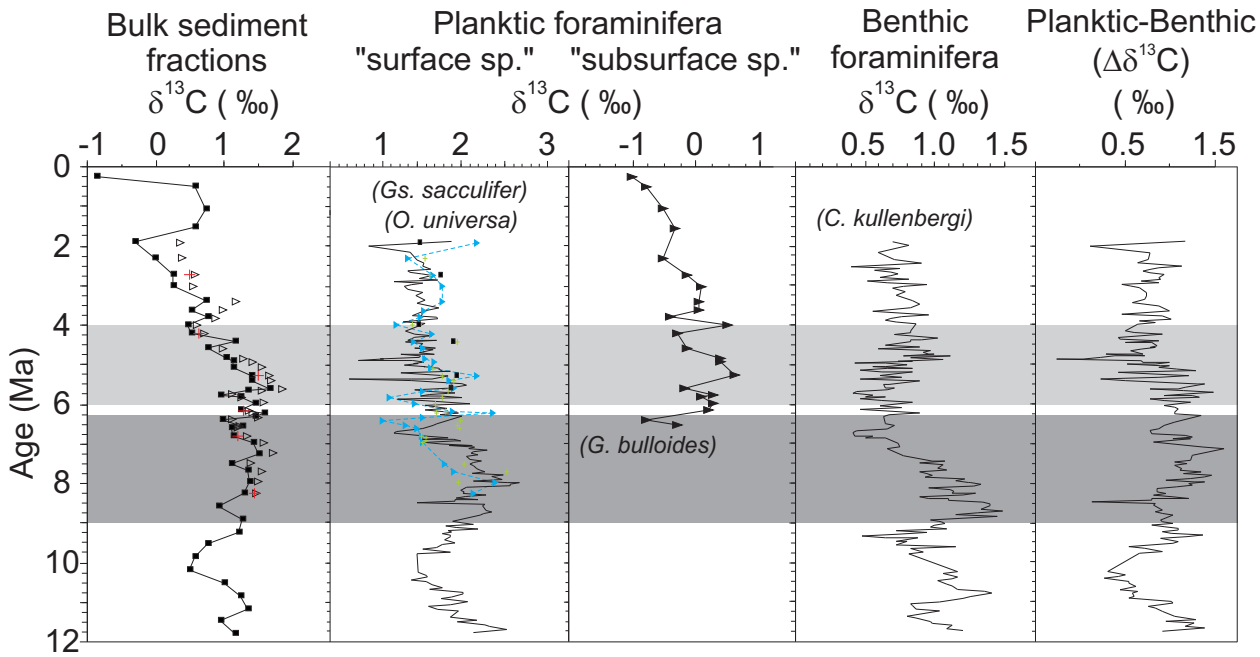

Fig. 5F5 The $\delta^{13}C$ of bulk sediment fractions, planktonic foraminifera, and benthic foraminifera from site 590. Bulk sediment fractions include bulk sediment (■), bulk fine-grained sediment (Δ), and bulk 'nannofossils' (+). Planktonic foraminifera have been grouped into surface-dwelling species [*Gs. sacculifer* 'w' (■), *Gs. sacculifer* 'w/o' (+), *Gs. sacculifer* 'mix' (-), *O. universa* (--▲--)] and subsurface-dwelling species [*G. bulloides*], where *Gs. sacculifer* 'mix' is the mixed-morphotype data from Elmstrom and Kennett (1986). The $\Delta\delta^{13}C$ record has been calculated from *Gs. sacculifer* 'mix' and *Cibicidoides kullenbergi* using data from Elmstrom and Kennett (1986). Foraminiferan $\delta^{13}C$ values have not been corrected for vital effects.

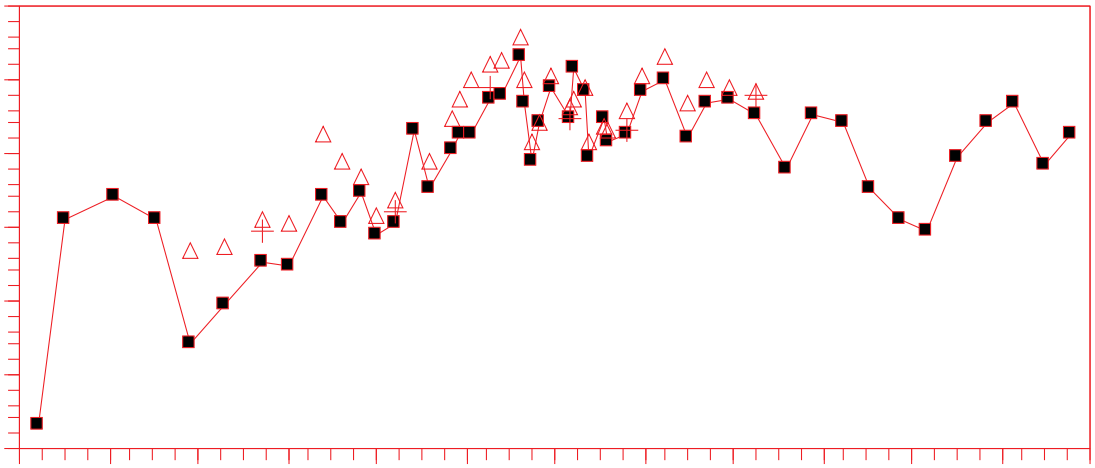

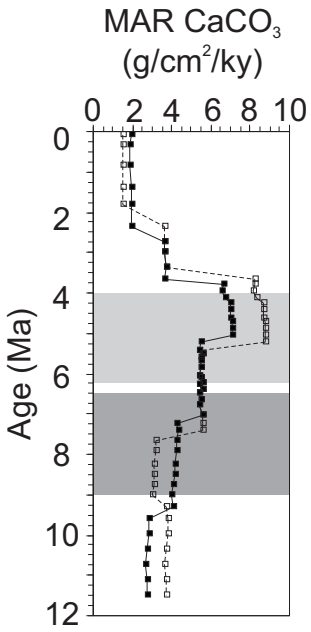

Fig.5F6 Possible deviations in the calculation of carbonate MARs as a function of varying the LSRs at site 590. Carbonate MARs have been calculated using LSRs derived from depth-averaged datums (■), and from the minimum (LAD) or maximum (FAD) depth in a sampling interval (□).

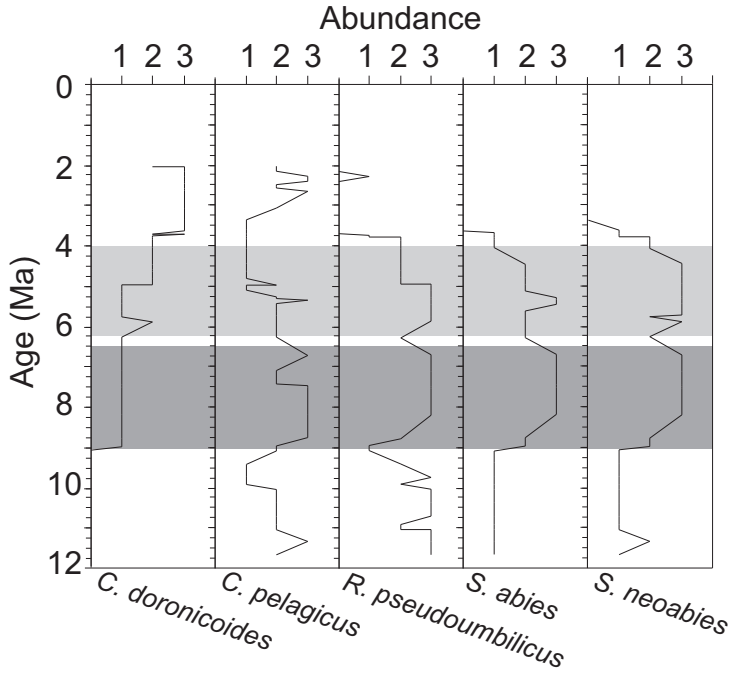

Fig.5F7 Variations in nannofossil abundance over time at site 590 (from Lohmann, 1986) for the five most abundant species at this site (*Crenalithus doronicoides, Coccolithus pelagicus, Reticulofenestra pseudoumbilicus, Sphenolithus abies,* and *Sphenolithus neoabies*). The *x*-axis is graded between 'rare' (1), 'common' (2), and 'abundant' (3).

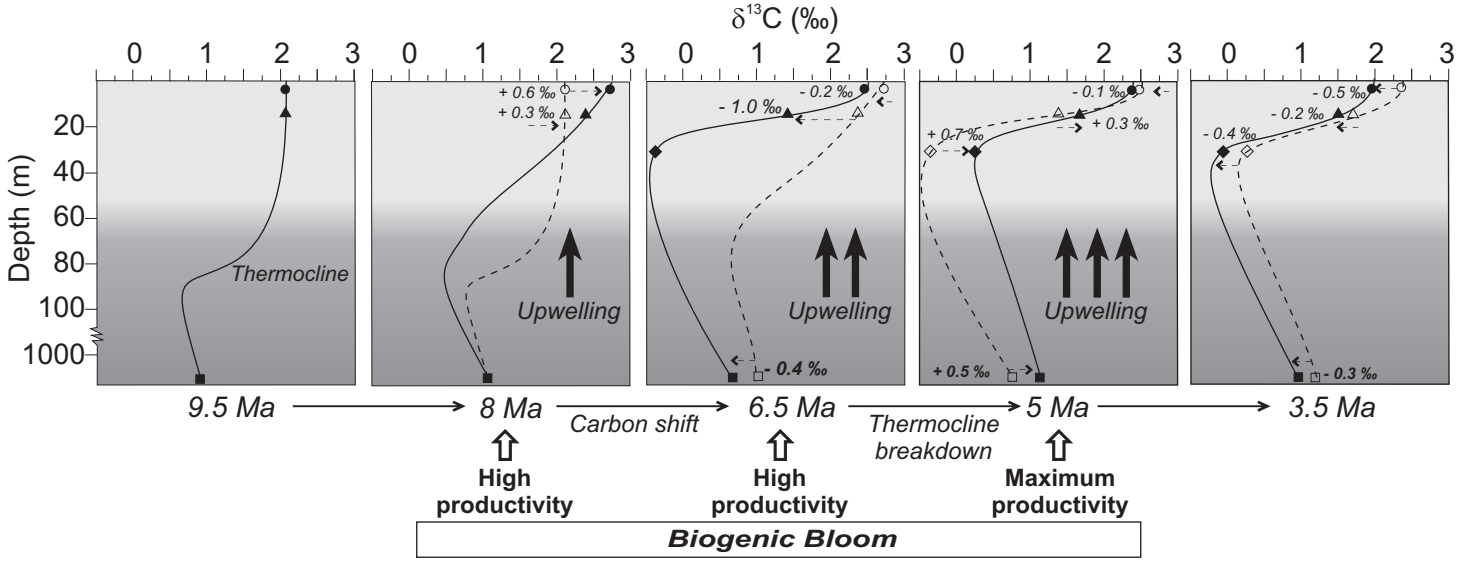

Fig.5F8 Carbon isotope vertical profiles at site 590 represented schematically based on the $\delta^{13}C$ records of bulk carbonate (●), *Gs. sacculifer* 'mix' (s), *G. bulloides* (♦) and *C. kullenbergi* (■) for the late Miocene and early Pliocene. Bulk carbonate $\delta^{13}C$ values have been corrected by + 1 ‰, given the assumption that the $\delta^{13}C$ gradient through the mixed layer was minimal prior to the start of the biogenic bloom and the Chron C3AR Carbon Shift. Recorded $\delta^{13}C$ shifts are quantified (e.g. + 1 ‰ →) so that the change in the $\delta^{13}C$ gradient between successive 1.5 My intervals (dashed line) can be inferred.

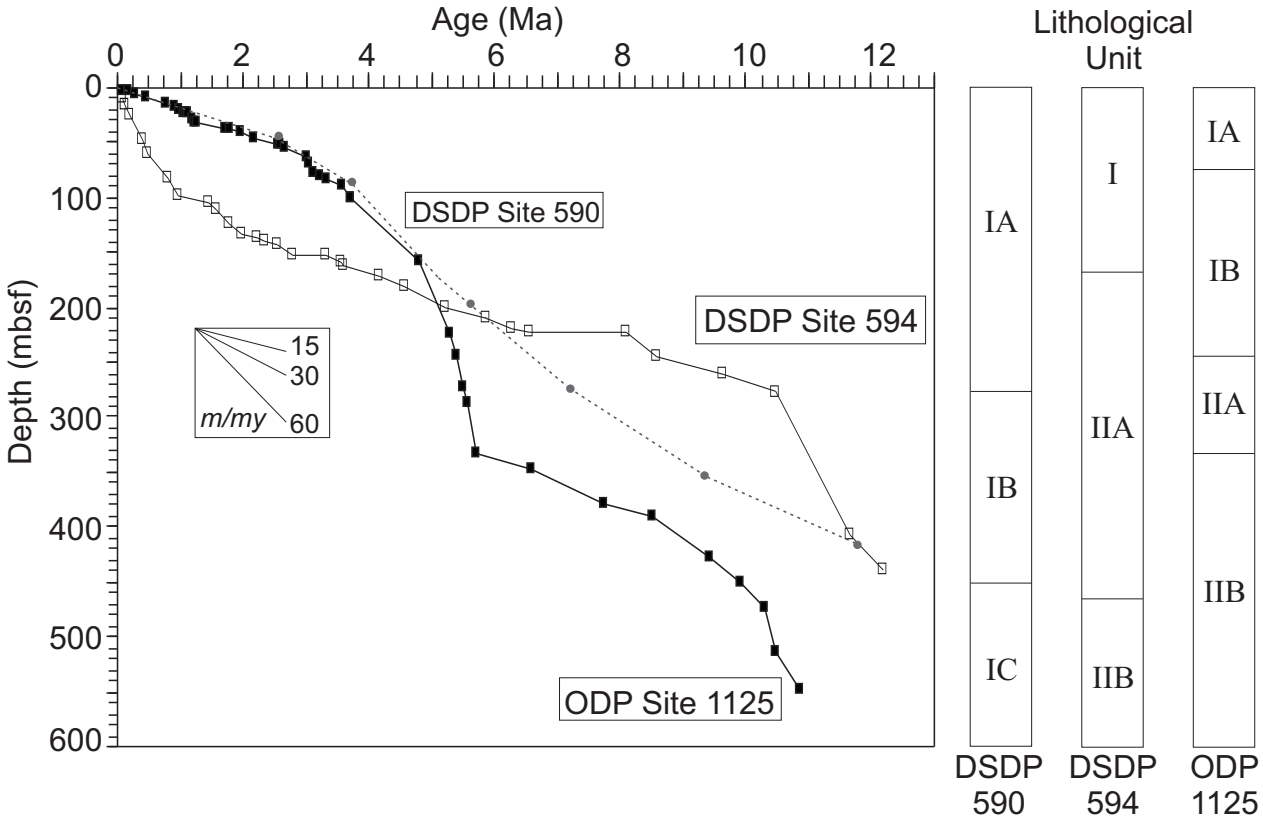

Fig. 6F1 Age-depth model for sites 590 (-●-), 594 (-▫-) and 1125 (-■-), based on the Berggren et al. (1995a,b) timescale. Site lithology from Kennett, von der Borch et al., 1986 (sites 590, 594) and Carter et al., 1999 (site 1125).

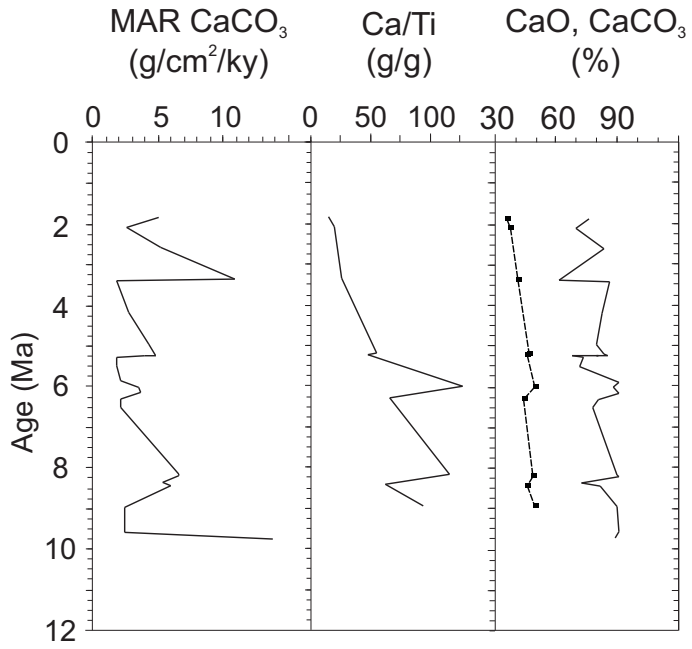

Fig.6F2 Downcore records of carbonate content - % CaO (dashed line) and % $CaCO_3$ (solid line) - and carbonate mass accumulation rates (MARs) at DSDP site 594.

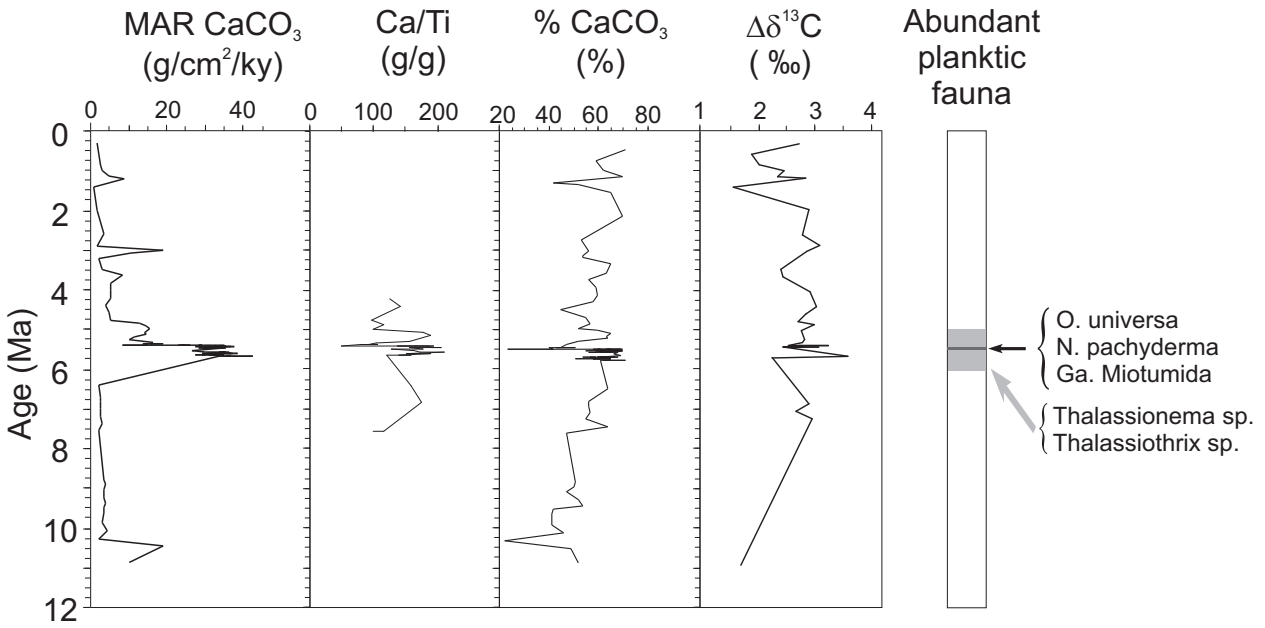

Fig.6F3 Downcore records of carbonate accumulation, Δδ13C (*O. Universa* - *Uvigerina* spp.), and significant faunal changes at ODP site 1125.

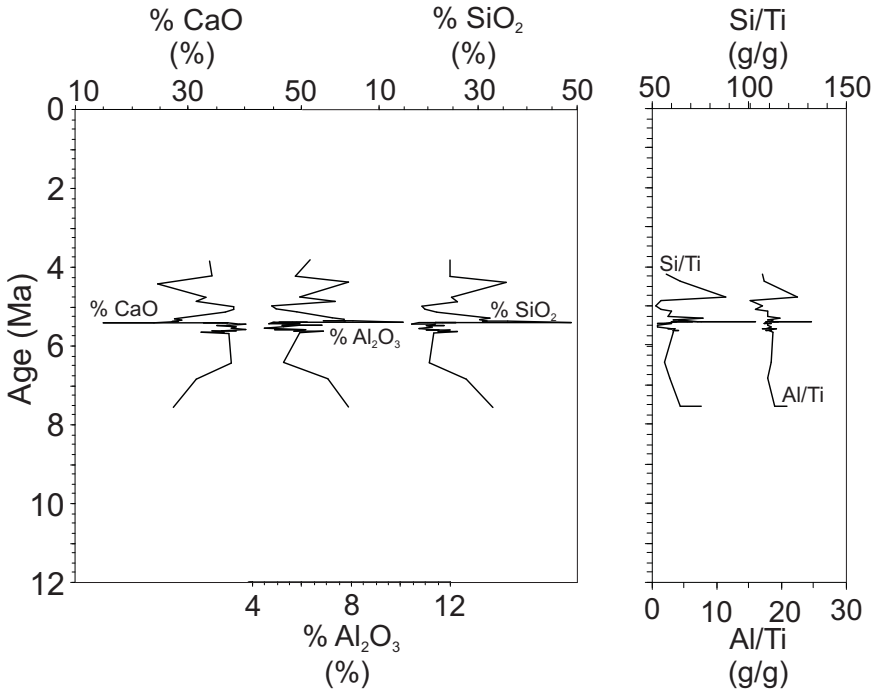

Fig. 6F4 Concentrations of major element oxides, and Si/Ti and Al/Ti ratios at site 1125.

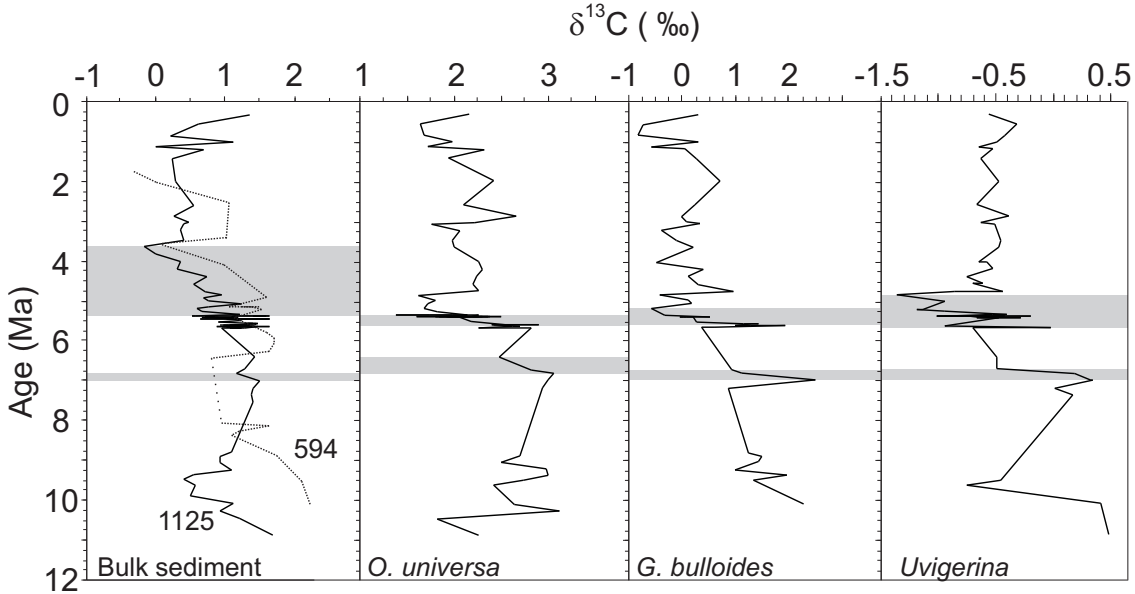

Fig. 6F5 The $\delta^{13}C$ of bulk sediment from site 594 (dashed line), and the $\delta^{13}C$ of bulk sediment, planktonic foraminifera, and benthic foraminifera from site 1125. Foraminiferan $\delta^{13}C$ values have not been corrected for vital effects. The shaded areas indicate intervals of $\delta^{13}C$ depletions (see section 6.5).

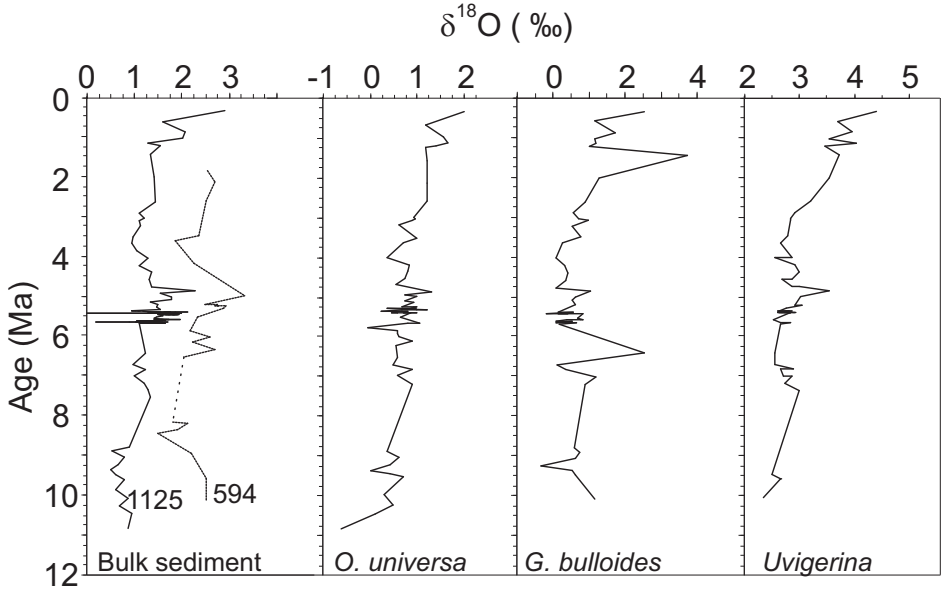

Fig. 6F6 The $\delta^{18}O$ of bulk sediment from site 594 (dashed line), and the $\delta^{18}O$ of bulk sediment, planktonic foraminifera, and benthic foraminifera from site 1125. Foraminiferan $\delta^{18}O$ values have not been corrected for vital effects.

Late Neogene Biogenic Sedimentation and Carbon Isotope Shifts in the southwest Pacific Ocean

Katherine Grant

ERRATA

p. iv	For "sholarship" read "scholarship"
p. 2	Correct the age for the Earth to 4.6 billion years
p. 2	For "Two observations that somehow reflect major perturbations" read "Two observations that require major perturbations"
p. 6 et seq.	For "planktonic" read "planktic"
p. 7	Add "FAD = First Appearance Datum"
p. 9	For "ageing" read "aging"
p. 13	For "variarions" read "variations"
p.14	Add "MAR = Mass Accumulation Rate"
p. 21	For "depostion" read "deposition"
p. 27	For "pertinant" read "pertinent"
p. 41 et seq.	For "Fig. 4F5" read "Fig. 5F4"
p. 48	For "Fig. 5F7" read "Fig. 5F8"
p. 57	For "aluminsilicate" read "aluminosilcate"
p. 64	For "Fig. 6F1" read "Fig. 6F3"
p. 65	For "drlling" read "drilling"
p. 70	For "Antartic" read "Antarctic"
p. 71	For "Fig. 6F5" read "Fig. 5F6"